Durham E-Theses

Molecular tailoring of solid surfaces

Evenson, Simon Alan

MOLECULAR TAILORING OF SOLID SURFACES

Simon Alan Evenson

Ph.D. Thesis

Department of Chemistry

University of Durham

September 1997

2 0 MAY 1998

DECLARATION

The work described in this thesis was carried out in the Department of Chemistry at the University of Durham between October 1994 and September 1997. It is the original work of the author except where otherwise acknowledged, and has not previously been submitted for a degree in this or any other university.

Langmuir-Blodgett film preparation (Chapters 2 and 3) was performed by Chris Pearson, School of Engineering and Centre for Molecular Electronics, University of Durham.

LIST OF PUBLICATIONS

Work in this thesis has been published or will be submitted for publication as follows:-

1. "Variation in Intermolecular Spacing with Dipping Pressure for Arachidic Acid LB Films"; Evenson, S. A.; Badyal, J. P. S.; Pearson, C.; Petty, M. C.; *J. Phys. Chem.* **1996**, *100*, 11672 - 11674.

2. "Skeletonization of Mixed Arachidic Acid / Cadmium Arachidate LB Films: A Study Using Atomic Force Microscopy"; Evenson, S. A.; Badyal, J. P. S.; Pearson, C.; Petty, M. C.; *Adv. Mater.* **1997**, *9*, 58 - 61.

3. "Self Assembled PAMAM Dendrimer Films"; Evenson, S. A.; Badyal, J. P. S.; Accepted for publication in *Advanced Materials.*

4. "Surface Esterification of Ethylene Maleic Anhydride Copolymer"; Evenson, S. A.; Badyal, J. P. S.; Submitted for publication.

5. "Aminolysis of Ethylene Maleic Anhydride Copolymer Surfaces"; Evenson, S. A.; Badyal, J. P. S.; Submitted for publication.

6. "Surface Functionalization of Maleic Anhydride Plasma Polymer Films"; Evenson, S. A.; Badyal, J. P. S.; Submitted for publication.

7. "Chemical Attachment of PAMAM Dendrimers to Solid Surfaces"; Evenson, S. A.; Badyal, J. P. S.; Submitted for publication.

8. "Controlled Polymerization of 1,2-Ethanedithiol"; Evenson, S. A.; Badyal, J. P. S.; Submitted for publication.

ACKNOWLEDGEMENTS

ABSTRACT

The overall performance of a material can be dramatically improved by tailoring its surface at the molecular level. The aim of this project was to develop a universal technique for attaching dendrimers (well-defined, nanoscale, functional polymers) and Jeffamines® (high molecular weight polymer chains) to the surface of any shaped solid substrate. This desire for controlled functionalization is ultimately driven by the need to improve material compatability in various biomedical applications.

Atomic force microscopy (AFM) was used initially to study the packing and structure of Langmuir-Blodgett films on surfaces, and subsequently resulted in the first visualization of individual, spherically shaped, nanoscopic polyamidoamine dendrimers. The next goal was to develop a methodology for attaching such macromolecules to inert surfaces. Thin copolymer films were deposited onto solid substrates to produce materials with a fixed concentration of surface anhydride groups. Vapor-phase functionalization reactions were then carried out with trifluorinated amines to confirm the viability of this technique to bond molecules to surfaces.

Finally, pulsed plasma polymerization of maleic anhydride took this approach one stage further, by forming well-adhered polymer films containing a predetermined concentration of reactive anhydride groups. Subsequent functionalization reactions led to the secure attachment of dendrimers and Jeffamines® at any desired packing density. An alternative route to biocompatibilization used 1,2-ethanedithiol to yield thiolated surfaces containing very high polymeric sulfur : carbon ratios.

TABLE OF CONTENTS

CHAPTER 3 : SKELETONIZATION OF MIXED ARACHIDIC ACID / CADMIUM ARACHIDATE LB FILMS: A STUDY USING ATOMIC FORCE MICROSCOPY

CHAPTER 4 : SELF-ASSEMBLED PAMAM DENDRIMER FILMS

CHAPTER 5 : SURFACE ESTERIFICATION OF ETHYLENE MALEIC ANHYDRIDE COPOLYMER

CHAPTER 6 : AMINOLYSIS OF ETHYLENE MALEIC ANHYDRIDE COPOLYMER SURFACES

CHAPTER 7 : SURFACE FUNCTIONALIZATION OF MALEIC ANHYDRIDE PLASMA POLYMER FILMS

CHAPTER 8 : CHEMICAL ATTACHMENT OF PAMAM DENDRIMERS TO SOLID SURFACES

CHAPTER 9 : CONTROLLED POLYMERIZATION OF 1,2-ETHANEDITHIOL

CHAPTER 10 : CONCLUSIONS

CHAPTER 1

AN INTRODUCTION TO SURFACES, THEIR

FUNCTIONALIZATION, AND

CHARACTERIZATION

1.1   SCOPE OF THESIS

This first chapter introduces the field of surface modification, concentrating on how plasma polymerization and surface functionalization can be used to tailor solid surfaces. An introduction into the analytical techniques used to study such surfaces is included at the end. The following eight chapters (2-9) are grouped into three parts, Scheme 1. The first part (Chapters 2-4) is an initial study on how atomic force microscopy can be used to image the packing and structure of molecules (Langmuir-Blodgett films and dendrimers) at surfaces. The second part (Chapters 5-7) tests the viability of vapour phase functionalization reactions between maleic anhydride copolymer surfaces and a selected range of alcohols and amines. X-ray photoelectron spectroscopy and infrared spectroscopy are used to examine the reaction rates and overall conversion factors of the different molecules and to characterize the resultant surfaces. Finally, the third part (Chapters 7-9) is a coming together of the previous two parts, dealing with the controlled molecular tailoring of surfaces via the pulsed plasma polymerization of maleic anhydride and 1,2-ethanedithiol. Subsequent functionalization reactions ultimately produce solid surfaces to which trifluorinated amines, Jeffamines, and dendrimers have been attached at a predetermined concentration with a view to improved interfacial properties including biocompatability, adhesion, and wettability.

Scheme 1. Scope of Thesis.

Molecular Tailoring of Solid Surfaces

Part 1

Part 2

Part 3

Silicon Substrate

LB Film

Dendrimer ○

2+3

4

Ethylene Maleic Anhydride Copolymer Film

HO —— CF₃

or

H₂N —— CF₃

Chapters 5+6

CF₃ CF₃ CF₃

NH₂ NH₂ NH₂ NH₂

Jeffamine

Maleic Anhydride Plasma Polymer

H₂N —— CF₃

Jeffamine

NH₂

H₂N

Dendrimer ○

1,2-Ethanedithiol Plasma Polymer

SH SH SH

9

8

CF₃ CF₃ CF₃

NH₂ NH₂ NH₂

7
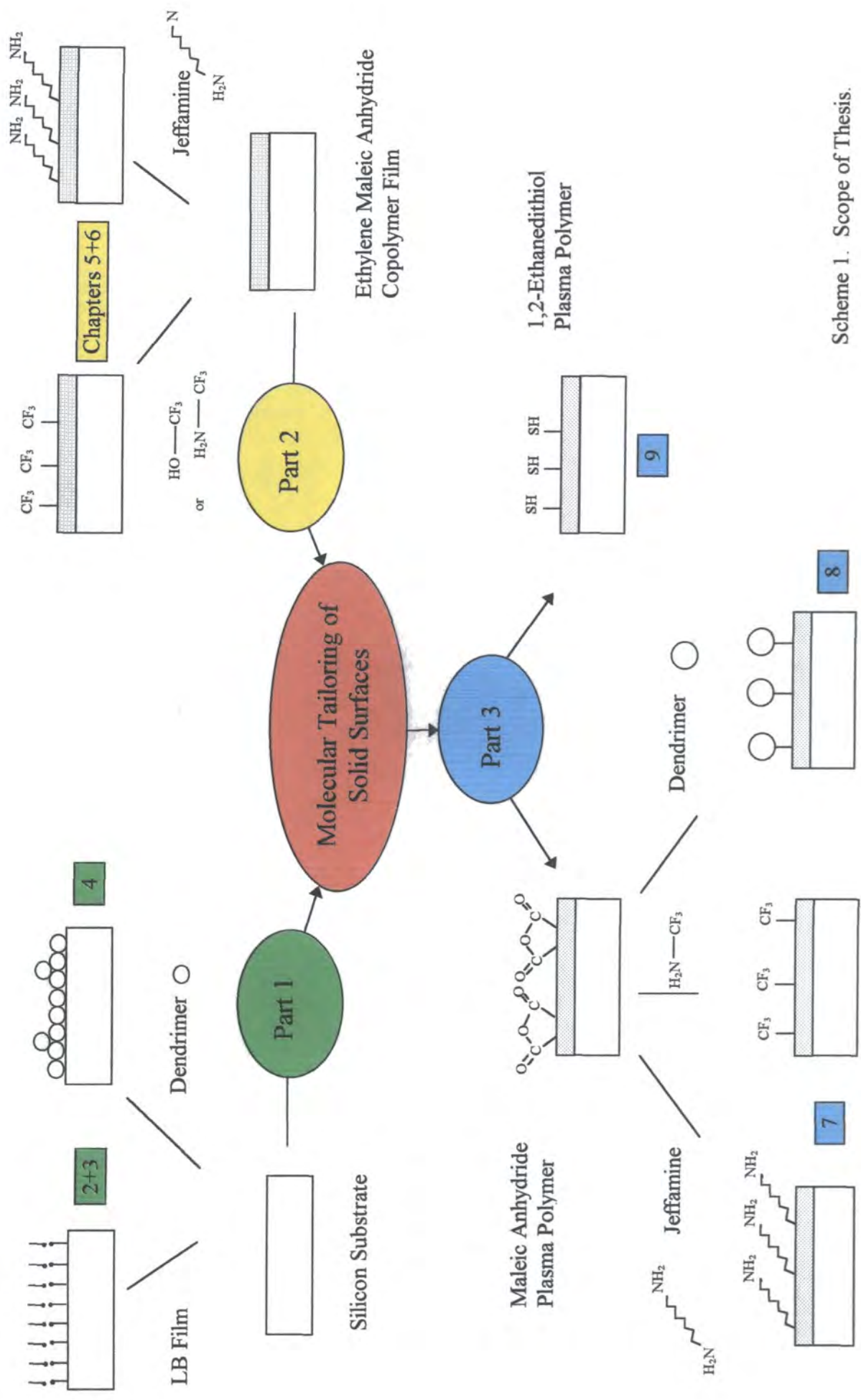
1.2   SURFACES

The interaction between a solid surface and the surrounding environment is critical to the overall performance of the device in its chosen application (biomedical, microelectronic, packaging, printing, etc.). It is very difficult to find a single material that possesses both the highly specialized surface properties and the bulk mechanical properties required for any given function. Therefore, the knowledge and creativity of the surface scientist is especially important in the design and development of new materials.

1.3   AIMS OF THESIS

The ultimate goal of this thesis is to produce solid surfaces to which selected macromolecules (dendrimers and high MW Jeffamines) are securely attached. This will involve developing a method whereby the surface of any shaped solid substrate can be tailored at the molecular level. The chemical inertness of many solids (especially the non-reactive character of polymers) stipulates the need for:

[A]   Introducing a predetermined concentration of reactive functional groups

 at their surface (achievable by physical methods), to which

[B]   Macromolecules can be chemically attached at a desired packing density.

The physical and chemical treatments currently available for modifying solid surfaces will be discussed in the next section.

1.4   SURFACE MODIFICATION TECHNIQUES

1.4.1   PHYSICAL SURFACE MODIFICATION

The activities aimed at physically modifying surfaces can be divided into two main categories: the first involves altering the surface layer, the second with depositing an extraneous layer on top of the existing material.[1] The former will be discussed in this section and the latter in the following section 1.4.2.

Flame and corona treatments are used to improve adhesion, wettability and paintability of polyolefin surfaces.[2] Laser and UV treatments are widely applied for selectively irradiating surfaces in the microelectronics industry. Permeability and diffusion coefficients of polymeric coatings have been altered by electron beam induced cross-linking. Surfaces can be coated by metal species (metallization) for electrical or packaging applications,[3] whereas sputtering and evaporation have been used for producing inorganic coatings to improve electro-optic performance.[4] Finally, the most successful application of low pressure plasmas is in the electronic industries.

Although these techniques all have their benefits and applications, none of them are able to fulfil all of the aforementioned criteria for the controlled molecular tailoring of solid surfaces. Furthermore, the high energy density involved with most of them results in bulk as well as surface modification. Flame treatments inherently involve high temperatures and plasma induced surface modifications are susceptible to ageing.[5] Uniformity has been difficult

to achieve for complex shaped substrates using corona treatments and electron and ion beams can cause damage to the underlying substrate.

Plasma polymerization offers an alternative technique whereby a well-adhered thin film containing surface functional groups (originally present in the parent monomer) can be deposited onto a solid substrate.[6] Utilising these groups in subsequent functionalization reactions enables one to control surfaces on the molecular level. Furthermore, treatment of complex shapes (e.g. car bumpers) has been routinely achieved.[1]

1.4.2 PLASMA POLYMERIZATION

Introduction

Plasma polymerization refers to the formation of polymeric materials under the influence of a plasma (partially ionized gas). The technique provides a relatively simple one-step approach to surface modifications without changing the bulk properties of the coated substrates. New kinds of materials can be prepared which are often highly branched, cross-linked, and amorphous in nature, and have a high thermal stability, high melting point and low solubility.[7] Plasma polymerization is characterized by several important features:[8] the resultant plasma polymers have no discernible repeat unit (unlike conventional polymers); their properties are determined both by the process parameters and the original monomer structure; and the monomers used do not have to contain a double bond for the polymerization to proceed.

Rapid step growth polymerization (RSGP) has been used to describe the complex nature of the plasma polymerization process.[9] The mechanism consists of three major steps all of which can occur heterogeneously or homogeneously.[8] Initiation involves free radical or ion formation of the monomer by the plasma. Addition of radical atoms to other radicals or molecules resulting in a growing radical chain is the propagation step of polymerization. Termination takes place by a process similar to propagation but ends in a closed polymer chain. Unlike conventional polymerization, neutral products formed in the termination step can undergo re-initiation and propagation reactions. Chain fragments are reconverted into radicals by collision with electrons in the gas phase or by impact of energetic particles on the surface of the polymer film.

Plasma Generation

Plasma polymerization experiments can be carried out in an electrodeless cylindrical glass reactor, Figure 1. A Radio Frequency (R.F.) signal is used to generate the plasma discharge.[10] The energy is supplied to the discharge via an inductive and capacitative (L-C) matching unit, which is used to couple the impedance of the partially ionized gas to the output impedance of the power supply.[8] The discharge can be achieved at low pressures (as low as 1 mTorr).

The Technique

Plasma polymerization studies encompass research involving a wide variety of monomers, techniques, and applications.[11] The ability of very stable molecules (saturated hydrocarbons and fluorocarbons) to undergo plasma polymerization
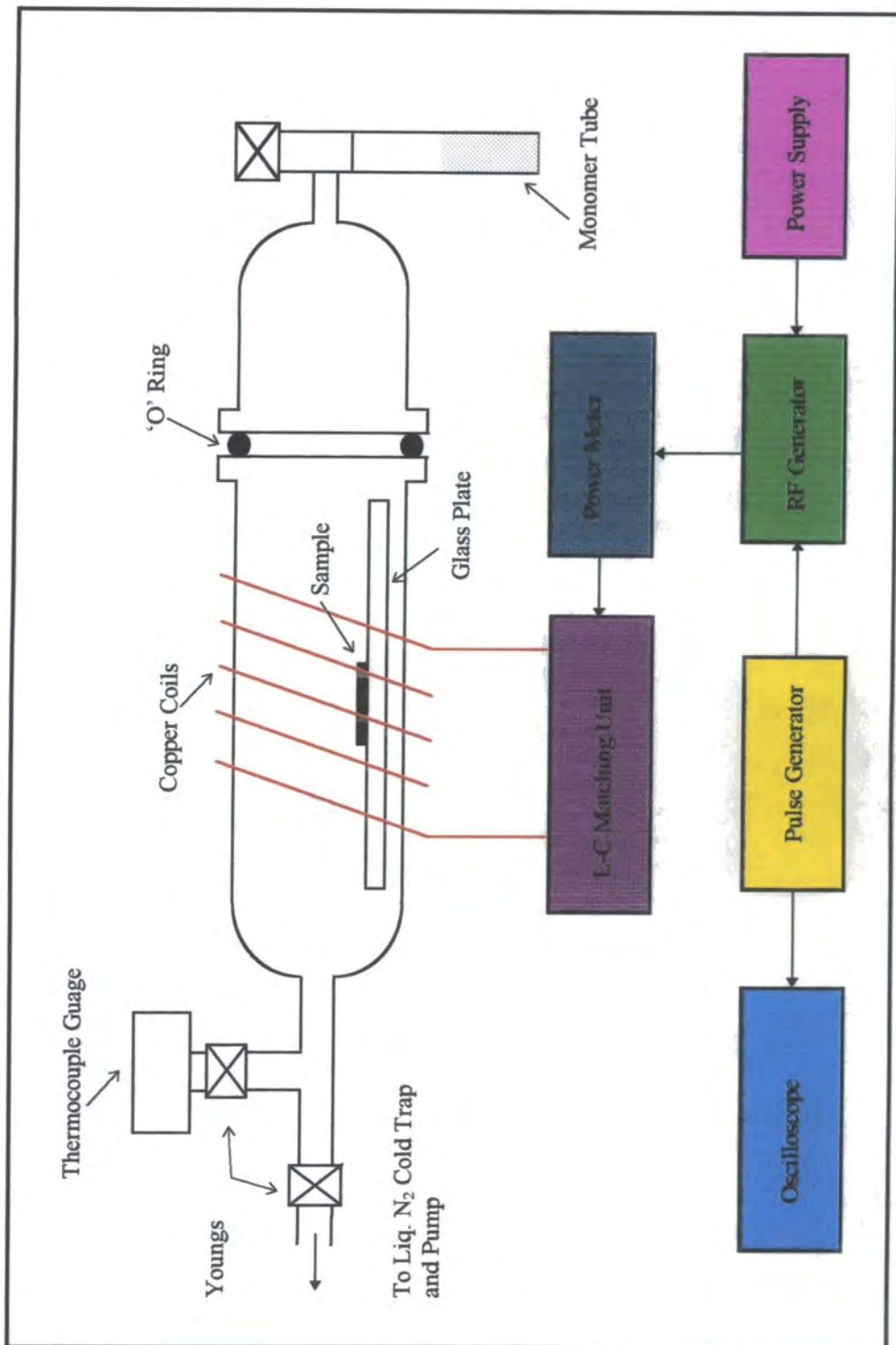
Figure 1. Schematic of Plasma Polymerization Apparatus.

reflects the fact that this deposition process typically involves very energetic conditions under which dissociation of even highly stable bonds occurs readily.[12] In many cases the structure of the deposited films bears little resemblance to the starting monomers, reflecting the relatively indiscriminate chemistry occurring in typical plasma depositions.

More recently, attempts have been made to achieve controllability over the molecular composition of films deposited under plasma conditions. For example, many studies have been devoted to the effect of absorbed R.F. power density[12] or the location of the substrate relative to the plasma discharge zone on film chemistry.[13] Control has also been achieved through variations of the substrate temperatures during deposition.[14,15]

Pulsed Plasma Polymerization

An alternative approach to compositional control of films deposited during R.F. plasma polymerizations involves employing a variable duty cycle pulsed R.F. plasma in lieu of the continuous wave (CW) discharges used in most other systems.[16-18] Spectroscopic characterization of the films reveal dramatic and progressive changes in the film chemistry obtained during systematic variations in pulsed R.F. duty cycles, while maintaining all other plasma variables constant. Additionally, interesting differences in film deposition rates and film composition are noted in contrasting pulsed versus CW plasma polymerizations. The greater retention and overall control of functionalities in the pulsed plasma polymer make these surfaces ideal for subsequent functionalization reactions.[19]

1.4.3 CHEMICAL SURFACE FUNCTIONALIZATION

Following the deposition of reactive functionalities onto solid substrates (via plasma polymerization) the final requirement is to choose suitable conditions for the subsequent reactions with a range of organic molecules. These chemical modifications can be achieved by either direct chemical reaction with a given solution (wet treatments) or by the covalent bonding of suitable macromolecular chains to the sample surface (functionalization/grafting).[1] Wet treatments are concerned with modifying existing surface chemistry, and the main drawback is that the reaction can often extend far into the substrate.

Surface functionalization involves the covalent bonding of new macromolecules on top of the substrate. Vapour-phase surface functionalization[20,21] has been shown to alleviate the problems associated with conventional solution-phase techniques (e.g. reorientation of surface functional groups and solvent extraction of low molecular weight species), ultimately producing a solid surface to which a controlled well-defined two dimensional array of organic molecules is securely attached.

1.5 ANALYTICAL TECHNIQUES

A selected range of analytical techniques have been used to characterize the solid surfaces before and after their molecular tailoring. The packing and structure of molecules at surfaces was imaged using Atomic force microscopy (AFM). X-ray photoelectron spectroscopy (XPS) provided information on the chemical composition of the functionalized surfaces, whilst infrared (IR) spectroscopy was used to examine both the bulk and surface properties of polymer thin films.

1.5.1 ATOMIC FORCE MICROSCOPY

Introduction

Atomic force microscopy (AFM) is an exciting technique available for a host of applications ranging from relatively simple visualization of morphology to more advanced examination of surface structure and properties on the nanometer scale.[22] The microscope can be operated in two modes (Contact or TappingMode) under atmospheric conditions and requires no special sample preparation.[23]

Contact Mode

In conventional contact mode AFM, a sharp tip mounted on the end of a cantilever is brought close enough to a sample such that it interacts with the atoms on the surface. Subsequently, the surface is rastered under the probe tip

using a piezoelectric scanner and the deflection of the tip is measured via a laser configuration, Figure 2. A feedback system is used to adjust the vertical position of the AFM tip above the sample surface to keep the deflection of the tip, and therefore the force, constant. Thus, the AFM is able to monitor the atomic force interactions between the tip and the surface and the resulting image is a topographical map of the sample.

While this technique has been very successful for many samples, particularly high resolution imaging on a molecular scale, it has some drawbacks. The dragging motion of the probe tip, combined with adhesive forces between the tip and the surface, can cause damage to the sample and the probe creating artefacts in the image.[24] Cantilevers with smaller spring constants can be used on softer samples which would otherwise be destroyed by imaging with high contact forces.[24]

TappingMode

TappingMode imaging overcomes the limitations of conventional scanning modes by alternately placing the tip in contact with the surface to provide high resolution and then lifting the tip away to avoid dragging it across the surface.[25] High resolution imaging is implemented by oscillating the cantilever assembly at or near the cantilever's resonance frequency using a piezoelectric crystal. The piezo motion causes the cantilever to oscillate with a high amplitude (> 20 nm) when the tip is not in contact with the surface. The oscillating tip is then moved towards the surface until it begins to lightly touch, or tap the surface. During scanning, the vertical oscillating tip alternately contacts the surface, and lifts off,
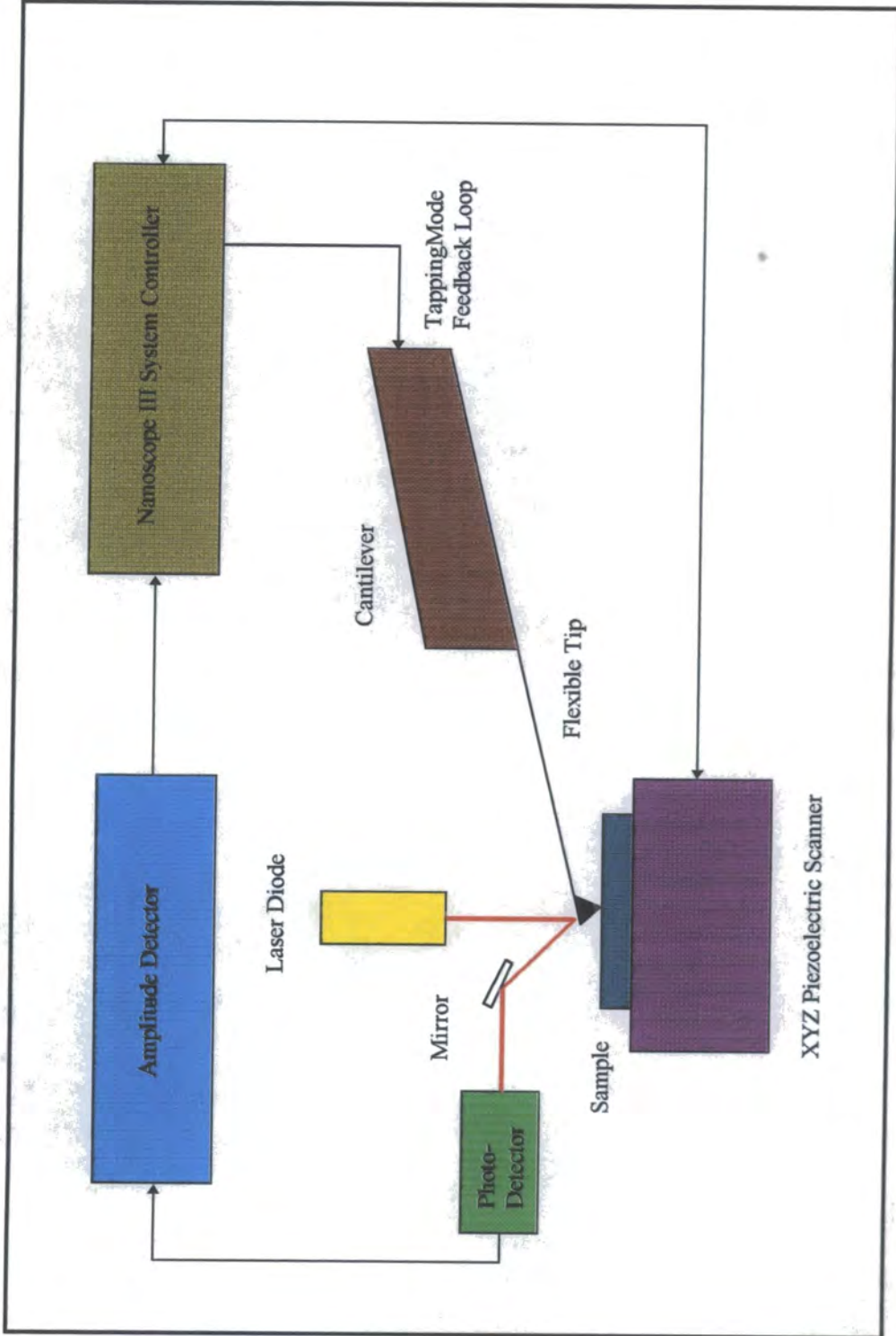
Figure 2. Schematic of an Atomic Force Microscope.

generally at a frequency of 50,00 to 500,000 cycles per second. As the cantilever interacts with the surface, the oscillation amplitude changes and it is this that is used to identify and measure surface features. The cantilever's oscillation amplitude is measured by a photo-detector and the digital feedback loop then adjusts the tip-sample separation to maintain a constant amplitude and force, Figure 2.[23]

TappingMode inherently prevents the tip from sticking to the surface and causing damage during scanning. Specifically, the technique is able to overcome problems associated with friction, adhesion, electrostatic forces, and other difficulties that plague conventional AFM scanning methods.[25] Overall, it has proven extremely successful for high resolution topographic imaging of sample surfaces that are easily damaged (polymers, biological samples),[26] loosely held to their substrate (thin films), or otherwise difficult to image by other AFM techniques.

Phase Imaging

Phase imaging is a powerful extension of TappingMode AFM that provides nanometer scale information about surface structure often not revealed by other AFM techniques.[27] In TappingMode AFM, the oscillation amplitude is used as a feedback signal to measure topographic variations of the sample. In phase imaging, the phase lag of the cantilever oscillation, relative to the signal sent to the cantilever's piezo driver, is simultaneously monitored. The phase signal changes when the probe encounters surface regions of different composition,

and the resultant phase shifts are registered as bright and dark regions in phase images. Resolution is comparable to that of TappingMode AFM.

Therefore, phase imaging goes beyond simple topographical imaging to detect variations in composition, adhesion, friction, viscoelasticity and other properties. Applications include identification of contaminants, defective films, mapping of different components in composite materials, and differentiating regions of high and low adhesion or hardness.[28] Furthermore, because phase imaging highlights edges and is not affected by large-scale height differences, it provides for clearer observations of fine features which can be obscured by rough topography.

1.5.2 X-RAY PHOTOELECTRON SPECTROSCOPY

Introduction

Surface analysis by X-ray photoelectron spectroscopy (XPS) involves irradiating a solid under vacuum with mono-energetic soft X-rays and analysing the energy spectrum of the emitted electrons.[29] As the inelastic mean free path of electrons in a solid is small, the detected electrons originate from only the top few atomic layers, making XPS an extremely surface sensitive technique. From photoemission spectra, quantitative data (surface concentrations) can be identified form peak areas and qualitative information (functional groups) can be obtained from exact measurements of peak positions and separations.[29]

Theory

Photoelectron spectroscopy is based on the photoelectric effect,[30] which describes the ejection of electrons from atoms or molecules upon exposure to electromagnetic radiation. Each atom present at the sample surface, except hydrogen, has valence electrons (involved in bonding) and core electrons (not directly involved in bonding).[31] The binding energy (E_b) of these core electrons to the nucleus is characteristic of the individual atom to which it is bound.

The XPS spectrum is obtained by irradiating the sample with an X-ray source, under UHV conditions. Photons collide with electrons in the sample surface giving them energy and photoionization occurs. Emitted electrons acquire a kinetic energy (E_k) which is equal to the difference between the energy of the incident photon ($h\nu$) and the sum of the binding energy and the work function (φ) of the solid, the Einstein relation:

$$E_k = h\nu - (E_k + \varphi)$$

Only the electrons which are generated near the surface (top 3 nm) have a finite probability of escaping from the material and therefore it is these that originate the XPS signal.[32]

The XPS instrumentation consists of a UHV chamber (10^{-9} Torr) containing the sample holder, an X-ray source (Mg K_α 1253.6 eV or Al K_α 1486.6 eV), a concentric hemispherical electron analyser, a channel electron multiplier, a pre-amplifier, and an output display, Figure 3.
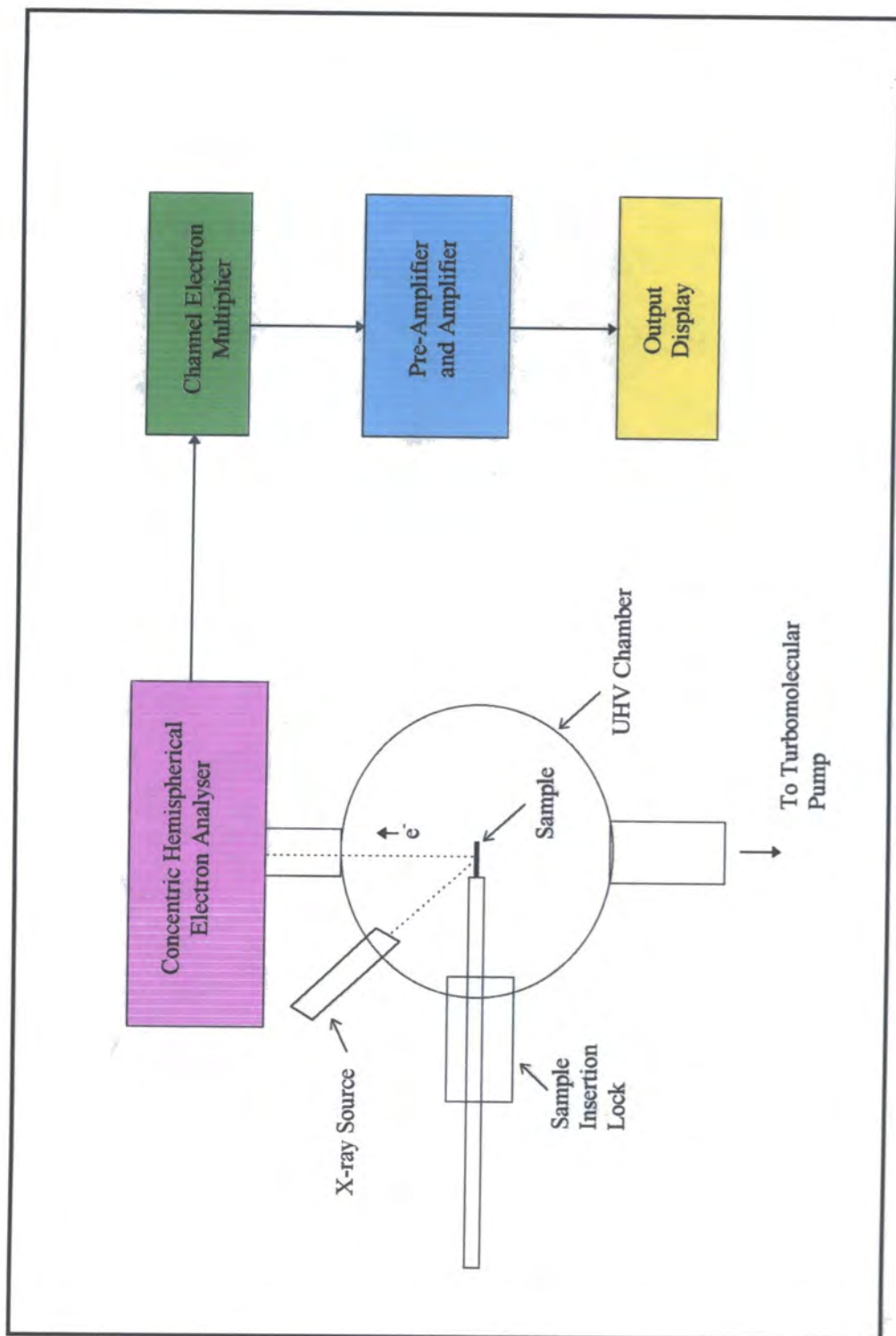
Figure 3. Schematic of an X-Ray Photoelectron Spectrometer.

Spectral Interpretation

The resultant spectrum is a plot of electrons counted per second versus electron binding energy. Core electrons, with high binding energies, originate the most important spectral features. Most information about polymer surfaces has been drawn from C(1s) peaks, since they are usually a sum of components relative to the different chemical states of the carbon atom at the surface.[1] Therefore, curve fitting of the C(1s) spectra allows semi-quantitative evaluation of the relative amounts of different functional groups at the surface. Peak width is a combination of X-ray line width and instrumentation conditions[29] and the magnitude of the shift is determined by the type of atom and strength of the bond. Large chemical shifts are observed for fluorocarbon polymers, owing to the electron attractive effect of fluorine.

Applications

Surfaces of polymers, copolymers, and polymer blends have been widely studied by XPS.[32] Modification of polymer surfaces, by chemical or physical methods (plasma, laser, flame, etc.) and grafting studies onto polymer surfaces have also been followed, often in conjunction with other techniques.[33] In such studies, observed chemical shifts are sometimes not sufficient to understand the chemistry at the surface and derivatization reactions have been proposed to introduce detectable ($-CF_3$) groups at the surface.[34]

1.5.3   INFRARED SPECTROSCOPY

Introduction

The previous two techniques (AFM and XPS) have enabled the structure and chemical composition of the modified solid surfaces to be examined. Transmission infrared (IR) spectroscopy can also prove very useful in elucidating the surface as well as the bulk chemistry of the plasma polymers before and after functionalisation.

Theory

Infrared (IR) radiation refers to the part of the electromagnetic spectrum between the visible and the microwave regions. The region between 400 and 4000 cm^{-1} is of most practical importance. Utilization of IR spectra in conjunction with other data is useful for determining molecular structure. Certain groups of atoms give rise to bands on or near the same frequency regardless of the rest of the molecule.[35] It is these characteristic bands that allow identification of useful structural information about the surface.

Infrared radiation in the range from 10,000 - 100 cm^{-1} is absorbed and converted by an organic molecule into energy of molecular vibration. This absorption is quantized, but the vibrational spectra appears as bands rather than lines because a single vibration energy is accompanied by a number of rotational energy changes. The frequency or wavelength of absorption depends on the relative masses of the atoms, the force constants of the bonds, and the geometry of the atoms. Band positions are presented here as wavenumbers whose unit is

the reciprocal centimetre (cm^{-1}); this unit is proportional to the energy of vibration. Band intensities can be expressed as transmittance or absorbance. Transmittance is the ratio of the radiant power submitted by a sample to the radiant power incident on the sample, and absorbance is the logarithm, to the base 10, of the reciprocal of the transmittance. There are two types of molecular vibrations, stretching and bending, and only those vibrations that result in a rhythmical change of the dipole moment of the molecule are observed in IR spectroscopy.[35,36]

Application to Plasma Polymers

Infrared spectra may be obtained for gases, liquids, or solids. Solids are usually examined as a mull, a pressed disc, or as a deposited film. The deposited film technique is particularly useful for obtaining spectra of polymers. The IR spectra of a solid may differ significantly from that of the free molecule due to intermolecular interactions restricting some bond movements, although spectra of plasma polymers often bear some relationship to the spectrum of the monomer. Peaks in the spectra tend to be broader and less well defined than in the monomer, indicating the large variety of chemical environments for each functional group within the plasma polymer.[37]

REFERENCES

[1]   Garbassi, F.; Morra, M.; Occhiello, E. *Polymer Surfaces From Physics to Technology*; Wiley: Chichester, **1994**.

[2]   Briggs, D.; Brewis, D. M.; Konieczko, M. B. *J. Mater. Sci.* **1979**, *14*, 1344.

[3]   Weiss, J.; Leppin, C.; Mader, W.; Salzberger, U. *Thin Solid Films* **1989**, *174*, 155.

[4]   Vossen, J. L.; Kern, W.; *Thin Film Processes*; Academic: New York, **1978**.

[5]   Occhiello, E.; Morra, M.; Garbassi, F. *Polymer* **1992**, *33*, 3007.

[6]   Yasuda, H. *Plasma Polymerization*; Academic: London, **1985**.

[7]   Yasuda, H. J. Poly. Sci.: *Macro. Rev.* **1981**, *16*, 199.

[8]   Grill, A.; *Cold Plasma in Materials Fabrication*; Iee Press: Piscataway NJ, **1993**.

[9]   Yasuda, H.; Iriyama, Y. *Comprehensive Polymer Science Vol. 4*; Pergammon: Oxford, **1989**, Chapter 21.

[10]   Hollahan, J. R.; Bell, A. T. *Techniques and Applications of Plasma Chemistry*; Wiley: New York, **1974**.

[11]   Panchalingham, V.; Chen, X.; Savage, C. R.; Timmons, R. B.; Eberhart, R. C. *J. Appl. Poly. Sci. : Appl. Poly. Symp.* **1994**, *54*, 123.

[12]   Yasuda, H. *Plasma Polymerization*; Academic: New York, **1986**.

[13]   O'Kane, D. F.; Rice, D. W.; *J. Macromol. Sci. Chem.* **1976**, *A10*, 567.

[14]   Lopez, G. P.; Ratner, B. D. *J. Appl. Poly. Sci. : Appl. Poly. Symp.* **1990**, *46*, 493.

[15]   Lopez, G. P.; Ratner, B. D. *Langmuir* **1991**, *7*, 766.

[16]   Savage, C. R.; Timmons, R. B. *Chem. Mater.* **1991**, *3*, 575.

[17]   Rinsch, C. L.; Chen, X.; Panchalingam, V.; Eberhart, R. C.; Wang, J.-H.; Timmons, R. B. *Langmuir* **1996**, *12*, 2995.

[18]   Chen, X.; Rajeshwar, K.; Timmons, R. B.; Chen, J.-J.; Chyan, O. M. R. *Chem. Mater.* **1996**, *8*, 1067.

[19]   Ryan, M. E.; Hynes, A. M.; Badyal, J. P. S. *Chem. Mater.* **1996**, *8*, 37.

[20]   Sutherland, I.; Sheng, E.-S.; Brewis, M.; Heath, R. J. *J. Mater. Chem.* **1994**, *4*, 683.

[21]   Popat, R. P.; Sutherland, I.; Sheng, E.-S. *J. Mater. Chem.* **1995**, *5*, 713.

[22]   Binning, G.; Quate, C. F.; Gerber, C. *Phys. Rev. Lett.* **1986**, *56*, 930.

[23]   *Nanoscope III MultiMode SPM Manual*; Digital Instruments: California, **1992**

[24]   Maganov, S. *Studies of Polymer Surfaces with Atomic Force Microscopy*; Digital Instruments: California, **1995**.

[25]   Prater, C. B.; Maivald, P. G.; Kjoller, K. J.; Heaton, M. G. *TappingMode Imaging: Applications and Technology*; Digital Instruments: California, **1997**.

[26]   Radmacher, M.; Fritz, M.; Hansma, H.; Hansma, P. K. *Science* **1994**, *265*, 1577.

[27]   Babcock, K. L.; Prater, C. B.; *Phase Imaging: Beyond Topography*; Digital Instruments: California, **1995**.

[28]   Ruddick, V. J.; Badyal, J. P. S. *J. Phys. Chem.* **1997**, *101*, 1791.

[29]   Chastain, J. *Handbook of X-ray Photoelectron Spectroscopy*; Plenum: New York, **1994**, Chapter 1.

[30]   Sherwood, P. M. A. In *Spectroscopy*; Straughan, B. P.; Walker, S. Eds.;

Chapman and Hall: London, **1976**, Chapter 7.

[31]   Christie, A. B. In *Methods of Surface Analysis*; Walls, J. M. Ed.; Cambridge

Uni. Press: Cambridge, **1989**, Chapter 5.

[32]   Beamson, G.; Briggs, D. *High Resolution XPS of Organic Polymers*; Wiley:

Chichester, **1992**.

[33]   Burrell, M. C.; Liu, Y. S.; Cole, H. S. *J. Vac. Sci. Technol. A* **1986**, *4*, 2459.

[34]   Batich, C. D. *Appl. Surf. Sci.* **1988**, *32*, 57.

[35]   Silverstein, R. M.; Bassler, G. C.; Morril, T. C. *Spectrometric Identification of*

Organic Compounds; Wiley: Singapore, **1991**.

[36]   Rao, C. N. R. *Chemical Applications of Infrared Spectroscopy*; Academic: New

York, **1963**.

[37]   Shard, A. *Plasma Assisted Thin Film Deposition*; PhD. Thesis: University of

Durham, **1992**.

CHAPTER 2

VARIATION IN INTERMOLECULAR SPACING WITH DIPPING PRESSURE FOR ARACHIDIC ACID LB FILMS

2.1 INTRODUCTION

The Langmuir-Blodgett (LB) technique is one of the few methods available that allows organic amphiphilic molecules to be organized at the molecular level.[1] This field has attracted many scientists from diverse backgrounds to work together for a common purpose - the fabrication and investigation of novel thin film architectures of electroactive materials. Such structures could find wide ranging uses in (or lead to design rules for) new electronic and electro-optic devices.

Condensed floating monolayers of long-chain fatty acids exhibit polymorphism. Several close-packed states are possible, depending on the precise details of temperature and surface pressure.[2] These phases, traditionally referred to as L_2, L_2', LS, S and CS, bear close similarities to the mesophases of smectic liquid crystals.[3] In the (high surface pressure) LS, S and CS phases, the tails of the fatty acids are oriented normal to the monolayer plane, whereas for the L_2 and L_2' states, they are tilted towards the nearest and next-nearest neighbours, respectively.

What happens as the floating film is transferred to a solid surface is less clear. There is certainly no reason to assume that the molecular order on the water surface is preserved on the solid substrate. For example, Leuthe and Riegler have shown that deposited LB films of behenic acid possessed a similar X-ray structure irrespective of the phase (L_2, L_2' or CS) from which deposition took place.[4] Fatty acid LB films tend to possess an orthorhombic subcell packing (i.e., packing of the C_2H_4 repeat units in the alkyl chain) and a monoclinic main

cell structure in which the alkyl chains are tilted away from the substrate normal (often in the direction of deposition).[5,6] A continuous variation in the tilt angle of the alkyl chain with deposition pressure has also been reported.[7]

Although a wide range of tools for the structural investigation of LB films are available,[1] most of the useful information about fatty acid films has been obtained with just a few techniques: X-ray and neutron reflection; electron diffraction; and infrared spectroscopy. Recently, atomic force microscopy (AFM) has been shown to be a further powerful method for studying LB films.[8-16] This allows the direct observation of the surface morphology of the organic structures on the molecular scale and in real space. While the early work concentrated on the stability and defect structure of fatty acid and other LB films, Schwartz et al.[13,14] recently demonstrated that AFM can be used to provide quantitative information on the ordering of the outermost layer of fatty acid salt multilayer films.

Here, we report a detailed AFM study on LB films of arachidic acid (eicosanoic acid). The variation in the LB lattice parameters with deposition pressure has been examined. All other variables including substrate, number of layers, pH and length of alkyl chain have been kept constant.

2.2   EXPERIMENTAL

LB films were prepared using a constant-perimeter barrier trough (home-made) located in a Class 10,000 microelectronics clean room. The subphase was ultrapure water obtained from a commercial reverse osmosis/deionization/UV sterilization system.

Figure 1 shows the surface pressure versus area isotherm for arachidic acid measured at a temperature of $19 \pm 1^{O}C$, pH 5.6 ± 0.1 and a compression rate of approximately 1×10^{-3} nm^{2} molecule s^{-1}. The condensed phases L_2, $L_2{}'$, LS and S are evident in the diagram; the phase transitions are marked with arrows.[2] A number of 12-layer films of arachidic acid were deposited onto hydrophobic silicon wafers over a range of deposition pressures (20, 25 ($L_2{}'$ phase), 30 (LS), and 50 (S) mN m^{-1}). The transfer ratios were 1.0 ± 0.05.

A Digital Instruments Nanoscope III atomic force microscope was used to examine the topographical nature of the arachidic acid film surface. All of the AFM images were acquired in air at room temperature using the contact mode and a 1 μm x 1 μm piezoelectric scan head. A 200 μm narrow legged silicon nitride cantilever with a low spring-constant (k = 0.06 N m^{-1}) was used in order to minimize any sample damage due to high contact forces. Several images were obtained, for each LB film, over a range of dimensions down to 5 nm x 5 nm. All of the images were stable with respect to time, and did not vary with repetitive scanning. The image shown in this article is presented as unfiltered data in gray-scale.
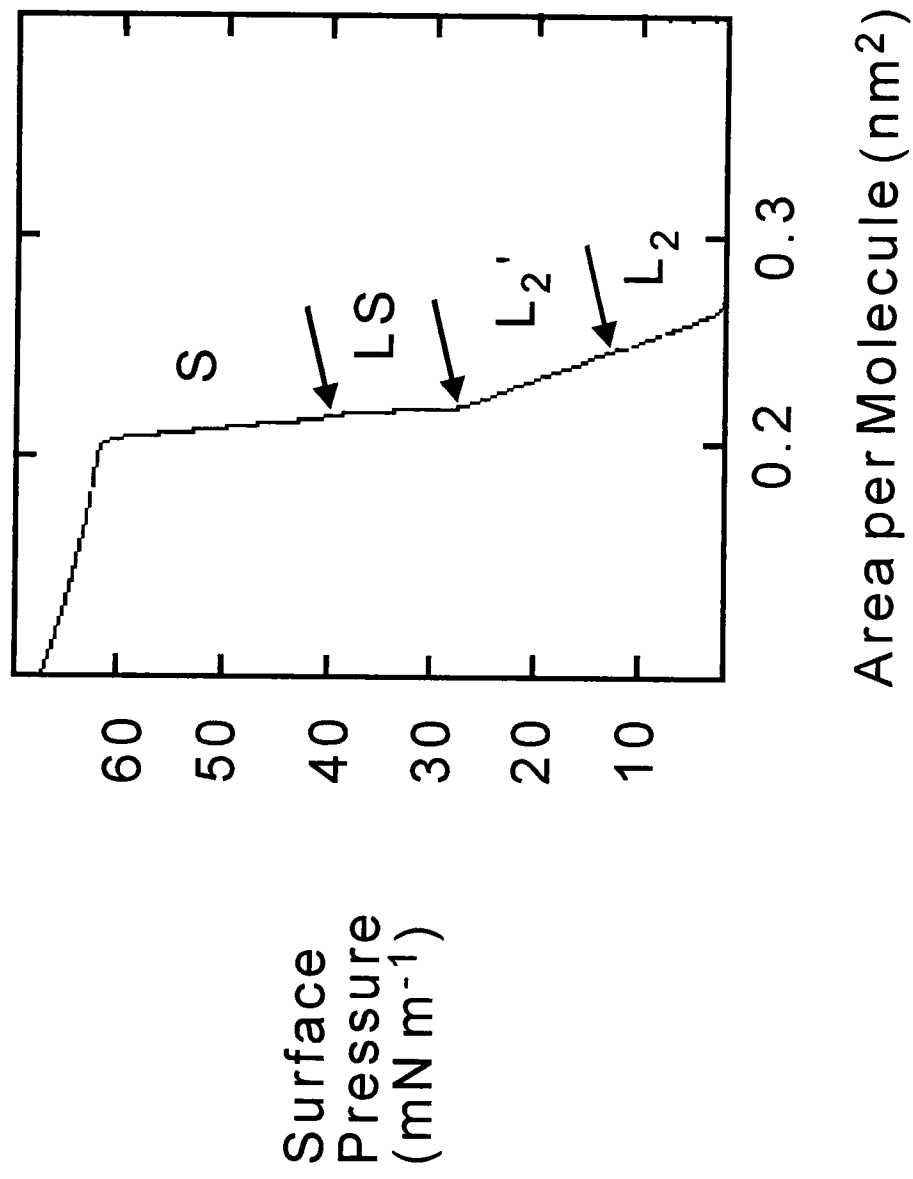
Figure 1. Surface pressure versus area isotherm for arachidic acid on a pure water subphase.

2.3   RESULTS

Molecular resolution AFM images for all four arachidic acid LB films were obtained. Figure 2(a) shows a typical 8.5 nm x 8.5 nm AFM image obtained for a sample deposited at 30 mN m^{-1} (LS phase). The lighter part of the image indicates the higher part of the surface and the darker regions correspond to deeper down. A two-dimensional periodic structure at molecular resolution is clearly discernible. Rows of chain ends appear at approximately 45° to the horizontal AFM scan direction. This is consistent with the relative orientation of the LB dipping direction with respect to the piezoelectric scan direction. In order to measure the periodicity contained within each AFM image, two-dimensional fast Fourier transform (FFT) analysis was undertaken. Figure 2(b) shows the FFT spectrum corresponding to the image shown in Figure 2(a). Inspection of the image reveals six bright spots. This is similar to that reported previously for LB films of cadmium arachidate.[13,14]   However, close examination of the pattern of spots suggests an oblique, rather than a rectangular, unit cell. It is therefore possible that the subcell of our arachidic acid multilayers is either monoclinic or triclinic, containing one molecule per unit cell.[17] An alternative explanation is that the molecular organization is based on a distortion of the orthorhombic subcell packaging, with a two-molecule unit cell. For the latter scheme, the unit cell dimensions a_0 and b_0, and the intermolecular spacings X and Y ($X \neq Y$) are labelled on the structural schematic of the surface, Figure 2 (c). Values of a_0 and b_0 can be calculated from experimental X and Y data using simple geometry.

24

0.5 nm

0.0 nm

8.0

6.0

4.0

2.0

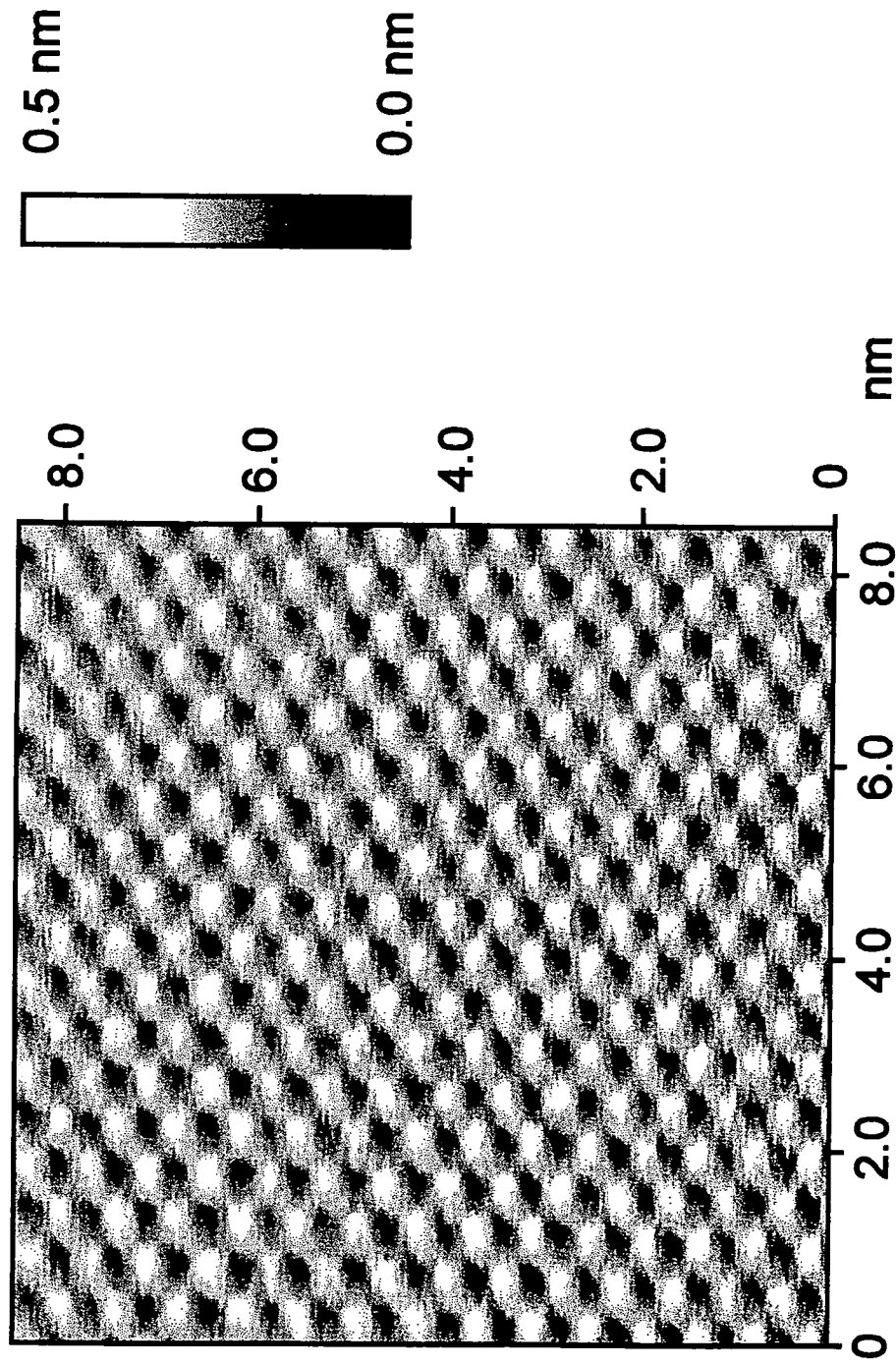0

nm

0   2.0   4.0   6.0   8.0

Figure 2(a). Molecular resolution AFM image of the surface of a 12 layer arachidic acid LB film.
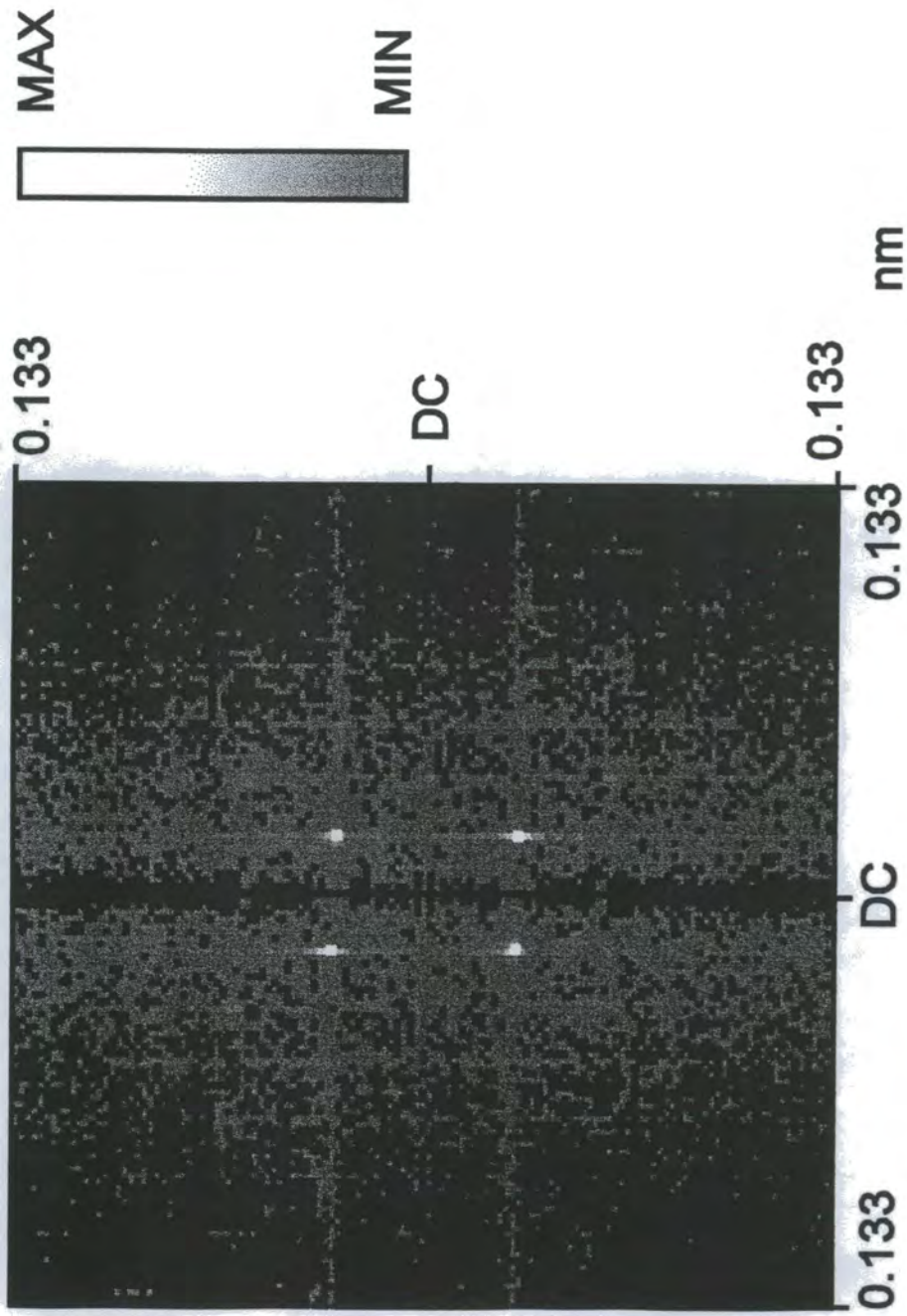
Figure 2(b).   Two dimensional FFT spectrum of the image shown in Figure 2(a).
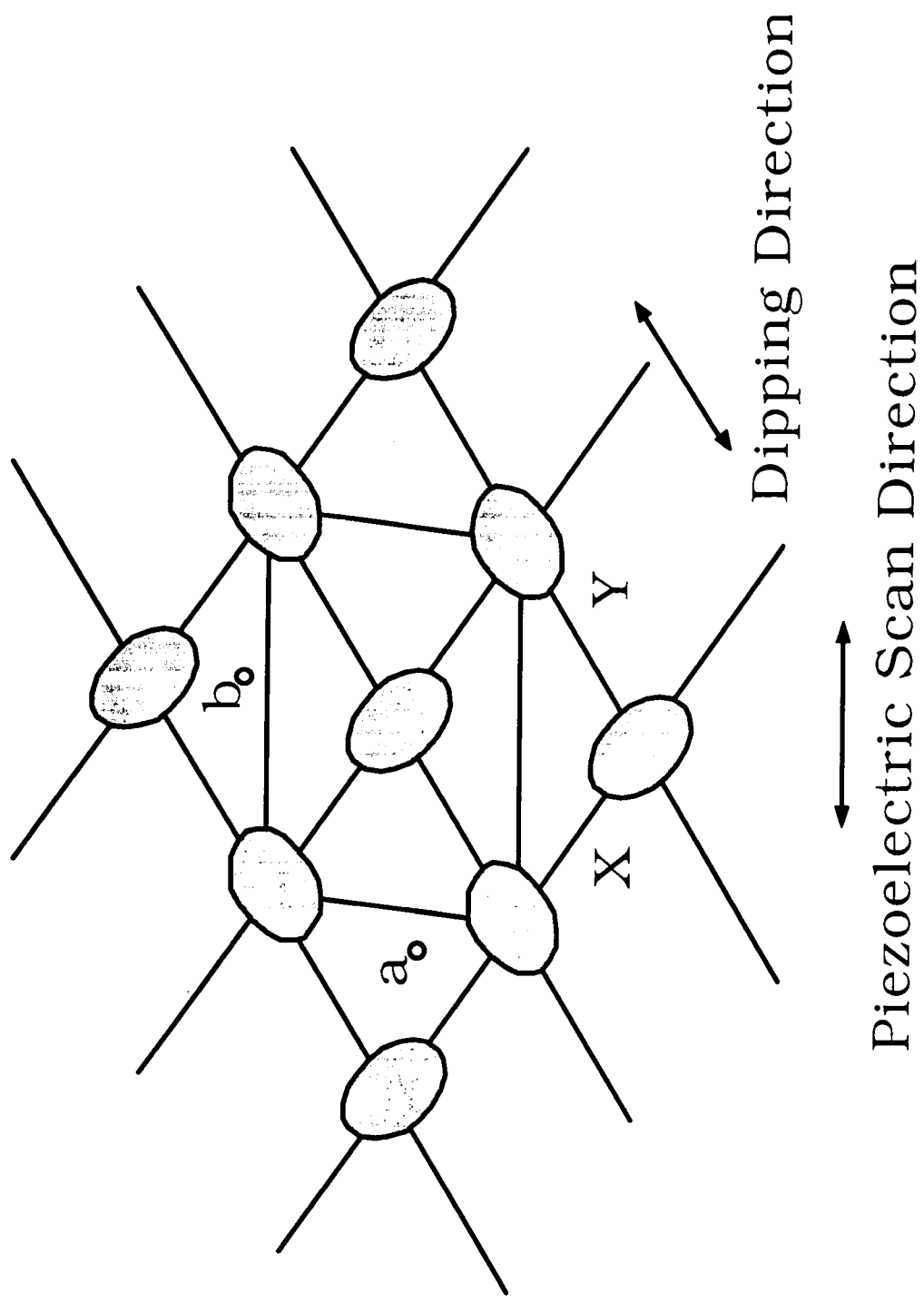
Figure 2(c). Schematic of the LB film surface showing the oblique two-molecule unit cell.

Comparable AFM images were obtained for the other arachidic acid LB films deposited at different surface pressures (20, 25, and 50 mN m^{-1}). Two-dimensional fast Fourier transform analysis of each corresponding AFM image produced similar diffraction patterns to that described above, although the unit cell dimensions differed, Table 1. This suggests that the type of unit cell (i.e., monoclinic, triclinic or orthorhombic) is the same for all the deposition pressures investigated. In all cases, the dimensions and standard deviations were calculated by averaging the FFT data obtained from a number of different images for each deposited LB film.

Table 1: Unit cell dimensions for arachidic acid LB films deposited at different surface pressures.

Surface Pressure (mN m^{-1})	a_o (nm)	b_o (nm)
20	0.52 ± 0.06	1.01 ± 0.04
25	0.55 ± 0.02	0.90 ± 0.02
30	0.58 ± 0.07	0.79 ± 0.03
50	0.46 ± 0.06	0.77 ± 0.02

2.4   DISCUSSION

A two-molecule unit cell similar to the one shown in Figure 2(c) has been used previously by Schwartz et al. to explain AFM images obtained for <u>fatty acid salt</u> LB layers.[13,14]   A comparable orthorhombic subcell has been reported for <u>fatty acid</u> LB films.[5,6]   In the present study, there is an increase in unit cell dimensions as the deposition pressure decreases, suggesting an increase in tilt of the alkyl chains with respect to the substrate normal, Table 1.   For the highest deposition pressure (50 mN m^{-1}), the lattice parameters are $a_0 = 0.52 \pm 0.06$ nm, $b_0 = 0.77 \pm 0.02$ nm.   These values are the same (within experimental error) as those obtained from AFM measurements on cadmium arachidate LB layers (0.482 $\pm$ 0.004 nm and 0.748 $\pm$ 0.006 nm).[13]   There is also good agreement with the orthorhombic (R) subcell dimensions for infinite aliphatic chains given by Kitaigorodski ($a_0 = 0.495$ nm; $b_0 = 0.740$ nm).[17]

The d-spacing (obtained from low-angle X-ray diffraction measurements) for Y-type LB films of long-chain fatty acid salts corresponds to twice the molecular length, inferring that the hydrocarbon chains are oriented with their long axes perpendicular to the substrate plane.[1]   We suggest that this is also the case for our arachidic acid films deposited at 50 mN m^{-1}.   As the deposition pressure is reduced, the alkyl chains tilt, hence increasing the dimensions of the unit cell.

Figure 3 shows how the intermolecular dimensions (X and Y) for the arachidic acid LB films vary with deposition pressure (Π).   An approximately linear relationship between X and Π is found where the intermolecular distance
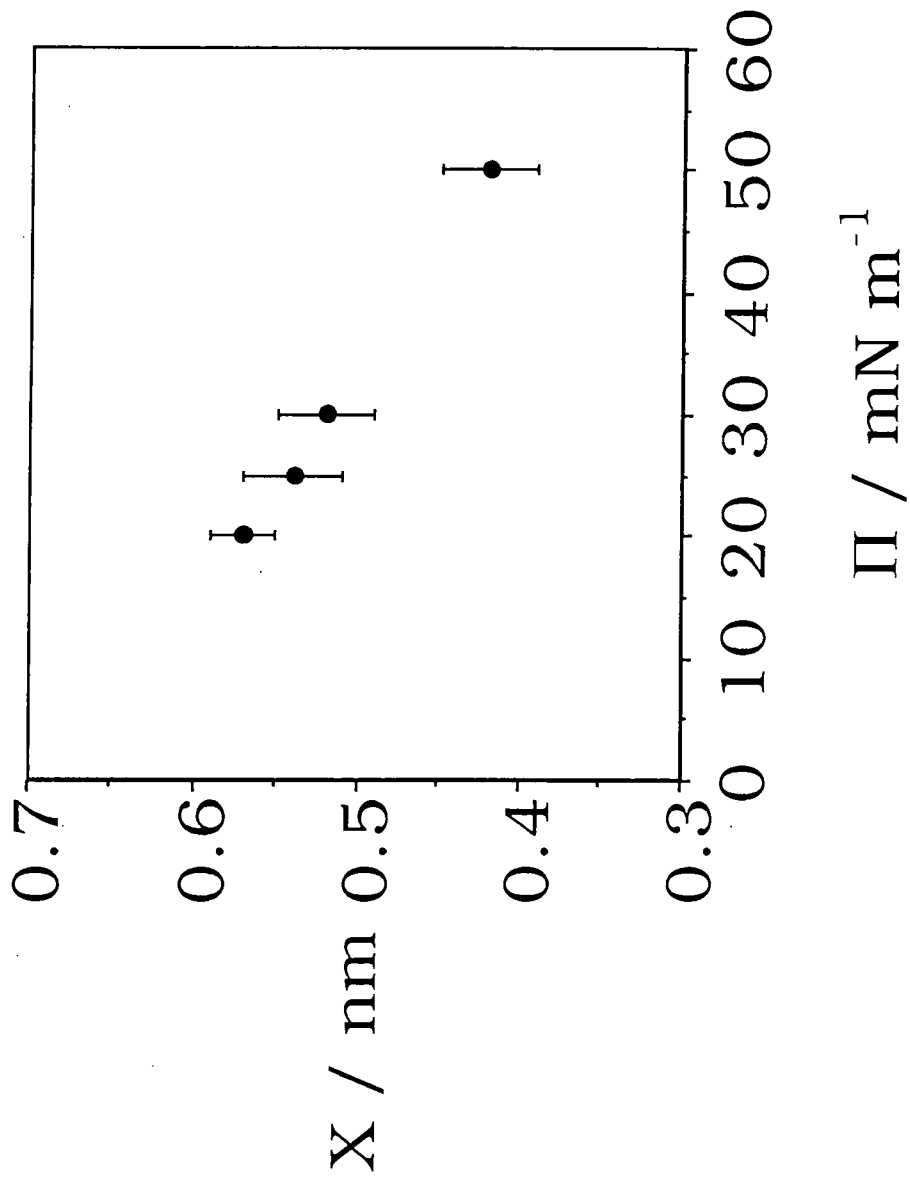
Figure 3(a). A graph of the intermolecular distance (X) versus surface deposition pressure.

decreases as the deposition pressure increases, Figure 3(a). In contrast, Figure 3(b) shows that the intermolecular Y dimension decreases with increasing pressure to a value of about 0.47 nm, remaining constant for further surface pressure increases. Again, these results do not indicate a change in the nature of the subcell. Although the phase of the floating film varies with deposition pressure (from $L_2^{\,|}$ to S), we suggest that the type of subcell in the deposited film is the same; it is only its dimensions that change.

For bulk fatty acids, the crystallographic structure is determined by the degree of tilt in the hydrocarbon chain. For example, the B and C crystal structures for bulk stearic acid possess an orthorhombic subcell and a monoclinic main cell which are derived from the basic orthorhombic structure.[20] In the B form the molecules are tilted along the a axis, increasing a_0 from 0.495 to 0.559 nm, whilst the C form has the molecules tilted over the b axis, increasing b_0 from 0.740 nm to 0.936 nm. For our LB films, the molecules are tilted along the dipping direction producing an increase in dimensions along both the a_0 and b_0 axes. This tilt also distorts the rectangular lattice, resulting in the oblique in-plane lattice observed in our studies.

The packing arrangements for layers of long-chain fatty acid molecules have been enumerated by Kitaigorodski.[17] A finite number of close-packed arrangements is possible depending on the type of subcell (orthorhombic, monoclinic, triclinic) and the relative displacements of neighbouring chains. This leads to just a few fixed orientations for the hydrocarbon chains relative to the substrate. However, there is an increasing amount of experimental evidence for a continuous change of tilt angle with, for example, deposition pressure. To

27
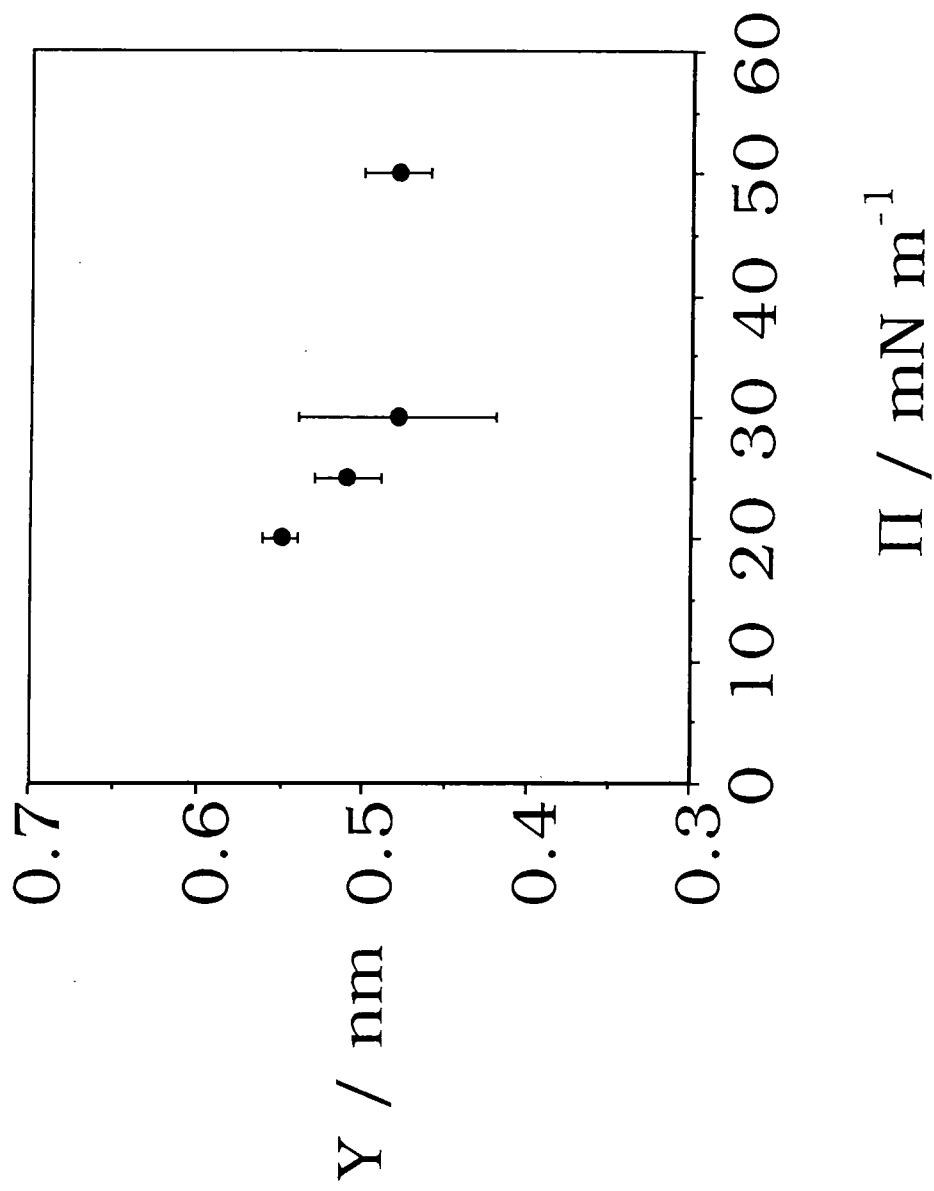
Figure 3(b). A graph of the intermolecular distance (Y) versus surface deposition pressure.

explain this, Robinson et al.[7] have proposed a model of small areas (nanometric order) of crystallinity in which grains are both inclined to the substrate with a distribution of tilt azimuths and permeated with holes. Theory predicts that a variation in tilt angles results in a 'buckling' superstructure in the LB molecular array due to a frustration in the packing of the molecules.[21] Schwartz et al.[13,14] have identified such a periodic superstructure for fatty acid salt films, although the experimental observations do not completely fit the theoretical model. Our present study certainly suggests that a range of tilt angles exists for fatty acid LB films. However, we have not directly observed the defects in the multilayer structure resulting from the models discussed above.

2.5   CONCLUSIONS

Atomic force microscopy has been used to provide molecular-resolution images of LB films of arachidic acid deposited onto hydrophobic silicon. Multilayer films have been built-up from the L_2^I, LS and S floating condensed phases.

In all cases, a similar molecular organization was observed in the transferred film. It is suggested that the AFM images correspond to a distorted orthorhombic subcell with two molecules per unit cell. For films built-up at high surface pressures (50 mN m^{-1} from the S phase), the unit cell dimensions (a_O = 0.52 ± 0.06 nm, b_O = 0.77 ± 0.02 nm) indicate that the long axes of the fatty acid molecules are aligned approximately parallel to the substrate normal. For lower deposition pressures, an increase in both the a_O and b_O unit cell dimensions was found. This suggested a progressive tilt in the long axes of the fatty acid molecules along the deposition direction with decreasing surface pressure.

REFERENCES

[1]   Petty, M. C. *Langmuir-Blodgett Films: An Introduction*, Cambridge University Press: Cambridge, **1996**.

[2]   Stenhagen, E. in *Determination of Organic Structures by Physical Methods*, Eds. Braude, E. A. and Nachod, F. C.; Academic Press: New York, **1995**, 325.

[3]   Kenn, R. M.; Böhm, C.; Bibo, A. M.; Peterson, I. R.; Möhwald, H.; Als-Nielsen, J.; Kjaer, K. *J. Phys. Chem.* **1991**, *95*, 2092.

[4]   Leuthe, A.; Riegler, H. *J. Phys. D: Appl. Phys.* **1992**, *25*, 1786.

[5]   Bonnerot, A.; Chollet, P. A.; Frisby, H.; Hoclet, M. *Chemical Physics*, **1985**, *97*, 365.

[6]   Kimura, F.; Umemura, J.; Takenaka, T. *Langmuir* **1986**, *2*, 96.

[7]   Robinson, I.; Sambles, J. R.; Peterson, I. R. *Thin Solid Films* **1989**, *172*, 149.

[8]   Meyer, E.; Howald, L.; Overney, R. M.; Heinzelmann, H.; Frommer, J.; Güntherodt, H.-J.; Wegner, T.; Schier, H.; Roth, S. *Nature* **1991**, *349*, 398.

[9]   Hansma, H. G.; Gould, S. A. C.; Hansma, P. K.; Gaub, H. E.; Longo, M. L.; Zasadzinski, J. A. N. *Langmuir* **1991**, *7*, 1051.

[10]   DeRose, D. A.; Leblanc, R. M. *Surface Science Reports* **1995**, *22*, 73.

[11]   Chi, L. F.; Anders, M.; Fuchs, H.; Johnston, R. R.; Ringsdorf, H. *Science* **1993**, *259*, 213.

[12]   Schwartz, D. K.; Viswanathan, R.; Zasadzinski, J. A. N. *J. Phys. Chem.*, **1992**, *96*, 10444.

[13] Schwartz, D. K.; Garnaes, J.; Viswanathan, R.; Chiruvolu, S.; Zasadzinski, J. A. N. *Physical Review E*, **1993**,*47*, 1, 452.

[14] Schwartz, D. K.; Viswanathan, R.; Garnaes, J.; Zasadzinski, J. A. N. *J. Am. Chem. Soc.* **1993**, *115*, 7374.

[15] Schwartz, D. K.; Garnaes, J.; Viswanathan, R.; Zasadzinski, J. A. N. *Science* **1992**, *257*, 508.

[16] Viswanathan, R.; Schwartz, D. K.; Garnaes, J.; Zasadzinski, J. A. N. *Langmuir* **1992**, *8*, 1603.

[17] Kitaigorodski, A. I. *Organic Chemical Crystallography*; Consultants Bureau: New York, **1961**.

[18] Peng, J. B.; Barnes, G. T. *Thin Solid Films* **1994**, *252*, 44.

[19] Blodgett, K. B.; Langmuir, I. *Physical Review* **1937**, *51*, 964.

[20] Malta, V.; Celotti, G.; Zannetti, R.; Martelli, A. F. *J. Chem. Soc. (B)* **1971**, *13*, 548.

[21] Carlson, J. M.; Sethna, J. P. *Phys. Rev. A.* **1987**, *36*, 3359.

CHAPTER 3

SKELETONIZATION OF MIXED ARACHIDIC ACID / CADMIUM ARACHIDATE LB FILMS: A STUDY USING ATOMIC FORCE MICROSCOPY

3.1 INTRODUCTION

Atomic force microscopy (AFM) is proving to be a valuable characterization tool for studying the surfaces of monolayer and multilayer Langmuir-Blodgett (LB) films.[1-8] The method allows direct observation of the surface morphology of the organic layers on the molecular scale and in real space. Schwartz et al.[5-8] have also shown that AFM can be used to provide quantitative information on the crystallographic structure of the outermost layer of fatty acid salt multilayer films. We have recently demonstrated that similar data can be obtained for fatty acid LB films.[9] In particular, the technique allowed us to investigate the variation in the dimensions of the unit subcell with deposition pressure.

Multilayer films of fatty acid salts containing divalent cations are generally easier to build up using the LB technique than films of the pure acid. The cations co-ordinate two carboxylic acid groups and this stabilizes the floating monolayer. The transferred LB films consist of a mixture of the salt and the free acid, the precise salt : acid ratio depending on the pH of the subphase during film growth. After deposition, the free acid can be removed by soaking the LB film in a suitable solvent. This process is called *skeletonization* and leads to a decrease in the refractive index of the film.[10] In this work we report on the use of AFM to provide an insight into the microscopic structure of skeletonized films of cadmium arachidate.

3.2 EXPERIMENTAL

Langmuir-Blodgett films of arachidic acid/cadmium arachidate were prepared using a constant-perimeter barrier trough (purpose-built) located in a Class 10,000 microelectronics clean room. The subphase was ultrapure water obtained from a commercial reverse osmosis/deionization/UV sterilization system. The arachidic acid (eicosanoic acid) was obtained from Sigma (99% purity). For salt formation, $CdCl_2$ (BDH, Analar Grade) was added to the subphase to give an overall concentration of 2.5 x 10^{-4}M. The pH was adjusted to 5.7 $\pm$ 0.1 by the addition of HC1 (BDH, Aristar Grade) or ammonia solution (BDH, Aristar Grade). Transfer of the floating monolayers onto hydrophilic silicon wafers ((100) orientation) was undertaken at a subphase temperature of 19 $\pm$ 1°C and a deposition pressure of 30 mN m^{-1}. The dipping speed was 2 mm min^{-1}. Transfer ratios for all the monolayers deposited were 1.00 $\pm$ 0.05.

A Digital Instruments Nanoscope III atomic force microscope was used to examine the topographical nature of the arachidic acid/ cadmium arachidate LB film surface following dipping and after washing in ethanol (to remove the free acid). All of the high resolution AFM images were acquired in air at room temperature using the Contact Mode and a 1 μm x 1 μm piezoelectric scan head. A 200 μm narrow legged silicon nitride cantilever with a small spring-constant (k = 0.06 N m^{-1}) was used to minimize film damage due to high contact forces. The lower resolution images were acquired in air using the Tapping Mode in conjunction with a 10 μm x 10 μm piezolectric scan head. This technique employs a stiff silicon cantilever oscillating at a large amplitude near its

resonance frequency (several hundred kilohertz) which is detected by an optical beam system. AFM images are presented as unfiltered data in gray-scale and were found to be stable and unchanged over long periods of observation.

3.3   RESULTS AND DISCUSSION

3.3.1   As-Deposited Films

A molecular resolution AFM image of an 11-layer mixed film of arachidic acid and cadmium arachidate prepared on a hydrophilic silicon wafer is shown in Figure 1(a). The lighter shading represents the raised part of the surface and the darker regions of the image correspond to deeper down. The AFM micrograph shows two-dimensional periodic structure at the molecular level. Rows of chain ends are aligned at approximately 45° to the horizontal AFM scan direction. This is consistent with the relative orientation of the LB dipping direction with respect to the piezoelectric scan direction. In order to assess the overall periodicity contained within each AFM image, two-dimensional fast Fourier transform (FFT) analysis was carried out. This technique is of considerable computational importance in the digital processing of two-dimensional waveforms, such as images, and enables the identification of specific frequencies in the AFM images. Figure 1(b) shows the two-dimensional FFT spectrum of the image shown in Figure 1(a). Inspection of the Fourier transform pattern reveals six bright spots. This is similar to that reported by other workers for LB layers of cadmium arachidate, which was interpreted as arising from a rectangular
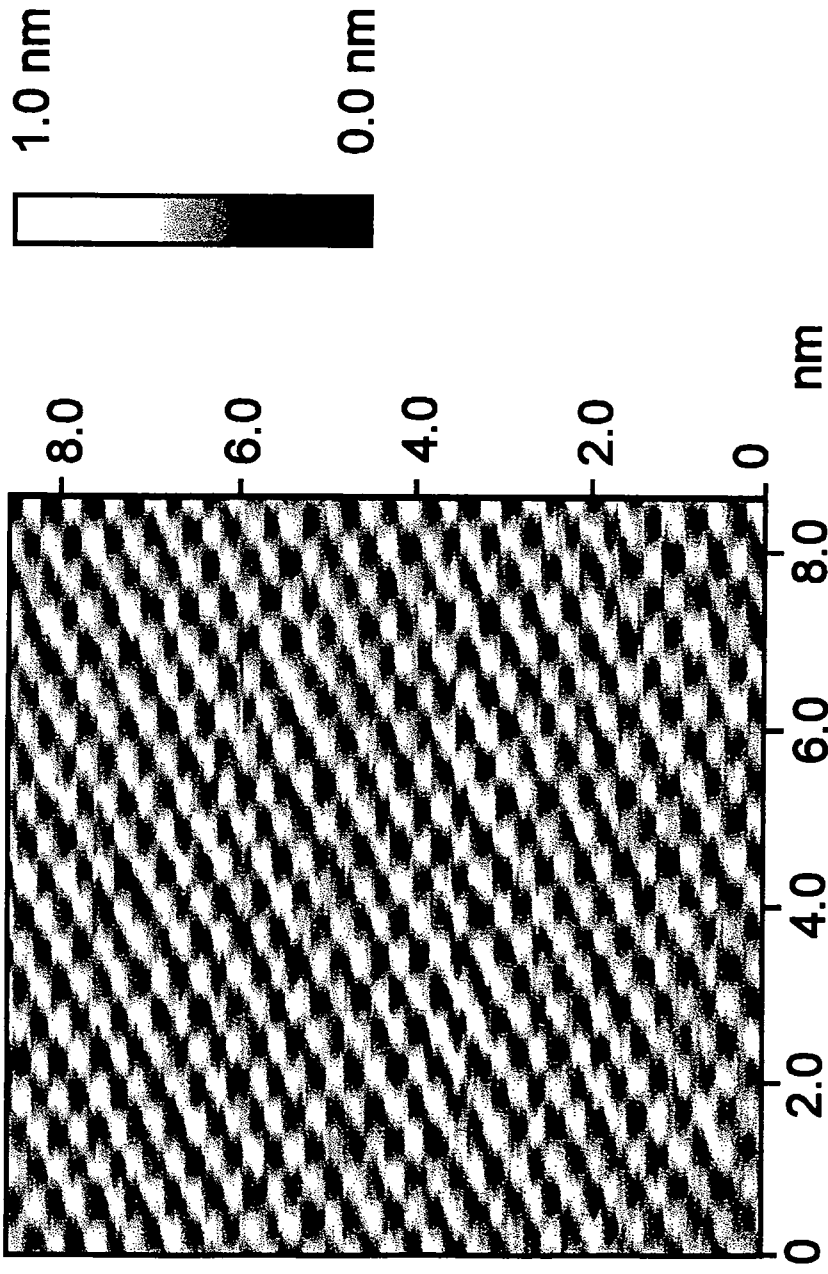
1.0 nm

0.0 nm

Figure 1(a). Molecular resolution AFM image of an 11-layer mixed LB film of arachidic acid / cadmium arachidate deposited onto a hydrophilic silicon substrtrate.
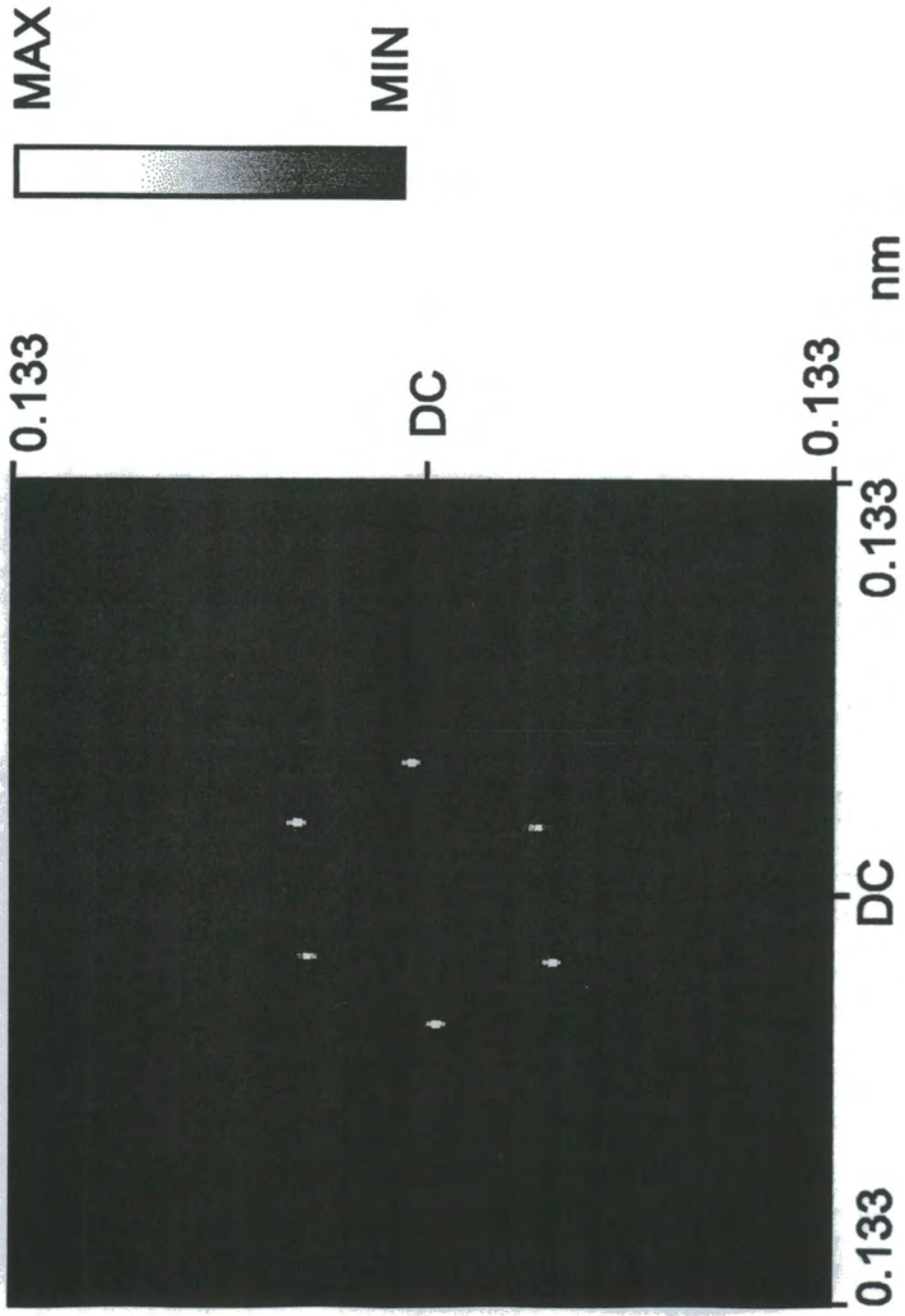
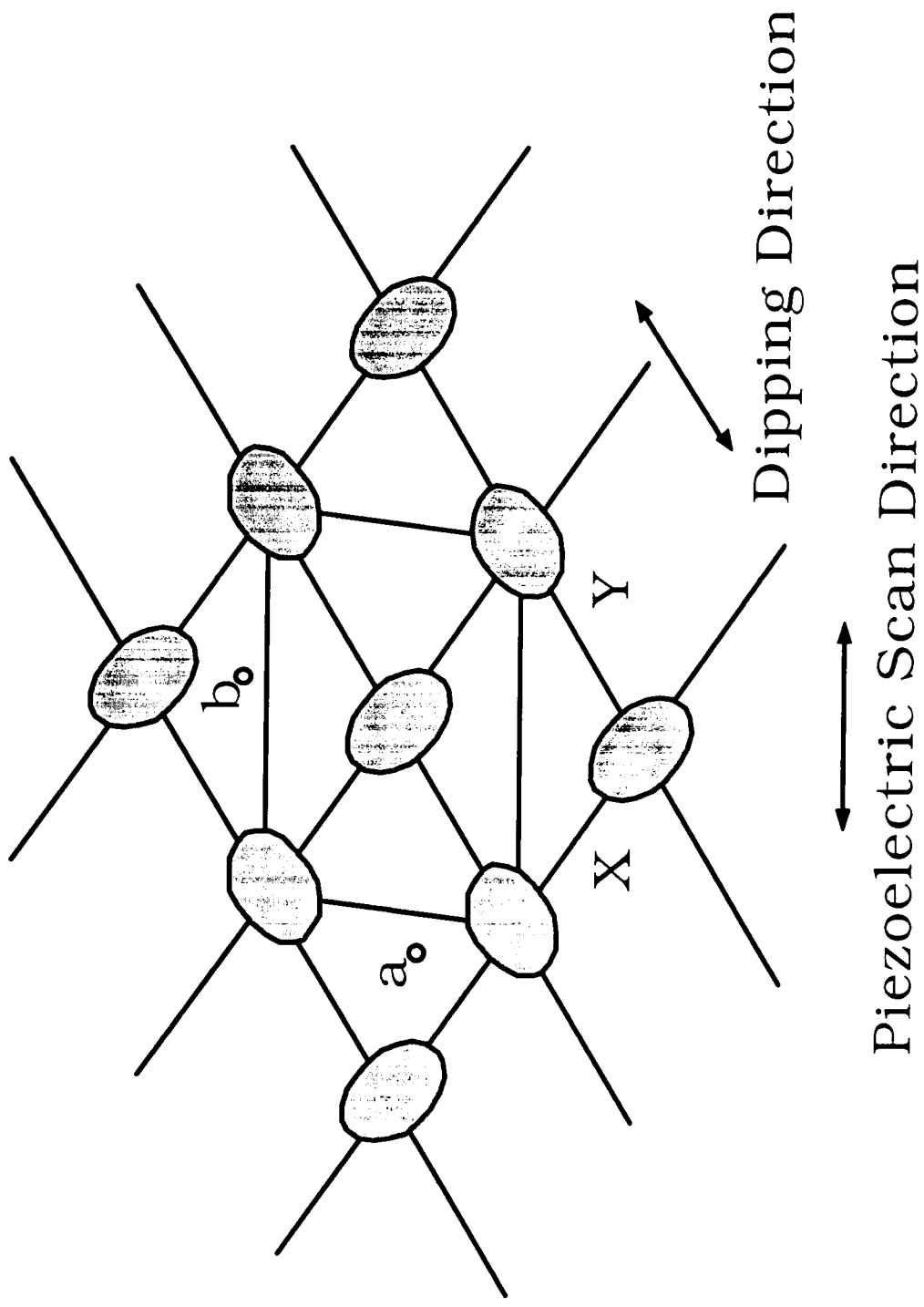Figure 1(b). Two dimensional FFT spectrum of the image shown in Figure 1(a).

Figure 1(c). Schematic of the LB film surface showing the oblique two-molecule unit cell.

lattice.[6,7] However, close examination of Figure 1(b) suggests a slightly oblique unit cell. We have recently noted a similar FFT pattern for arachidic acid LB films and have proposed that the molecular organization is based on a distortion (resulting from the deposition conditions) of the two-molecule orthorhombic subcell.[9] This structure is shown in Figure 1(c); the unit cell dimensions a_o, b_o and the intermolecular spacings X, Y (X ≠ Y) are labelled. Values of a_o and b_o can be calculated from experimental X and Y data using simple geometry.

The unit cell parameters obtained for our mixed film, a_0 = 0.48 $\pm$ 0.02 nm and b_0 = 0.74 $\pm$ 0.03 nm, are the same (within experimental error) as those obtained from AFM measurements on cadmium arachidate LB layers (0.482 $\pm$ 0.004 nm and 0.748 $\pm$ 0.006 nm).[6] There is also good agreement with the orthorhombic (R) subcell dimensions for infinite aliphatic chains given by Kitaigorodski (a_0 = 0.495 nm; b_0 = 0.740 nm).[11]

On inspection of the large scan area (2 μm x 2 μm) of the nominally 11-layer film, the image appears to be flat and homogeneous except for some small pinholes, rough patches, and a number of large regions of different contrast indicating discrete levels of height, Figure 2(a). Cross-section analysis shows that the domains are raised by discrete steps of 6.0 $\pm$ 0.6 nm, Figure 2(b). This is equivalent to the thickness of a bilayer of cadmium arachidate molecules,[10] confirming that the molecular chains are fully extended and approximately normal to the silicon substrate. It is apparent from Figure 2(b) that some regions of the nominally 11-layer LB film have rearranged to produce small areas of 9- and 13-layers (this gives rise to the different contrast regions seen in Figure 2(b)).
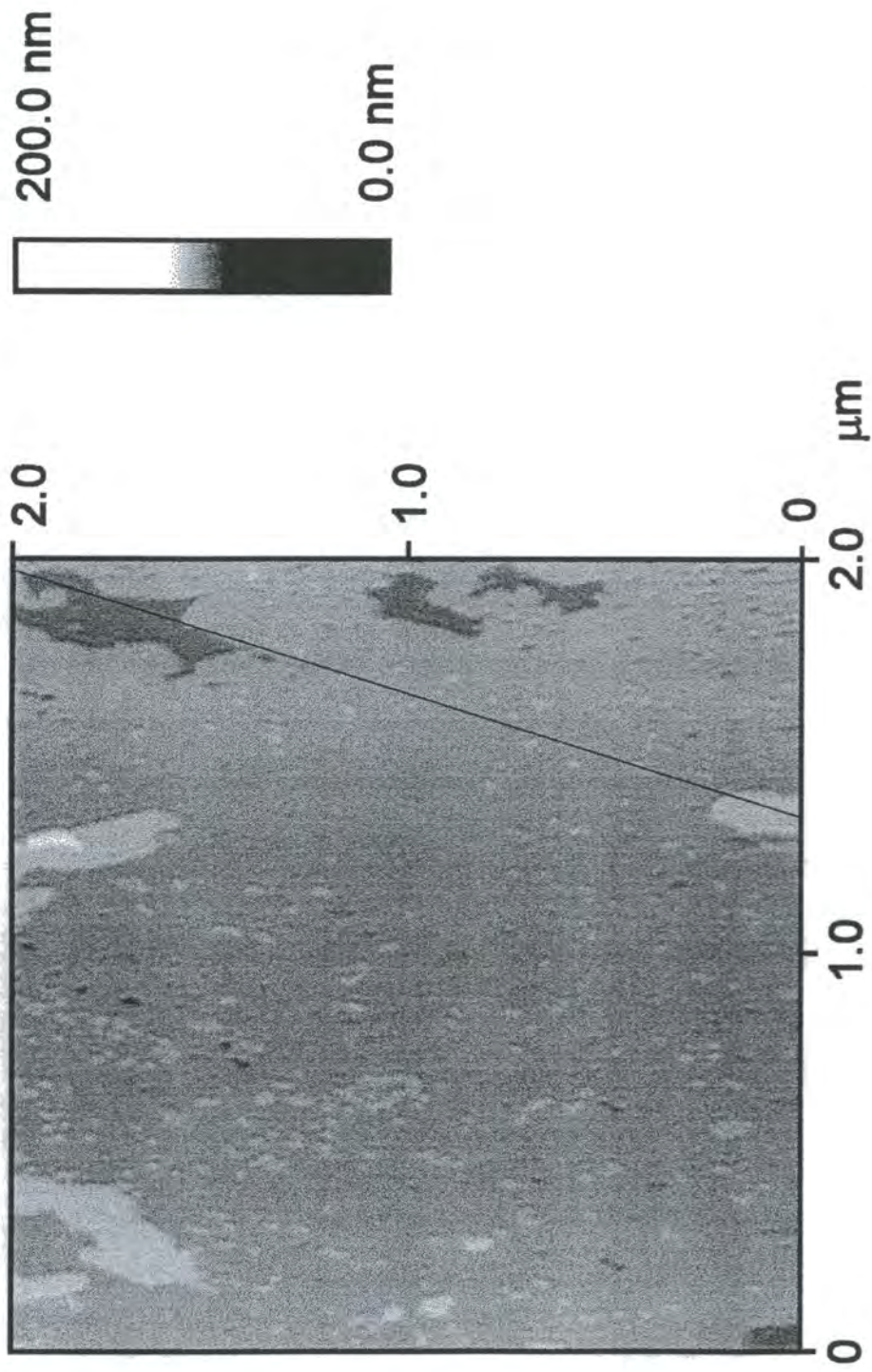
200.0 nm

0.0 nm

2.0

1.0

0

μm

2.0

1.0

0

Figure 2(a). Low resolution AFM image of an 11-layer mixed LB film of arachidic acid and cadmiun arachidate deposited onto a hydrophilic silicon substrate.
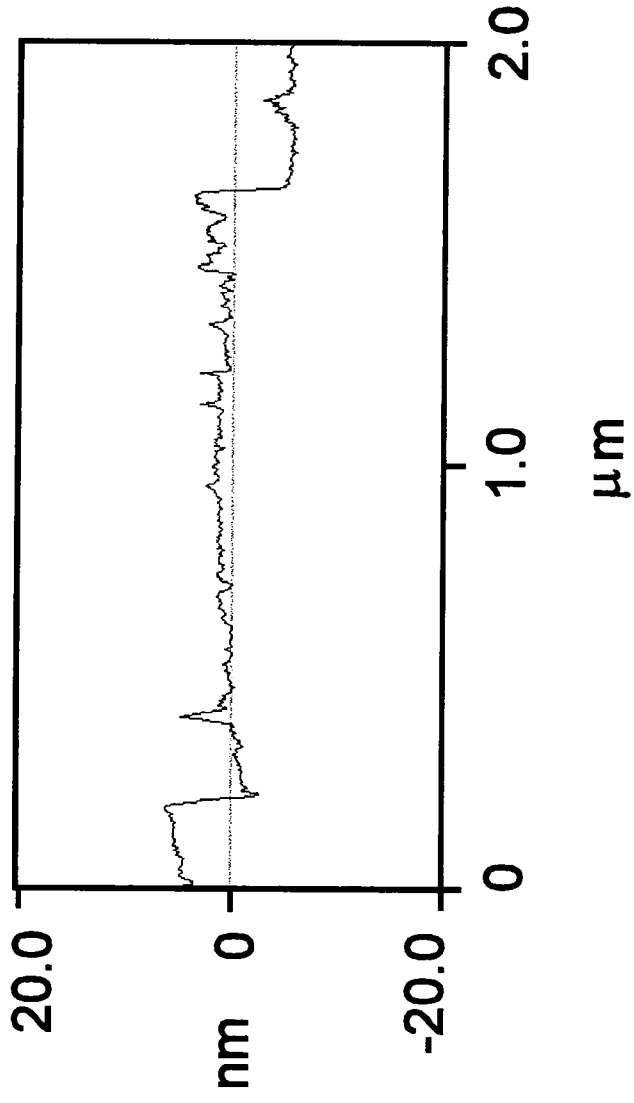
Figure 2(b). Cross-section analysis along the line drawn Figure 2(a).

Previous work on cadmium arachidate LB films, deposited at a pH of 6.5, has shown that this reorganization, leading to terraces of bilayer steps, is dependent on the time that the film is allowed to 'age' in the aqueous subphase.[5] The effect is driven by the very strong headgroup-to-headgroup interactions (in contrast to the interactions between the headgroups and the water or the headgroups and the substrate). For example, when the substrate is left submerged between the transfer of the 10th and 11th layers, some of the deposited film rearranges to form regions of 8- and 12-layers. On withdrawal through the air/water interface (thereby depositing an additional layer) the final film is mostly 11-layers thick, but with regions of 9- and 13-layers. The similar sizes of these latter regions indicates, as noted previously,[5] that the arachidic acid/cadmium arachidate is not being lost, but merely reorganising on the surface.

3.3.2 Skeletonized Films

The LB film shown in Figure 2(a) was rinsed in ethanol for five minutes, to remove the arachidic acid, and then dried[12]. The AFM micrograph of the washed film is shown in Figure 3(a). Examination of the AFM image shows that four distinct thickness regimes are discernible. The higher (brighter) areas superimposed onto the lower (darker) ones gives the impression of islands. These are aggregates of salt molecules, with air filling the spaces previously occupied by the acid molecules. Both the salt islands and the individual bilayers are discernible in the cross-section analysis of the AFM image, Figure 3(b). The
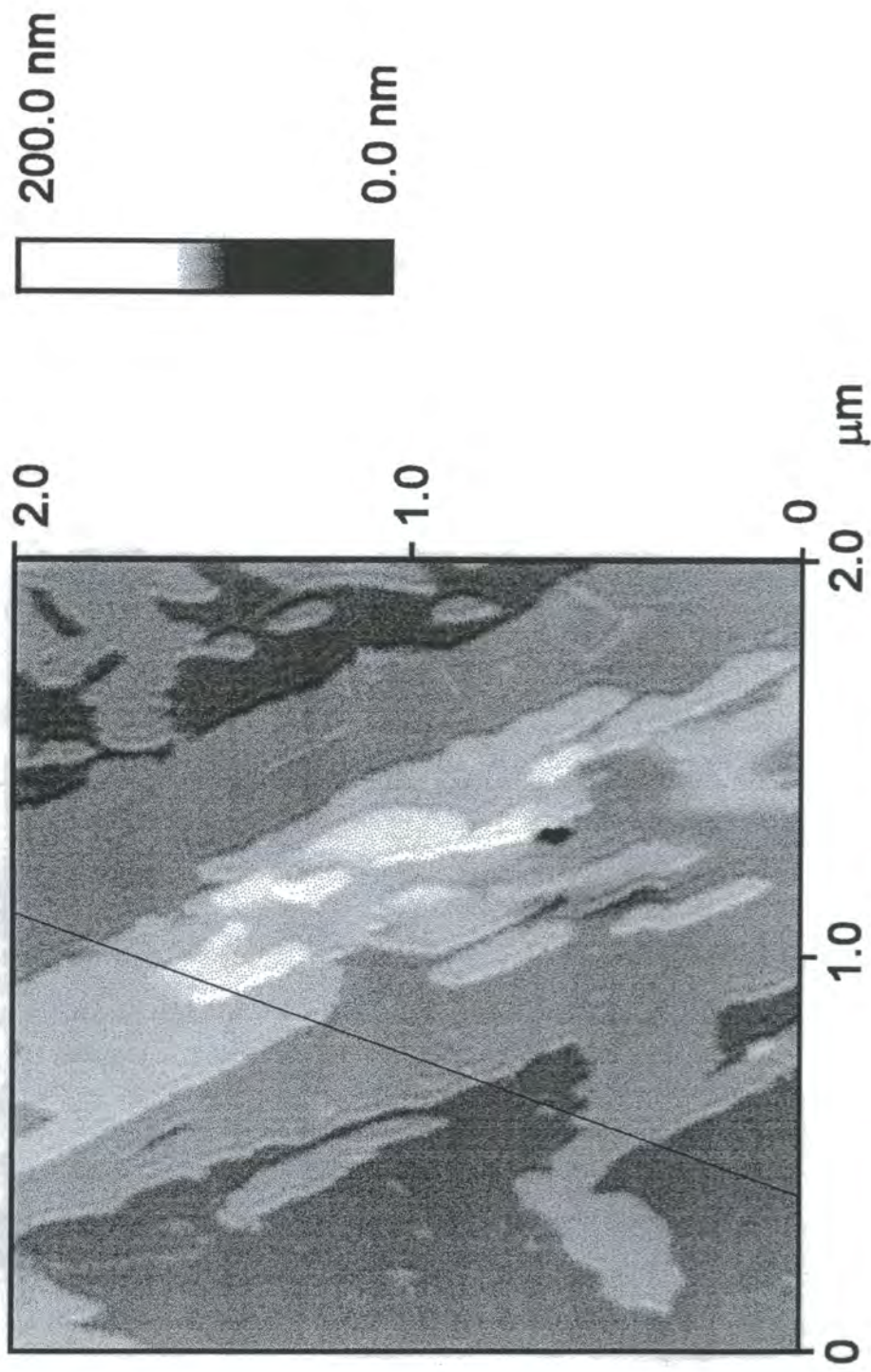
Figure 3(a) : Low resolution AFM image of an 11-layer mixed LB film of arachidic acid and cadmiun arachidate after washing in ethanol.
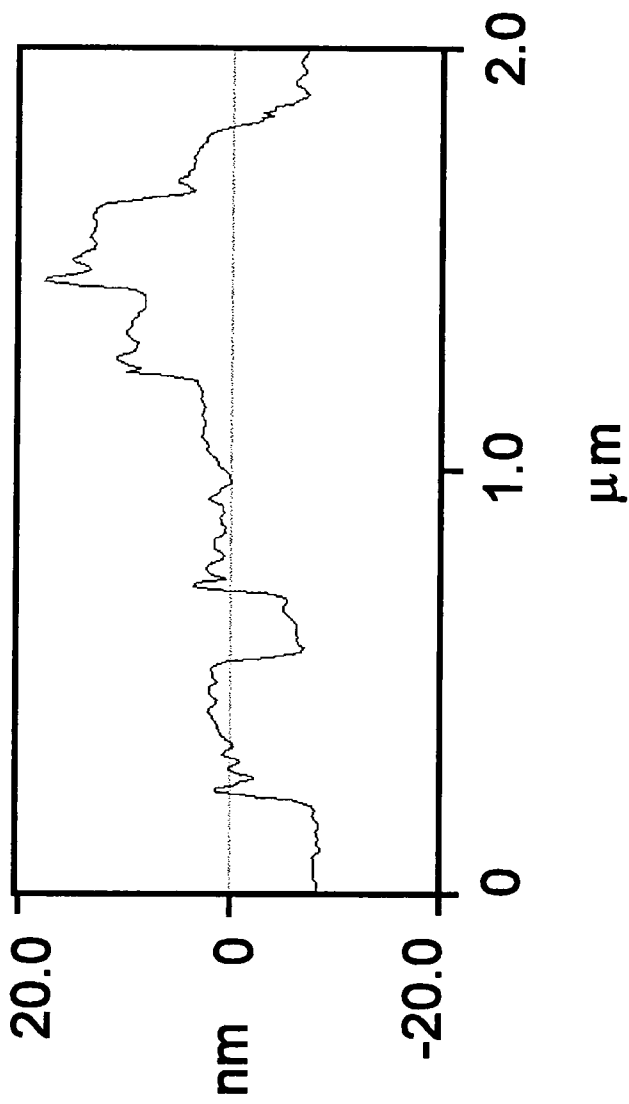
Figure 3(b). Cross-section analysis along the line drawn Figure 3(a).

maximum height of the islands (18.0 ± 0.6 nm) is equivalent to three bilayers of cadmium arachidate molecules. These results are consistent with ethanol washing out the majority of the arachidic acid, down to layer 5, to leave behind islands of cadmium arachidate molecules.

The overall cadmium arachidate content in the transferred LB film is determined by the pH of the aqueous subphase and its cadmium concentration.[10] Salt formation increases with subphase pH. It is approximately 50% complete at pH 5.5 and reaches full conversion at pH 6.5.[13] The deposition conditions adopted in this study (pH 5.7 ± 0.1) can therefore be expected to result in a film containing slightly more than 50% salt. This is in approximate agreement with the surface area of the islands (above layer 5) observed in Figure 3(a).

3.4   CONCLUSIONS

Atomic force microscopy has been used to study mixed LB films of arachidic acid/cadmium arachidate. Molecular resolution images are observed and it is proposed that these correspond to a distorted orthorhombic subcell. Some structural reorganization is evident in the transferred film, resulting in terraces of bilayer steps. The regions of arachidic acid in the mixed LB film can be removed by washing in ethanol to leave behind islands of cadmium arachidate molecules.

REFERENCES ·

[1]   Meyer, E.; Howald, L.; Overney, M. F.; Heinzelmann, H.; Frommer, J.; Güntherodt, H.-J.; Wegner, T.; Schier, H.; Roth, S. *Nature*, **1991**, *349*, 398.

[2]   Hansma, H. G.; Gould, S. A. C.; Hansmas, P. K.; Gaub, H. E.; Longo, M. L.; Zasadzinksi, J. A. N. *Langmuir*, **1991**, *7*, 1051.

[3]   DeRose, D. A.; Leblanc, R. M. *Surface Science Reports*, **1995**, *22*, 73.

[4]   Chi, L. F.; Anders, M.; Fuchs, H.; Johnston, R. R.; Ringsdorf, H. *Science*, **1993**, *259*, 213.

[5]   Schwartz, D. K.; Viswanathan, R.; Zasadzinksi, J. A. N. *J Phys Chem*, **1992**, *96*, 10444.

[6]   Schwartz, D. K.; Garnaes, J.; Viswanathan, R.; Chiruvolu, S.; Zasadzinksi, J. A. N. *Physics Review E*, **1993**, *47*, 1, 452.

[7]   Schwartz, D. K.; Viswanathan, R.; Garnaes, J.; Zasadzinksi, J. A. N. *J Am Chem Soc*, **1993**, *115*, 7374.

[8]   Schwartz, D. K.; Garnaes, J.; Viswanathan, R.; Zasadzinksi, J. A. N. *Science*, **1992**, *257*, 508.

[9]   Evenson, S. A.; Badyal, J. P. S.; Pearson, C.; Petty, M. C. *J Phys Chem*, **1996**, *100*, 11672.

[10]   Petty, M. C. *Langmuir Blodgett Films: An Introduction*, Cambridge Univeristy Press: Cambridge **1996**.

[11]   Kitaigorodski, A. I. *Organic Chemistry Crystallography*, Consultant Bureau: New York **1961**.

[12] Blodgett, K. B. *Phys. Rev.*, **1939**, *55*, 391.

[13] Viswanathan, R.; Schwartz, D. K.; Garnaes, J.; Zasadzinksi, J. A. N. *Langmuir*, **1992**, *8*, 1603.

CHAPTER 4

SELF-ASSEMBLED

PAMAM DENDRIMER FILMS

4.1   INTRODUCTION

Dendrimers are well defined, 3-dimensional, branched, functional polymers.[1] They can serve as useful starting materials for the fabrication of supramolecular structures. Existing applications include hybrid block copolymers,[2] liquid crystalline dendrimers,[3] unimolecular micelles,[4] and amphiphiles.[5] In this article it is reported that solvent cast polyamidoamine dendrimers undergo self-assembly into closely packed cells, made up of a complex network of intertwined dendritic microfibrils.

The polyamidoamine (PAMAM) family of starburst dendrimers (SBDs) is synthesized by repeat grafting of layers of amidoamine units onto an ethylenediamine core.[1] Each shell of the amidoamine units constitutes a "full" generation (terminated by amine groups), whilst the "half" generations are terminated by sodium carboxylate groups.

4.2   EXPERIMENTAL

Generation 9.5 PAMAM SBDs (5 wt. % dissolved in methanol, Aldrich) were solvent cast under a nitrogen atmosphere onto hydrophilic silicon substrates, and kept under nitrogen for at least 48 hours in order to ensure complete evaporation of the methanol solvent. A Nikon MM-11U optical microscope and a Digital Instruments Nanoscope III atomic force microscope were used to examine the respective macroscopic and microscopic structures of the dendrimer films in air. The atomic force microscope was operated in two modes: tapping

42

mode, where changes in the oscillation amplitude of the cantilever tip serves as a feedback signal for measuring topographic variations across a surface; and phase imaging mode,[6] where any shifts in the phase of the tip oscillation are detected. In both cases, a large root-mean-square amplitude was used to overcome the capillary attraction of the surface layer. The possibility of the dendrimers imaging the AFM tip was checked by using different generations of dendrimers.

4.3. RESULTS

On the macroscopic scale, optical microscopy showed that the dendrimer layer comprised a close packed array of cellular structures which completely covered the underlying silicon substrate, Figure 1 (this was confirmed by X-ray photoelectron spectroscopy by checking for the absence of the Si (2p) signal). The number of vertices contained within each cellular polygon ranges from three to seven with diameters varying between 50 - 230 μm. Cross-sectional analysis showed that the cell walls are raised approximately 1 μm above the bottom of each cell floor, Figure 2. These cellular features bear a strong resemblance to structures commonly found in plants[7] and soap foams.[8]

At the microscopic level, tapping mode atomic force microscopy unveiled a complex network of randomly intertwined PAMAM dendrimer microfibrils, Figure 3. The microfibril cross-sections were measured to be multiples of 150 Å, i.e. n150 Å (where n = 1-5). The packing and alignment of individual dendrimers contained within the microfibrils could be seen by phase imaging
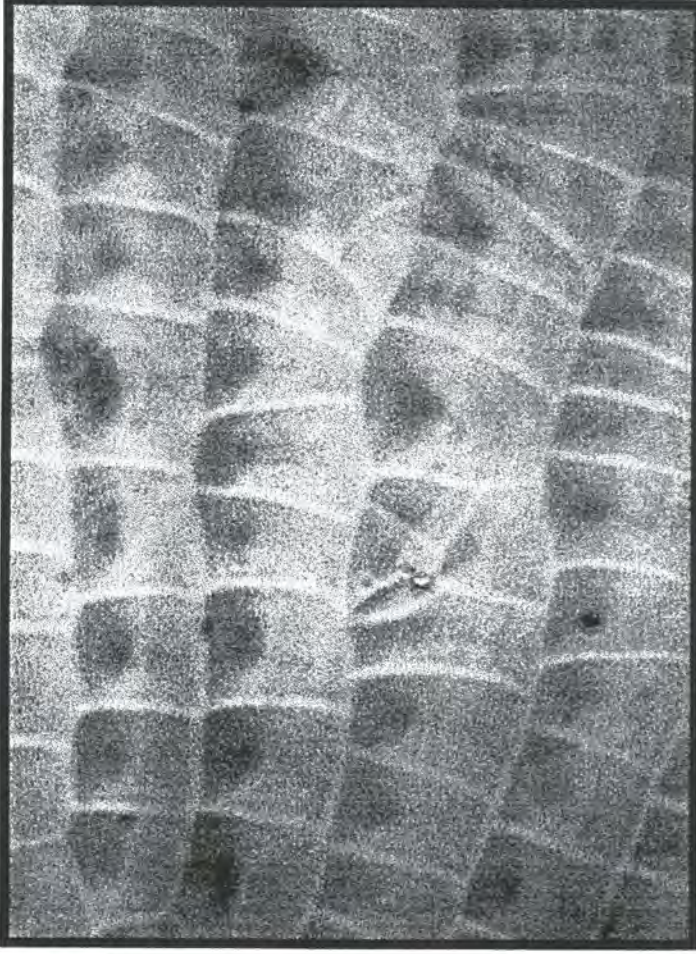
100 μm

Figure 1. Optical micrograph of the dendritic cellular structures formed during solvent casting of the generation 9.5 PAMAM dendrimer film (the lighter parts correspond to the raised cell walls).
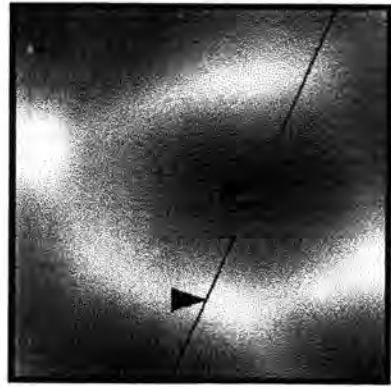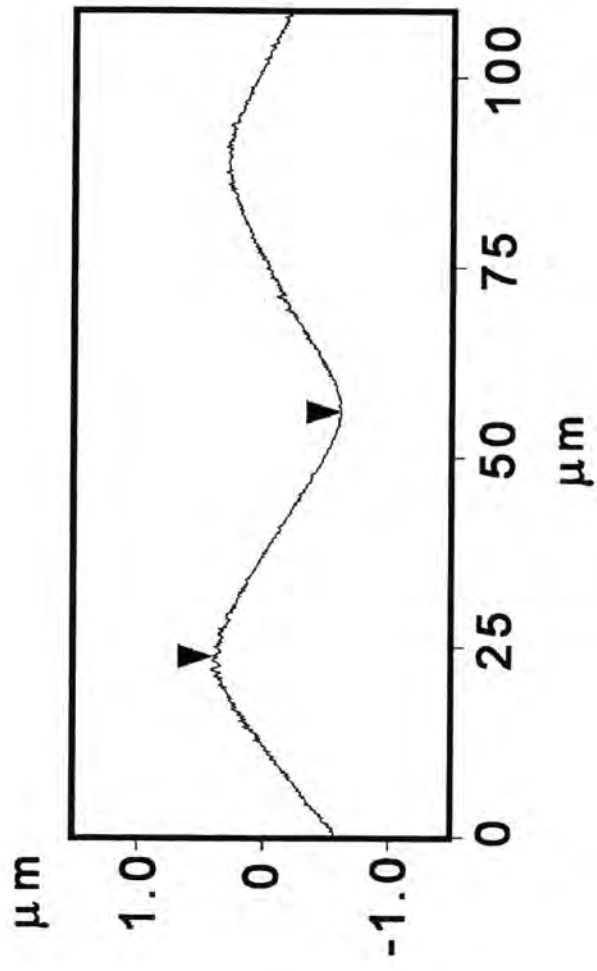
Figure 2. Low resolution tapping mode atomic force micrograph of an individual dendritic cell. The cross-section depicts the height of the cell walls.
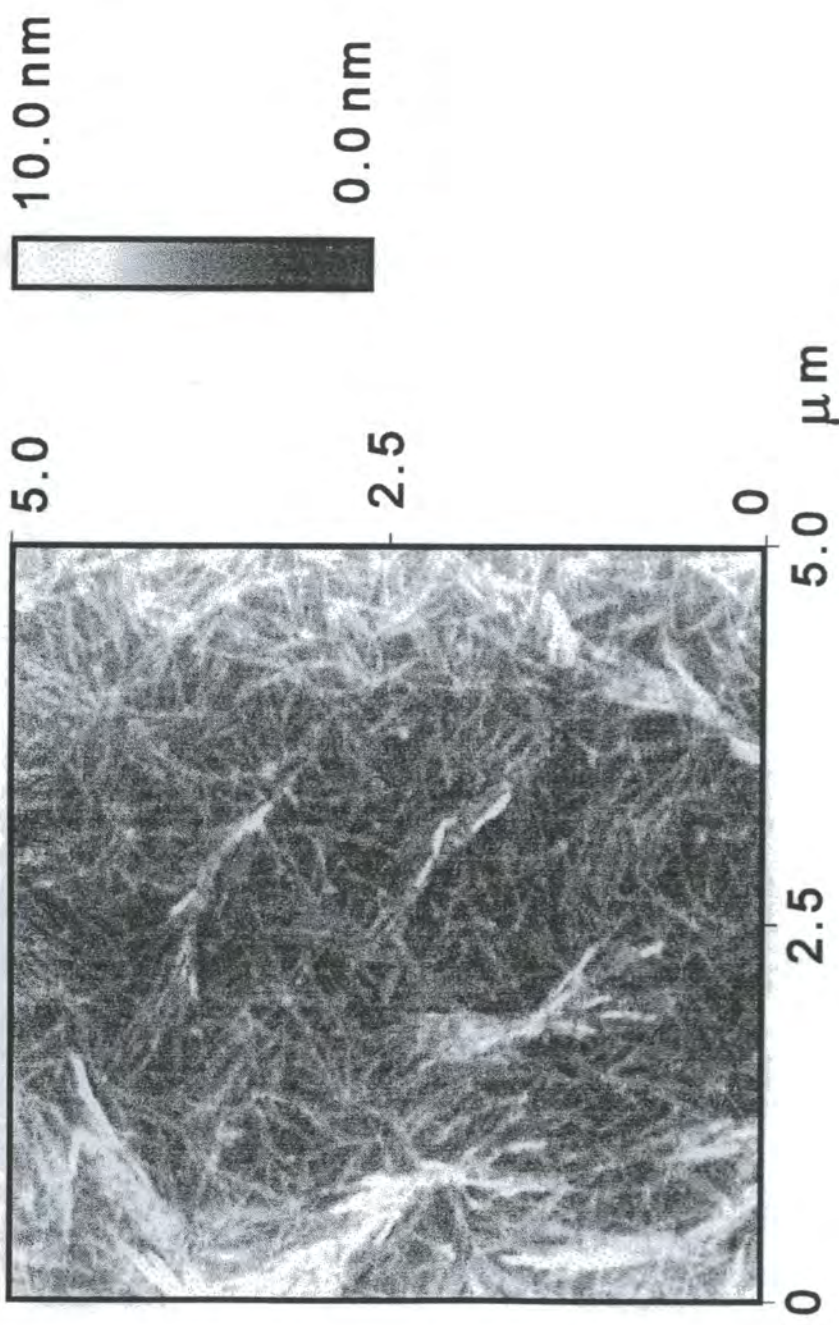
Figure 3. High resolution tapping mode AFM image of generation 9.5 PAMAM dendrimer microfibrils.

atomic force microscopy; this provides enhanced contrast of the structural features (dendrimers) because it highlights edges and is not affected by large-scale height differences[9,10] (i.e. the cell walls), Figure 4. The diameter of these generation 9.5 PAMAM dendrimers was measured from these images to be approximately 150 Å.

4.4   DISCUSSION

Clearly, these novel surface morphologies and patterns are formed during the dewetting or drying of the dendrimer film. Minimization of the overall surface tension of the system will occur during cell formation; which corresponds to aggregates of dendrimer material moving outwards from low surface energy regions at the centre of the cells towards the higher surface energy edges.[11] This process results in the formation of the observed dendritic cells which are reminiscent of Bénard cells found in coatings.[11] It is known that the surface tension driving force governing Bénard cell growth can be attributed to two reinforcing factors: firstly, evaporation of solvent causes cooling (and higher surface tension) which results in cellular convection, and secondly, the polymer concentration increases during the evaporation process. The spherical generation 9.5 PAMAM dendrimers can be considered as unimolecular micelles[4] consisting of an interior hydrophobic core surrounded by a hydrophilic surface layer of sodium carboxylate groups. During solvent casting, the dendrimer concentration gradually increases as methanol evaporates from the film leading to the self-assembly of dendrimers into microfibrils in an analogous fashion to
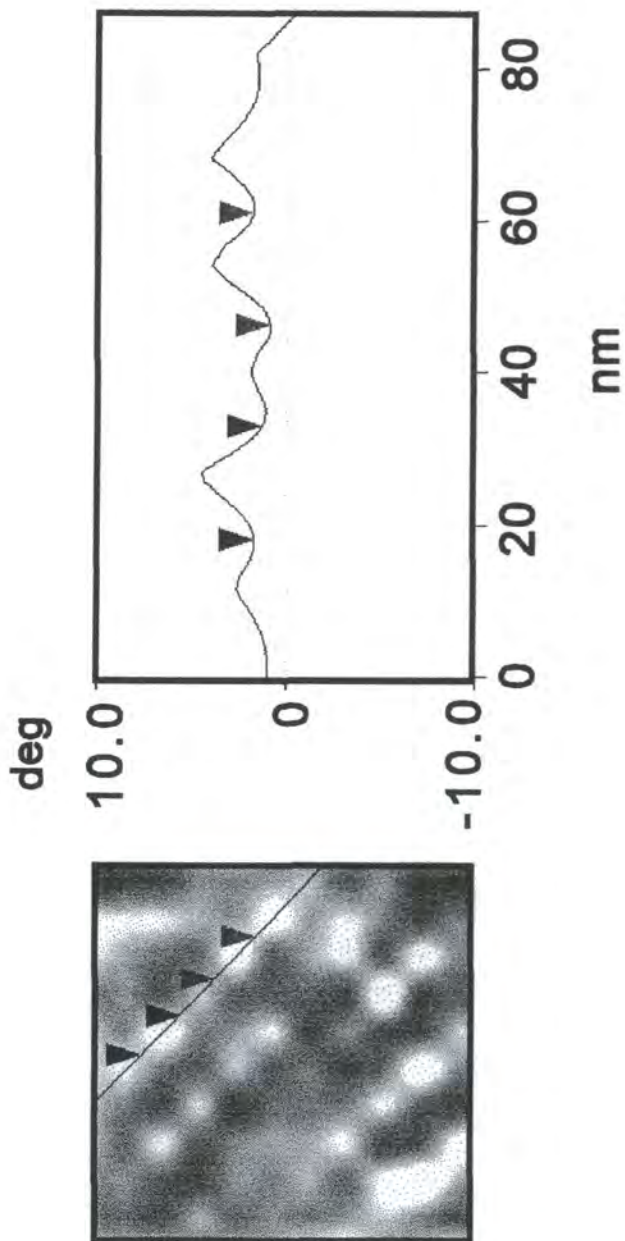
Figure 4. High resolution phase image of an individual dendrimer microfibril and the associated cross-section. The distance between consecutive markers corresponds to the size of individual dendrimers.

that reported for micellar systems (fiber- and rod-like assemblies) at high concentrations,[12] and inorganic carbonate and phosphonate precipitates.[13] The packing of dendrimers within the fibrils can be attributed to the co-ordination of surface carboxylate groups between adjacent dendrimers via shared sodium cations. This again is similar to previously observed complexation behaviour for generation 5.5 PAMAM dendrimers in a surfactant solution,[14] and micelles at high concentrations.[15] The measured cross-section of the dendrimer microfibrils correlates well with multiples of the monomeric dendrimer diameter (n150 Å). In fact the measured dendrimer diameter is slightly greater than the theoretical value (~130 Å),[1] and can be attributed to the flattening down and spreading out of dendrimers onto the underlying substrate.[16,17]

Other types of dendrimer superstructure have previously been observed and found to depend upon the class of multifunctional dendrimer building block utilized: low generation phenylacetylene dendrimers yield crystallites;[18] octaferrocenyl dendritic systems produce a layered compact morphology;[19] generation 8.0 PAMAM dendrimers form colourless sheet assemblies;[1] acid-functionalized amphiphiles derived from dendrimers can cluster into micellar aggregates;[5] and hybrid linear-dendritic copolymers are able to crystallize into spherulites and axialites.[2]

4.5 CONCLUSIONS

In the present case, a new type of cellular structure has been observed using generation 9.5 PAMAM dendrimers. The dimensions and surface functionality of these dendrimer assemblies could be tailored further by simply fine-tuning the type of dendrimer and solvent casting conditions used. Such novel surfaces may find potential applications in cell growth, compartmentalization, controlled permselectivity, electronic circuitry, catalysis, and adhesion enhancement.

REFERENCES

[1]   Tomalia, D. A.; Naylor, A. M.; Goddard III, W. A. *Angew. Chem. Int. Ed. Engl.* **1990**, *29*, 138.

[2]   Fréchet, J. M. J.; Gitsov, I. *Macromol. Symp.* **1995**, *98*, 441.

[3]   Percec, V.; Kawasumi, M. *Macromolecules* **1992**, *25*, 3843.

[4]   Newkome, G. R.; Moorefield, C. N.; Baker, G. R.; Saunders, M. J.; Grossman, S. H. *Angew. Chem. Int. Ed. Engl.* **1991**, *30*, 1178.

[5]   van Hest, J. C. M.; Baars, M. W. P.; Elissen-Román, C.; van Genderen, M. H. P.; Meijer, E. W. *Marcromolecules* **1995**, *28*, 6689.

[6]   Maganov, S. N.; Ellings, V.; Papkov, V. S. *Polymer* **1997**, *38*, 297.

[7]   Fosket, D. E. *Plant Growth and Development - A Molecular Approach,* Academic: San Diego **1994**, Chapter 5.

[8]   Boys, C. V. *Soap Bubbles and the Forces Which Mould Them,* Heinmann: London **1959**.

[9]   Babcock, K. L.; Prater, C. B. *Phase Imaging: Beyond Topography,* Digital Instruments Application Note: California **1995**.

[10]   Ruddick, V. J.; Badyal, J. P. S. *J. Phys. Chem.* **1997**, *101*, 1791.

[11]   Hansen, C. M.; Pierce, P. E. *Ind. Eng. Chem., Prod. Res. Develop.* **1974**, *13*, 218.

[12]   Magonov, S. N.; Whangbo, M.-H. *Surface Analysis with AFM and STM,* VCH: Weinheim **1996**, Chapter 12.

[13]   Pach, L.; Duncan, S.; Roy, R.; Komareni, S. *J. Mat. Sci.* **1996**, *31*, 6565.

[14] Ottaviani, M. F.; Turro, N. J.; Jockusch, S.; Tomalia, D. A. *J. Phys. Chem.* **1996,** *100,* 13675.

[15] Yoshikiyo, M. *Micelles : Theoretical and Applied Aspects,* Plenum Press, New York **1992**.

[16] Mansfield, M. L. *Polymer* **1996,** *37,* 3835.

[17] Wells, M.; Crooks, R. M. *J. Am. Chem. Soc.* **1996,** *118,* 3988.

[18] Buchko, C. J.; Wilson, P. M.; Xu, Z.; Zhang, J.; Moore, J. S.; Martin, D. C. *Polymer* **1995,** *36,* 1817.

[19] Alonso, B.; Morán, M.; Casado, C. M.; Lobete, F.; Losada, J.; Cuadrado, I. *Chem. Mater.* **1995,** *7,* 1440.

CHAPTER 5

SURFACE ESTERIFICATION OF ETHYLENE

MALEIC ANHYDRIDE COPOLYMER

5.1   INTRODUCTION

Modification of polymer surfaces can be used to tailor substrate wettability, permeability, biocompatability, adhesion, etc. This can be achieved by either surface activation methods (sensitizers,[1] plasma treatment,[2] high energy radiation,[3] etc.) or alternatively via direct functionalization of reactive groups along the polymer backbone. The former is usually very quick and produces negligible waste, whereas the latter can potentially offer greater chemical specificity.

Most chemical surface functionalization reactions are carried out in the solution phase. The major drawbacks of this approach include reorientation of surface functional groups and solvent extraction of low molecular weight species. Vapour phase treatments can help to alleviate these problems.[4] In this study, the surface esterification of ethylene maleic anhydride copolymer is explored using a range of alcohols with increasing nucleophilicities, i.e. 2,2,2-trifluoroethanol, 4,4,4-trifluorobutanol, and ethanol. The aim of this investigation was to establish how well conventional solution phase chemistry can be extended to reactions at polymer surfaces.
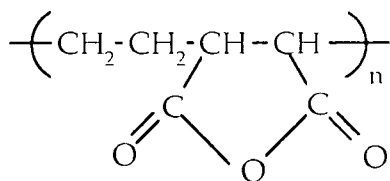
Ethylene maleic anhydride copolymer

5.2   EXPERIMENTAL

Ethylene maleic anhydride copolymer (Zeeland Chemicals) films were prepared by spin-coating a 2% wt./vol. solution of the powdered copolymer dissolved in acetone onto a glass slide. Infrared spectroscopy was used to confirm the purity of the film (and the absence of hydrolysis), whilst complete coverage of the glass substrate was checked by X-ray photoelectron spectroscopy (as signified by the absence of any Si(2p) signal from the glass slide). For each experiment, a freshly coated substrate was placed into a vapour phase labelling apparatus,[5] Figure 1, and evacuated to a base pressure of better than 1 x 10^{-2} mbar using an Edwards double stage mechanical rotary pump fitted with a liquid nitrogen cold trap. The reaction cell was then isolated from the pumping system. Next, alcohol vapour was allowed to equilibrate into the empty volume at ambient temperature (25 °C): trifluoroethanol (68.5 mbar), trifluorobutanol (10.6 mbar), or ethanol (63.2 mbar). At this stage, timing of the functionalization reaction commenced. Upon termination of exposure, the alcohol reservoir was isolated, and the whole apparatus pumped back down to its initial base pressure. Typical reaction profiles were compiled by varying the length of contact time of each alcohol with the copolymer followed by XPS quantification of the extent of esterification.

XPS analysis was carried out using a Kratos ES300 electron spectrometer equipped with a Mg $K\alpha_{1,2}$ X-ray source (1253.6 eV) and a concentric hemispherical analyser. Photo-emitted electrons were collected at a take-off angle of 30° from the substrate normal, with electron detection in the fixed
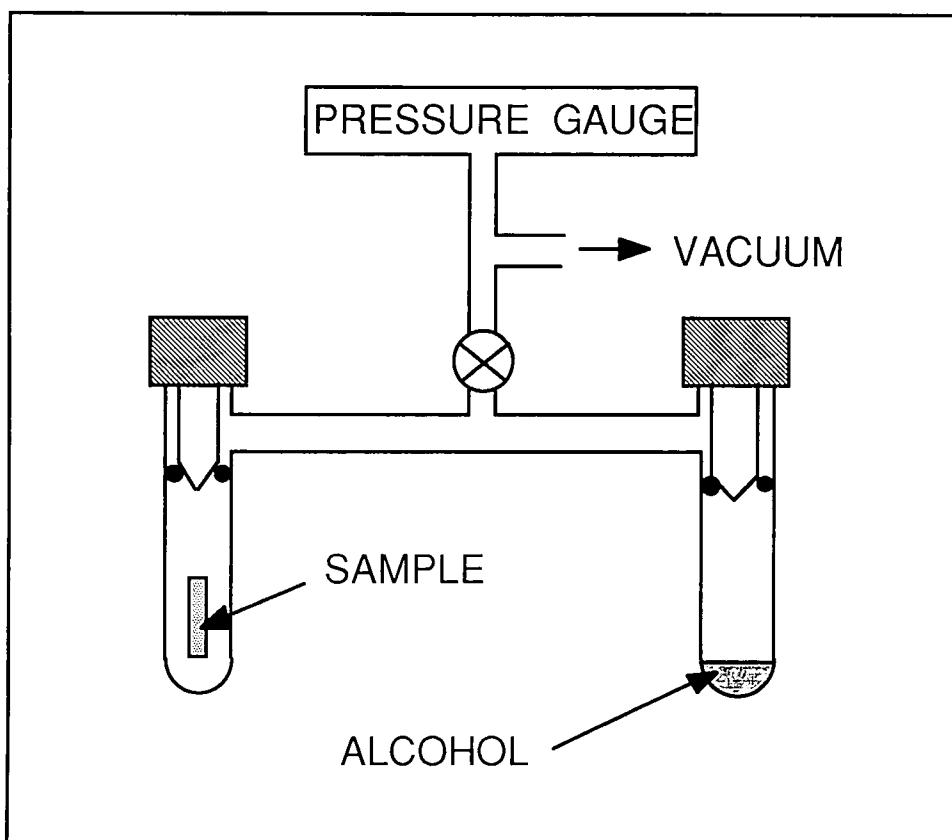
Figure 1. Vapor phase functionalization apparatus.

retarding ratio (FRR, 22:1) mode. XPS spectra were accumulated on an interfaced PC computer. Instrumentally determined sensitivity factors were taken as C(1s) : O(1s) : F(1s) equals 1.00 : 0.55 : 0.53.

For infrared analysis, sample preparation comprised spin coating thin films of ethylene maleic anhydride copolymer onto pre-formed KBr discs from a 2% wt./vol. acetone solution. Infrared absorption spectra were acquired on a Mattson Polaris instrument at 4 cm^{-1} resolution in the range 400 to 4000 cm^{-1}.

5.3   RESULTS

5.3.1. Characterization of the Copolymer

The C(1s) XPS envelope of ethylene maleic anhydride copolymer can be fitted to the following range of carbon functionalities:[6] hydrocarbon ($\underline{C}H_x$ ~ 285.0 eV), carbon adjacent to an anhydride group ($\underline{C}$-C-O(=O) ~ 285.8 eV), and anhydride groups (O=$\underline{C}$-O-$\underline{C}$=O ~ 289.4 eV) in a 1.3 : 1 : 1 ratio, Figure 2(a), i.e. there was a slight excess of hydrocarbon. The carbon/oxygen elemental ratio was measured to be 2.3 ± 0.1, which is higher than the expected theoretical value of 2.0, and can be attributed to one or more of the following possibilities: orientation of the anhydride groups away from the near surface, or the presence of a small amount of hydrocarbon contamination, or -$CH_2CH_2CH_2CH_2$- residues in the copolymer backbone.

Infrared absorption spectroscopy of the copolymer displayed absorbance bands at:[7] 2947 cm^{-1} (CH_2 stretching vibrations), 1778 cm^{-1} and 1713 cm^{-1} (C=O in
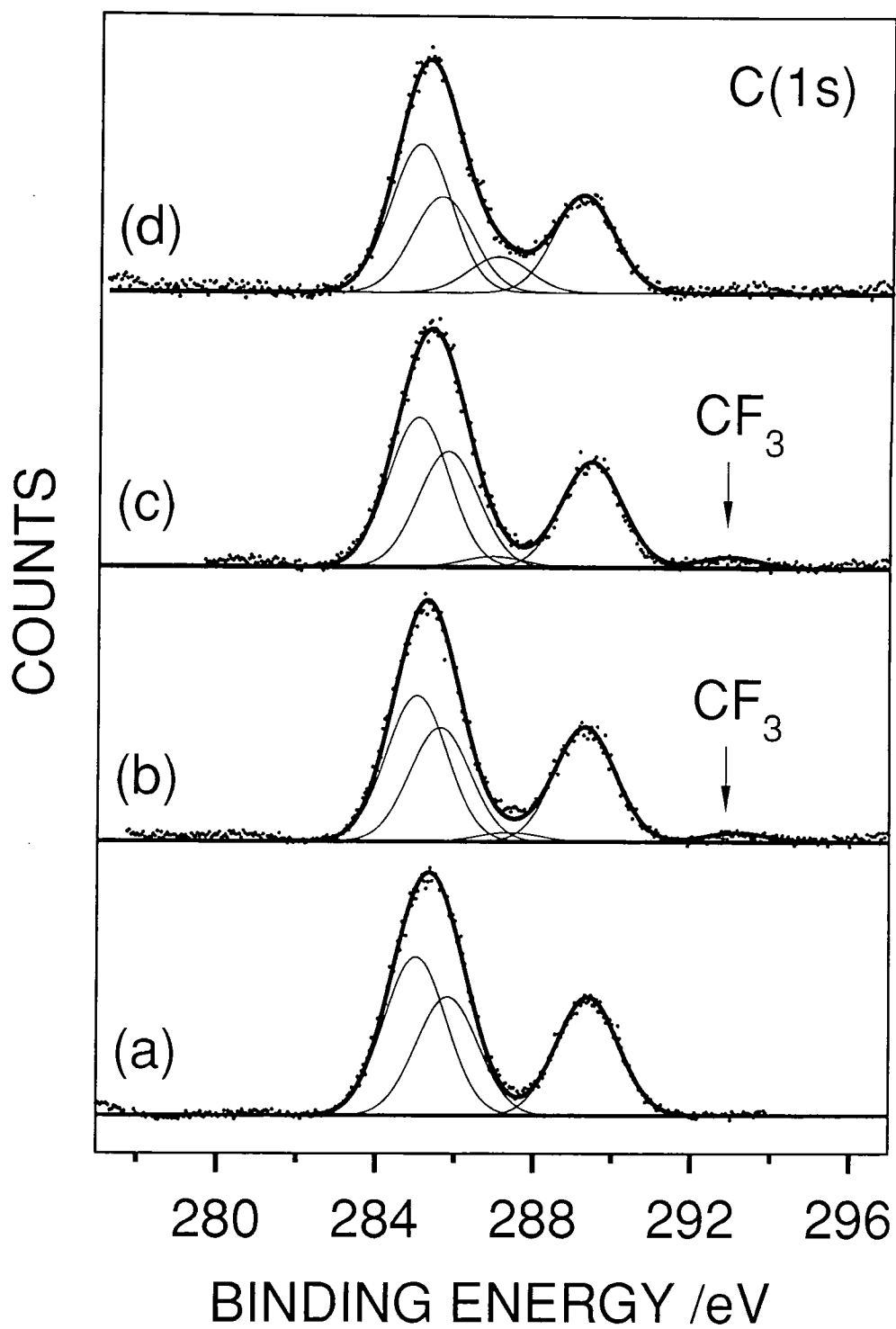
Figure2. C(1s) XPS spectra of ethylene maleic anhydride copolymer: (a) untreated; and functionalised with (b) trifluoroethanol; (c) trifluorobutanol; and (d) ethanol.
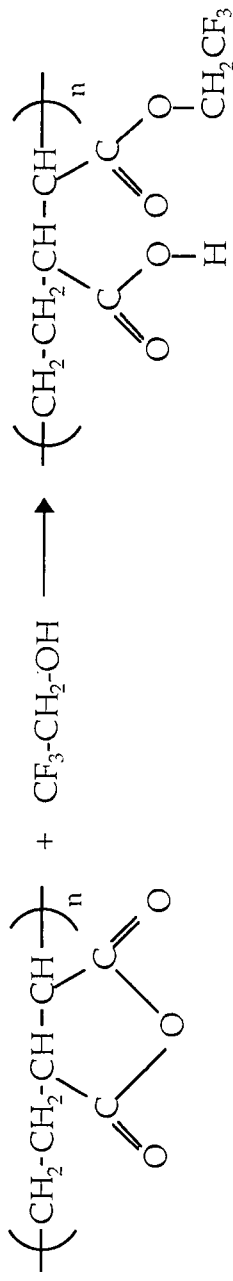
cyclic anhydride), 1460-1370 cm^{-1} (CH$_2$ deformations), and 1224 cm^{-1} (C-O in anhydride). All of these features are consistent with the known structure of ethylene maleic anhydride copolymer. A very weak absorption band was noted at 725 cm^{-1} due to skeletal vibrations of -CH$_2$CH$_2$CH$_2$CH$_2$- residues.[7]

5.3.2 Surface Functionalization with Trifluoroethanol

Monoester formation is a key reaction between polymeric derivatives of maleic anhydride and primary alcohols.[7] For instance, ethylene maleic anhydride copolymer should react with trifluoroethanol to form a half ester as shown in Scheme 1. The efficiency of this condensation reaction can be calculated from the measured surface fluorine concentration following functionalization.[8,9] For each anhydride group which undergoes reaction, there is an overall increase by six in the number of atoms detected by XPS, corresponding to two carbon, one oxygen, and three fluorine atoms. Thus by taking the conversion factor of anhydride to half ester groups to be x (where $x = 0$ in the case of no reaction and $x = 1$ in the case of complete reaction) and assuming that all elements are homogeneously distributed within the XPS sampling depth both before and after functionalization, the theoretical percentage of surface oxygen and fluorine concentrations can be predicted according to Equations 1(a) and 1(b):

$$\%\,[O] = \frac{[O]_0\,(1+x/3)}{[C]_0 + [O]_0\,(1 + 2x)} \times 100 \qquad \text{Equation 1(a)}$$

Scheme 1. Reaction of ethylene maleic anhydride copolymer with trifluoroethanol.

$$\left(CH_2\text{-}CH_2\text{-}CH\text{-}CH\right)_n \quad + \quad CF_3\text{-}CH_2\text{-}OH \quad \longrightarrow \quad \left(CH_2\text{-}CH_2\text{-}CH\text{-}CH\right)_n$$

Scheme 2. Reaction of ethylene maleic anhydride copolymer with trifluorobutanol.

$$\left(CH_2\text{-}CH_2\text{-}CH\text{-}CH\right)_n \quad + \quad CF_3\text{-}CH_2\text{-}CH_2\text{-}CH_2\text{-}OH \quad \longrightarrow \quad \left(CH_2\text{-}CH_2\text{-}CH\text{-}CH\right)_n$$
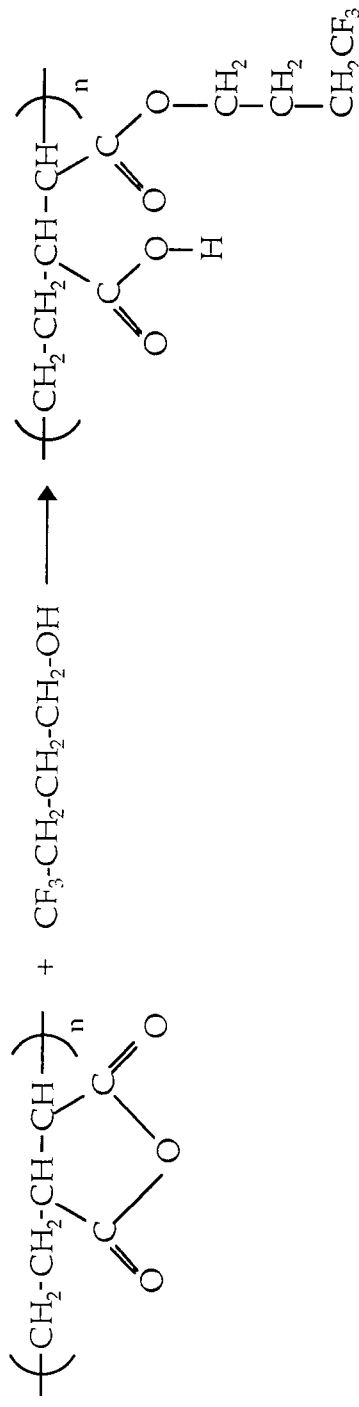
Scheme 3. Reaction of ethylene maleic anhydride copolymer with ethanol.

$$\left(CH_2\text{-}CH_2\text{-}CH\text{-}CH\right)_n \quad + \quad CH_3\text{-}CH_2\text{-}OH \quad \longrightarrow \quad \left(CH_2\text{-}CH_2\text{-}CH\text{-}CH\right)_n$$
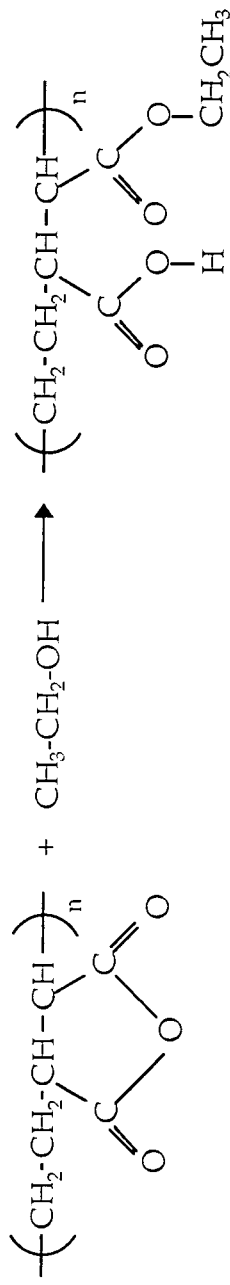
$$\% \, [F] = \frac{x \, [O]_0}{[C]_0 + [O]_0 \, (1 + 2x)} \times 100 \qquad \text{Equation 1(b)}$$

where $[O]_0$ and $[C]_0$ represent the oxygen and carbon concentrations contained in the untreated ethylene maleic anhydride copolymer (determined by experiment to be 30 % and 70 % respectively).

The high resolution C(1s) spectra of the alternating copolymer functionalized with trifluoroethanol, Figure 2(b), can be fitted to five different carbon functionalities:[6] hydrocarbon ($\underline{C}H_x$ ~ 285.0 eV), carbon singly bonded to an ester / carboxylic acid group ($\underline{C}$-C-O(=O) ~ 285.6 eV), carbon singly bonded to oxygen and to a trifluoromethyl carbon (O-$\underline{C}$-CF_3 ~ 287.3 eV), ester / carboxylic acid group (O-$\underline{C}$=O ~ 289.3 eV), and trifluoromethyl carbon (-$\underline{C}F_3$ ~ 293.1 eV). The presence of the trifluoromethyl carbon peak is indicative of surface functionalization. The exact amount of fluorine associated with the functionalized copolymer surface was measured from the area of the F(1s) peak, Figure 3(b), since each trifluoromethyl group contributes 3 fluorine atoms (-$C\underline{F}_3$ ~687.7 eV).[6] This fluorine concentration was used in conjunction with Equation 1(b) to generate a graph of experimental conversion factor (x) vs. reaction time, Figure 4. It can be seen that the esterification reaction proceeds reasonably well, leading to a limiting amount of fluorine incorporation after a reaction time of approximately 16 hours. Since all of the oxygen atoms associated with the untreated copolymer surface exist as anhydride functionalities, use of Equation 1(a) yields a conversion factor of $x = 0.19 \pm 0.01$ following 16 hours of reaction.
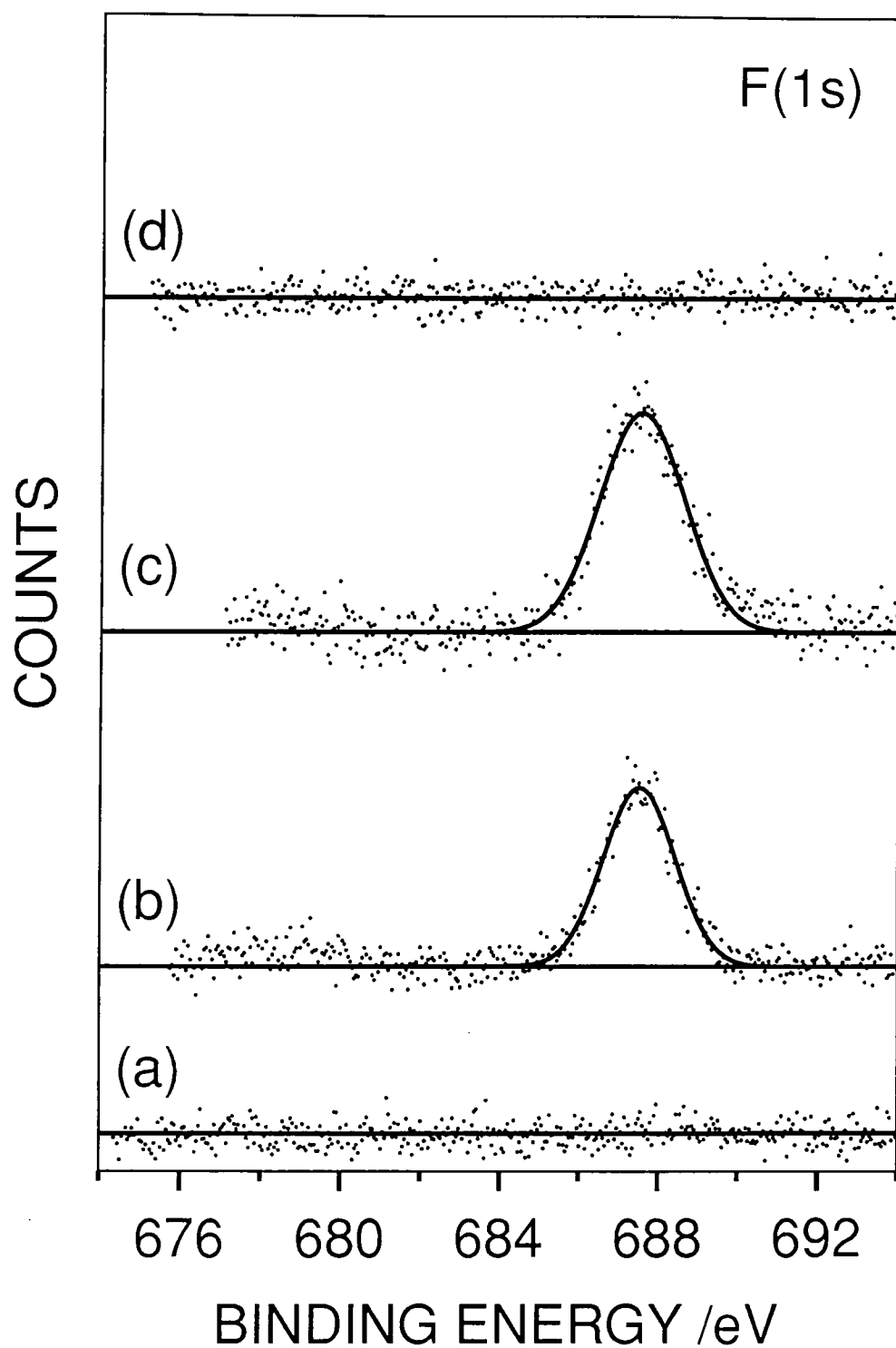
Figure 3. F(1s) XPS spectra of ethylene maleic anhydride copolymer:
(a) untreated; and functionalised with (b) trifluoroethanol; (c) trifluorobutanol;
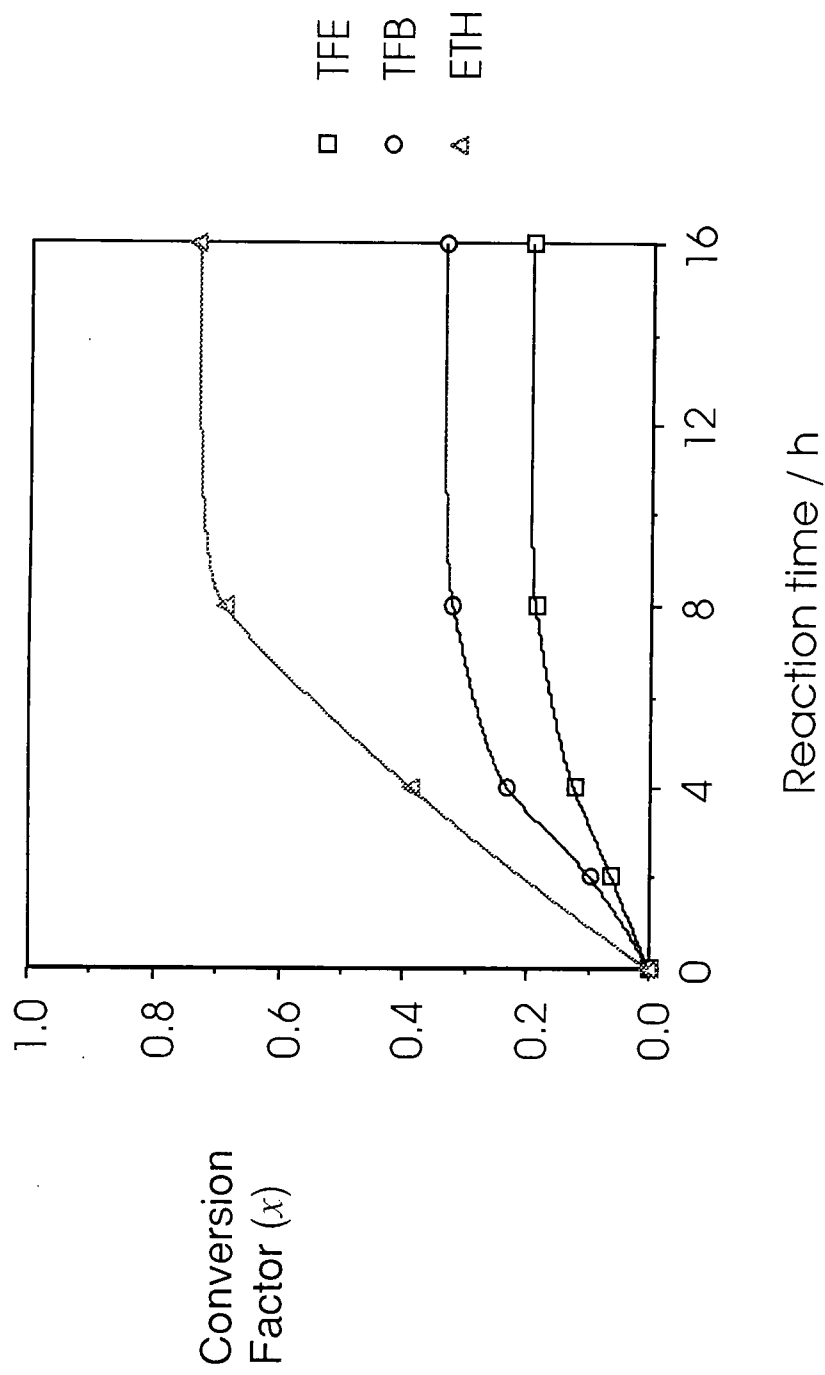and (d) ethanol.

Figure 4. Experimental conversion factors as a function of reaction time for the copolymer functionalised with: (a) trifluoroethanol; (b) trifluorobutanol; and (c) ethanol.

5.3.3 Surface Functionalization with Trifluorobutanol

The expected reaction of trifluorobutanol with ethylene maleic anhydride copolymer is shown in Scheme 2. The C(1s) XPS spectra of the copolymer reacted with trifluorobutanol, Figure 2(c), could be fitted to five different carbon functionalities:[6] hydrocarbon ($\underline{C}H_x$ ~ 285.0 eV), carbon singly bonded to an ester / carboxylic acid group ($\underline{C}$-C-O(=O) ~ 285.6 eV), carbon singly bonded to oxygen and to a trifluoromethyl carbon (O-$\underline{C}$-CF$_3$ ~ 287.3 eV), ester / carboxylic acid group (O-$\underline{C}$=O ~ 289.3 eV), and trifluoromethyl carbon (-$\underline{C}$F$_3$ ~ 293.1 eV). The area of the F(1s) peak was again taken to be a measure of the concentration of trifluoromethyl groups, Figure 3(c). Therefore, as described previously in the case of trifluoroethanol, the oxygen and fluorine concentrations measured following functionalization of the copolymer surface with trifluorobutanol can be related to the conversion factor (x):[8,9]

$$\% \; [O] = \frac{[O]_0 \, (1+x/3)}{[C]_0 + [O]_0 \, (1 + 8x / 3)} \times 100 \qquad \text{Equation 2(a)}$$

$$\% \; [F] = \frac{x \, [O]_0}{[C]_0 + [O]_0 \, (1 + 8x / 3)} \times 100 \qquad \text{Equation 2(b)}$$

In this case, surface functionalization was found to be faster and more extensive compared to the corresponding experiments with trifluoroethanol, Figure 4. A conversion factor of x = 0.34 ± 0.01 was reached following 16 hours of reaction.

5.3.4 Surface Functionalization with Ethanol

Ethanol was employed as the third functionalizing reagent, and its reaction with the ethylene maleic anhydride copolymer surface is described in Scheme 3. The obtained C(1s) spectra, Figure 2(d), could be fitted to four different types of carbon functionality:[6] hydrocarbon ($\underline{C}H_x$ ~ 285.0 eV), carbon singly bonded to an ester / carboxylic acid group ($\underline{C}$-C-O(=O) ~ 285.5 eV), carbon singly bonded to oxygen ($\underline{C}$-O-C=O ~ 287.0 eV), and ester / carboxylic acid groups (O-$\underline{C}$=O ~ 289.2 eV). Although ethanol does not contain the trifluoromethyl labelling group, one can still calculate the conversion factor using Equation 3:

$$\% \, [O] = \frac{[O]_o \, (1+x/3)}{[C]_o + [O]_o \, (1 + x)} \times 100 \qquad \text{Equation 3}$$

It can be seen that on a theoretical basis, the oxygen concentration for ethylene maleic anhydride copolymer functionalized with ethanol does not vary much with increasing conversion factor (x). Therefore, the conversion factor has to be calculated by comparing the area ratio of the 3rd and 4th peaks contained in the C(1s) spectra taken for the ethanol functionalized copolymer surface, Figure 2(d); where the 3rd peak corresponds to the number of ester functionalities ($\underline{C}$-O-C=O) and the 4th peak encompasses the total number of ester and carboxylic acid groups (O-$\underline{C}$=O). The conversion factor was calculated to be x = 0.74 ± 0.04 following 16 hours of reaction. Figure 4 highlights the increased rate of reaction

and greater conversion factors for ethanol compared to trifluoroethanol and trifluorobutanol.

5.4 DISCUSSION

The reaction of an alcohol (nucleophile) with a carboxylic acid derivative (such as an anhydride group) is known as 'Nucleophilic Acyl Substitution'.[10] The tetrahedral intermediate formed during nucleophilic attack at the anhydride centre expels one of the substituents originally bonded to the anhydride carbon, thereby resulting in the formation of a half ester, Scheme 4. Such esterification reactions are usually acid / base catalysed, hence explaining why trifluoroethanol alone has been reported to be an ineffective reagent for the vapour phase functionalization of carboxylic acid groups.[9] This also accounts for the slow conversion of anhydride groups to half esters in the present study.

Since the overall experimental conditions were similar for each alcohol study, a comparison can be made between their reactivities towards the ethylene maleic anhydride copolymer surface. The relative initial rates of esterification have been calculated to be 1 : 1.7 : 3.5 for trifluoroethanol : trifluorobutanol : ethanol respectively. This ranking of reaction rates can be attributed to the influence of the CF_3 group upon the nucleophilicity of the alcohols. The electron withdrawing nature of CF_3 makes trifluoroethanol, and to a lesser extent trifluorobutanol, much weaker nucleophiles compared to ethanol. Hence their overall nucleophilicity is expected to be trifluoroethanol < trifluorobutanol < ethanol, which is consistent with the initial reaction rates and conversion factors

57

Scheme 4. Nucleophilic acyl substitution reaction of ethylene maleic anhydride copolymer with an alcohol to yield a half ester.
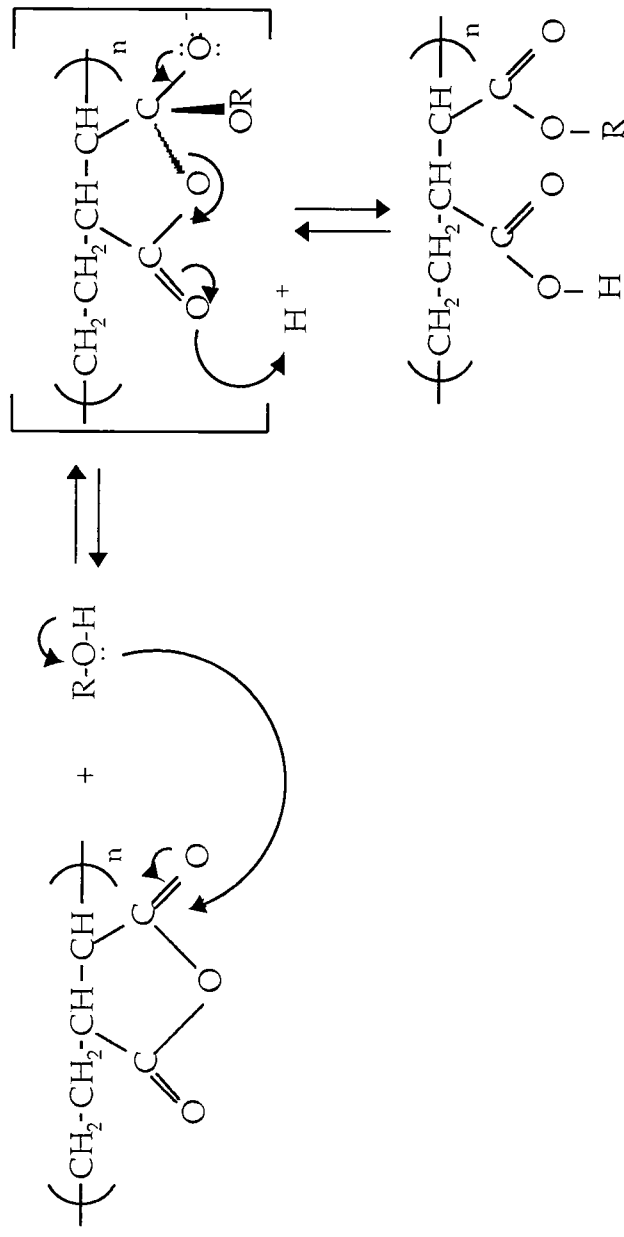
measured during reaction with the ethylene maleic anhydride copolymer surface. Therefore, in the general case, an alcohol of the type XCH_2CH_2OH (where X could be a protected reactive group, or a long alkyl chain, etc.) can undergo esterification at the surface of ethylene maleic anhydride copolymer.

5.5   CONCLUSIONS

Vapour phase chemical functionalization of ethylene maleic anhydride copolymer surfaces with trifluoroethanol, trifluorobutanol, and ethanol has been studied by XPS. All three alcohols are found to react with the anhydride groups contained along the copolymer backbone, forming half esters. The observed difference in relative esterification rates and yields between these alcohols can be attributed to their increasing order of nucleophilicity: trifluoroethanol < trifluorobutanol < ethanol.

REFERENCES

[1]   Goldblatt, R. D.; Park, J. M.; White, R. C.; Matienzo, L. J.; Huang, S. J.; Johnson, J. F. *J. Appl. Polym. Sci.* **1989**, *37*, 335.

[2]   Shard, A. G.; Badyal, J. P. S. *J. Phys. Chem.* **1991**, *95*, 9436.

[3]   Nho, Y. C.; Sugo, T.; Tsuneda, S.; Makuuchi, K. *J. Appl. Polym. Sci.* **1994**, *51*, 1269.

[4]   Nakayama, Y.; Takahagi, T.; Soeda, F.; Hatada, K.; Nagaoka, S.; Suzuki, J.; Ishitani, A. *J. Polym. Sci.* **1988**, *26*, 559.

[5]   Tasker, S.; Badyal, J. P. S. *Polymer* **1994**, *35*, 22.

[6]   Beamson, G.; Briggs, D. *High Resolution XPS of Organic Polymers*; Wiley: Chichester, **1992**.

[7]   Trivedi, B. C.; Culbertson, B. M. *Maleic Anhydride*; Plenum: New York, **1982**.

[8]   Sutherland, I.; Sheng, E. -S.; Brewis, M.; Heath, R. J. *J. Mater. Chem.* **1994**, *4*, 683.

[9]   Popat, R. P.; Sutherland, I.; Sheng, E. -S. *J. Mater. Chem.* **1995**, *5*, 713.

[10]   McMurry, J. *Organic Chemistry*; Brooks/Cole: California, **1988**; pp 652-653.

CHAPTER 6

AMINOLYSIS OF ETHYLENE MALEIC

ANHYDRIDE COPOLYMER SURFACES

Scheme 3. General mechanism of the nucleophilic acyl substitution reaction of ethylene maleic anhydride copolymer with an amine to yield a half amide.
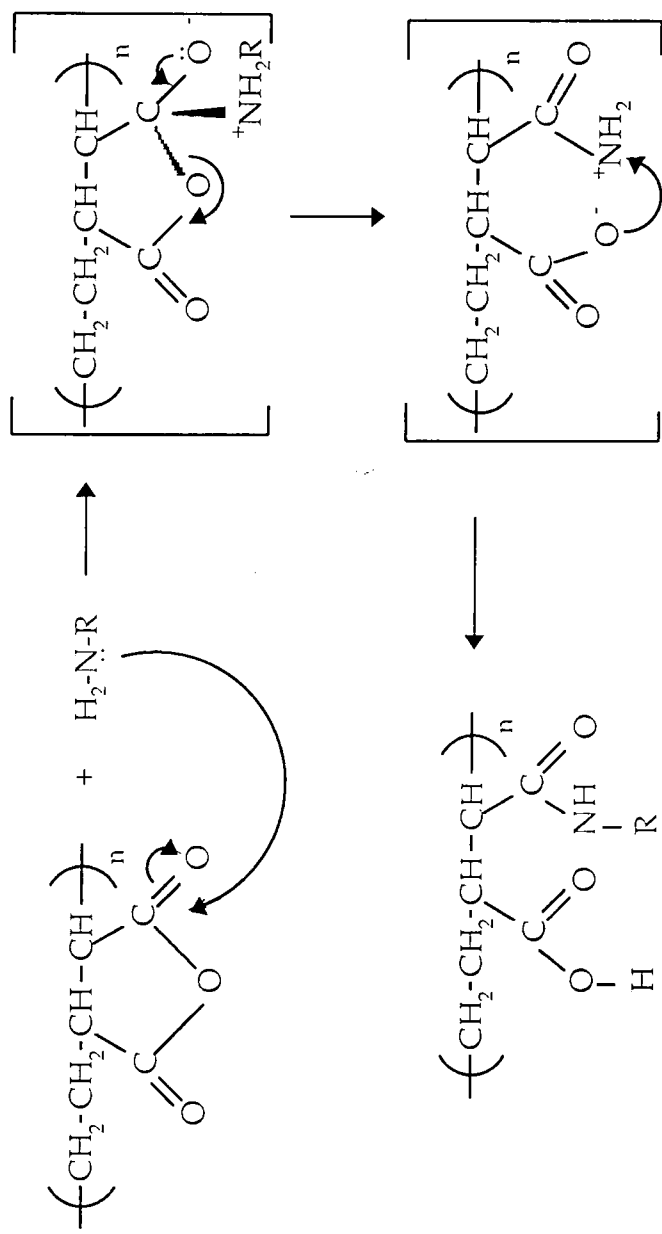
6.1   INTRODUCTION

Functionalized side chains bonded to polymer surfaces are important for a variety of industrial applications (e.g. adhesion, water repellency, lubrication, biocompatability). Such attachment can be achieved by either surface grafting methods (sensitizers[1], plasma treatment[2], high energy radiation[3], etc.), or alternatively via direct chemical reaction with groups contained within the parent polymer backbone. A good example of the latter approach is the functionalization of anhydride groups present at the surface of ethylene maleic anhydride copolymer films. Anhydride group chemistry offers a whole range of possibilities including esterification and aminolysis reactions.[4]

Typically, direct surface functionalization reactions are carried out in the solution phase.[5] Some of the major drawbacks associated with this type of approach are reorientation of surface groups within the reaction medium and solvent extraction of product species.[5] Vapour phase treatments can potentially alleviate these pitfalls.[6] In this article, the surface aminolysis of ethylene maleic anhydride copolymer using trifluoroethylamine and a Jeffamine are described.

6.2   EXPERIMENTAL

Ethylene maleic anhydride copolymer (Zeeland Chemicals, ~ 100% purity) films were prepared by spin-coating from a 2% wt./vol. acetone solution onto a glass substrate. Fourier transform (FT) infrared spectroscopy was used to check the purity of the polymeric film and the absence of anhydride group hydrolysis.[4] X-ray photoelectron spectroscopy (XPS) was used to confirm complete coverage of the substrate by the copolymer, as signified by the absence of any Si(2p) signals showing through from the underlying glass slide. Ethylene maleic anhydride copolymer surfaces were reacted with 2,2,2-trifluoroethylamine (Fluorochem, 99.5%), and poly(propylene glycol) bis(2-aminopropyl ether) also known as Jeffamine[®]-D (Aldrich, average molecular weight M_n = 230).

The reaction procedure comprised placing the polymer coated substrate into a vapour phase labelling apparatus,[7] Figure 1, followed by evacuation to a pressure of better than 1 x 10^{-2} mbar using an Edwards double stage mechanical rotary pump fitted with a liquid nitrogen cold trap. The reaction cell was then isolated from the pumping system and amine vapour was allowed to fill and equilibrate into the empty volume (trifluoroethylamine: 68.5 mbar; Jeffamine: 10.6 mbar) at ambient temperature (~25° C). At this stage, timing of the surface functionalization reaction commenced. Upon termination of exposure, the amine reservoir was isolated, and the whole apparatus pumped back down to its initial base pressure. Typical reaction profiles were compiled by varying the length of contact time between the copolymer surface and each amine, followed by XPS quantification of the extent of aminolysis. XPS and IR analysis were carried out
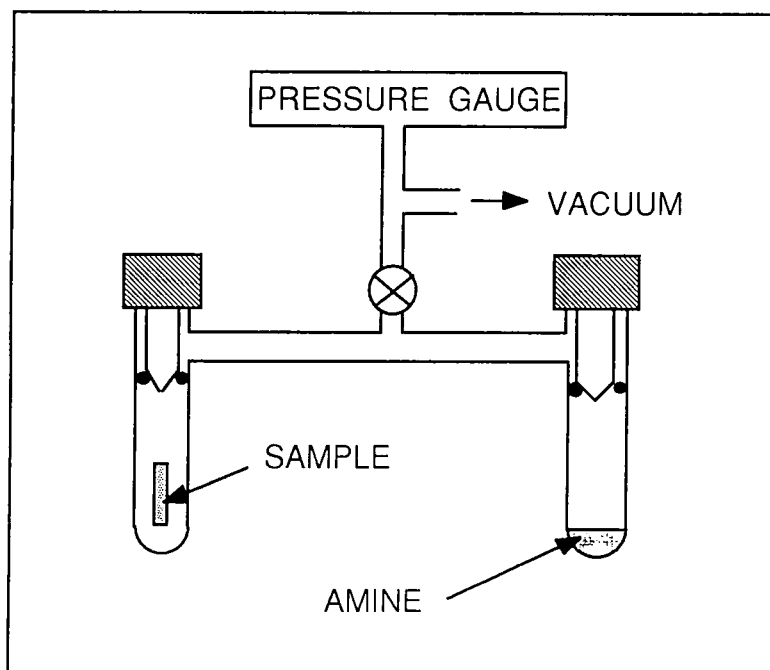
Figure 1. Vapor phase functionalization apparatus

as in Chapter 5. Instrumentally determined sensitivity factors were taken as C(1s) : O(1s) : F(1s) : N(1s) equals 1.00 : 0.55 : 0.67 : 0.74.

6.3   RESULTS

6.3.1   Characterization of Ethylene Maleic Anhydride Copolymer Films

The C(1s) XPS envelope obtained for ethylene maleic anhydride copolymer could be fitted to equal amounts of the following carbon functionalities:[8] hydrocarbon ($\underline{C}H_x$ ~ 285.0 eV), carbon adjacent to an anhydride group ($\underline{C}$-C-O(=O) ~ 285.8 eV), and an anhydride group (O=$\underline{C}$-O-$\underline{C}$=O ~ 289.4 eV), Figure 2(a); this is in good agreement with the theoretically predicted 1 : 1 : 1 ratio. The surface O : C ratio was measured to be 1.00 : 2.33 ± 0.02, which is slightly lower than the expected theoretical value of 1.00 : 2.00, and can be attributed to: the orientation of the anhydride groups away from the near surface towards the bulk, or the presence of a small amount of hydrocarbon contamination, or - $CH_2CH_2CH_2CH_2$- residues contained within the copolymer backbone.

Infrared absorption spectroscopy of the copolymer displayed vibrational features at:[4] 2947 cm^{-1} (CH_2 stretching), 1778 cm^{-1} and 1713 cm^{-1} (C=O in cyclic anhydride), 1460-1370 cm^{-1} (CH_2 deformations), and 1224 cm^{-1} (C-O in anhydride). A very weak absorption band was noted at 725 cm^{-1} associated with skeletal vibrations of -$CH_2CH_2CH_2CH_2$- residues[4] (this could account for the discrepancy between theoretically predicted and experimentally measured O : C XPS ratios).
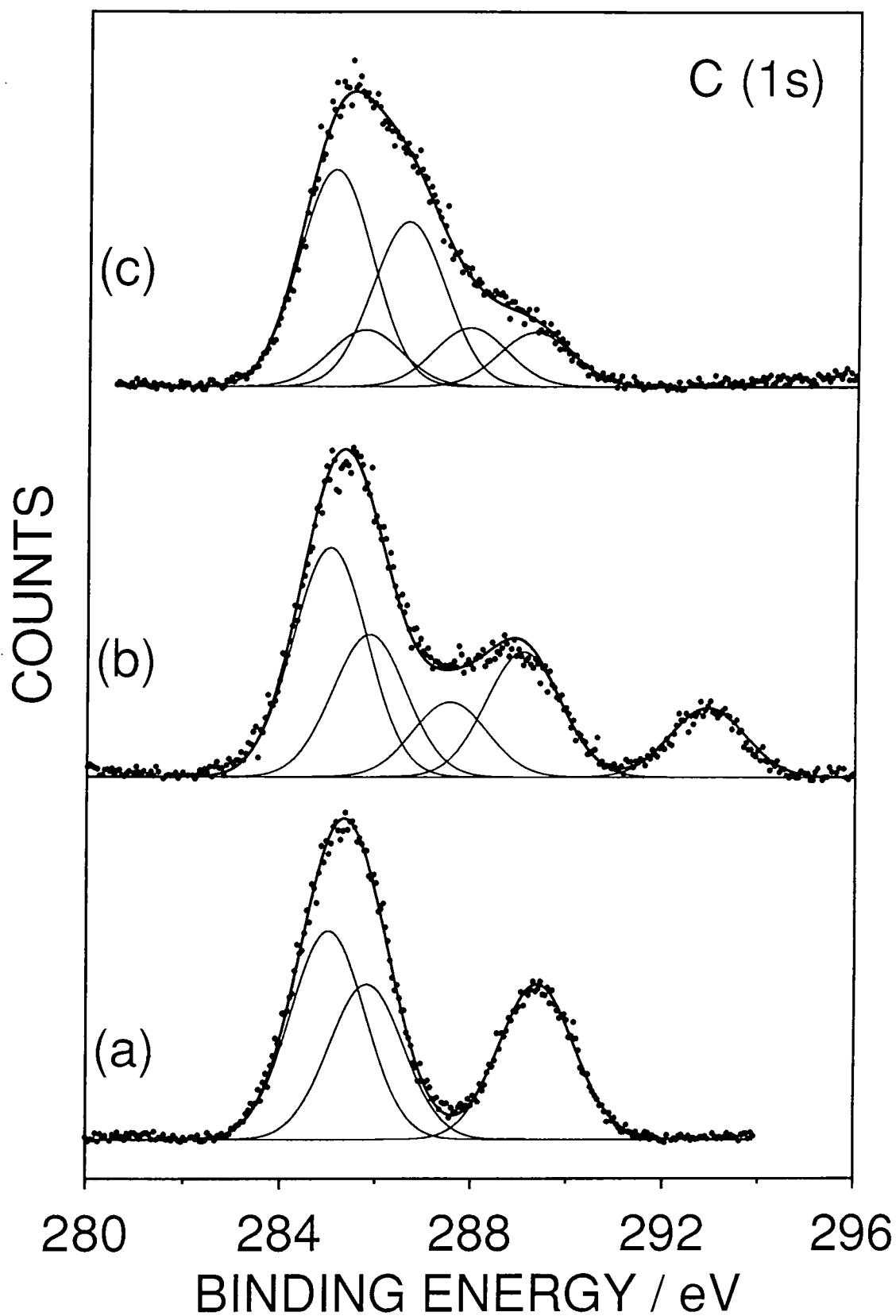
63

Figure 2. C(1s) XPS spectra of ethylene maleic anhydride copolymer:
(a) untreated; (b) functionalized with trifluoroethylamine; and (c) functionalized
with Jeffamine.

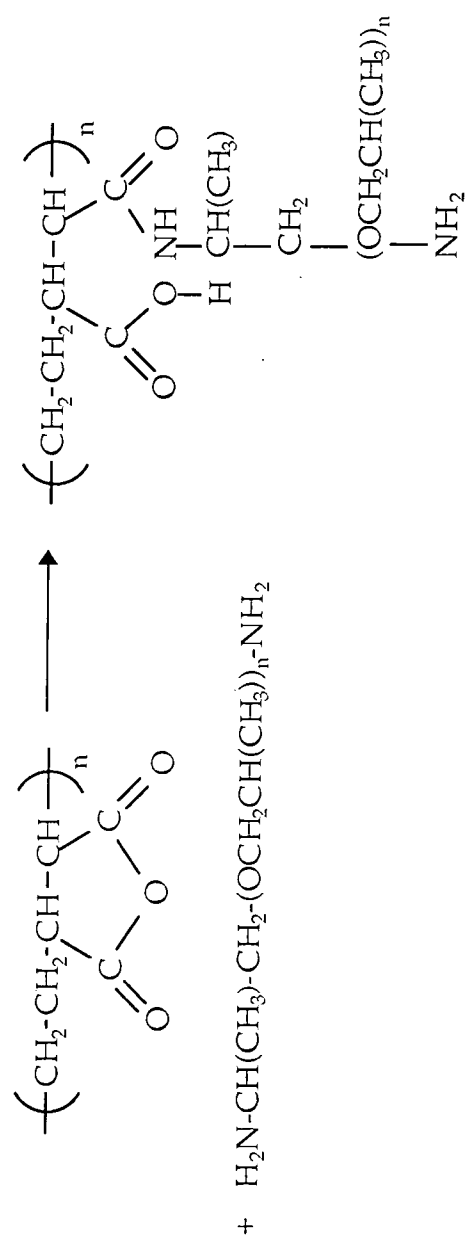### 6.3.2 Functionalization of the Copolymer Surface with Trifluoroethylamine

The high resolution C(1s) spectrum of ethylene maleic anhydride copolymer functionalized with trifluoroethylamine, Figure 2(b), can be fitted to five different carbon functionalities:[8] hydrocarbon ($\underline{C}H_x$ ~ 285.0 eV), carbon singly bonded to an amide / carboxylic acid group ($\underline{C}$-C-NHR(=O) / $\underline{C}$-C-OH(=O) ~ 285.7 eV), carbon singly bonded to nitrogen and to a trifluoromethyl carbon (N-$\underline{C}$-CF$_3$ ~ 287.3 eV), amide / carboxylic acid group (RHN-$\underline{C}$=O / O-$\underline{C}$=O ~ 289.1 eV), and trifluoromethyl carbon (-$\underline{C}$F$_3$ ~ 292.9 eV). The presence of the trifluoromethyl C(1s) peak, and the contribution of the three trifluoromethyl fluorines[8] (-C$\underline{F}_3$ ~687.7 eV) to the F(1s) region confirm that surface functionalization has indeed taken place.

The key reaction between polymeric derivatives of maleic anhydride and primary amines is aminolysis.[9] In the case of ethylene maleic anhydride copolymer and trifluoroethylamine, this leads to the formation of a half amide, as shown in Scheme 1. Overall aminolysis efficiency can be calculated from the measured surface nitrogen concentration following functionalization.[10,11] For each anhydride group which undergoes reaction, there should be an overall increase by six in the number of atoms detected using XPS (since H is not measured by this technique), corresponding to two carbon, one nitrogen, and three fluorine atoms. Thus by taking the conversion factor of anhydride to half amide groups as being x (where $x = 0$ in the case of no reaction and $x = 1$ in the case of complete reaction) and by assuming that all elements are homogeneously distributed within the XPS sampling depth both before and after

Scheme 1. Reaction of ethylene maleic anhydride copolymer with trifluoroethylamine.

$$\left(CH_2\text{-}CH_2\text{-}CH\text{-}CH\right)_n + CF_3\text{-}CH_2\text{-}NH_2 \longrightarrow \left(CH_2\text{-}CH_2\text{-}CH\text{-}CH\right)_n$$
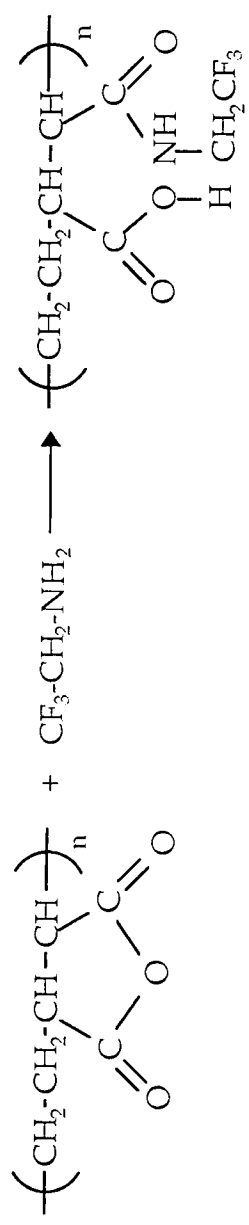
Scheme 2. Reaction of ethylene maleic anhydride copolymer with Jeffamine.

$$\left(CH_2\text{-}CH_2\text{-}CH\text{-}CH\right)_n + H_2N\text{-}CH(CH_3)\text{-}CH_2\text{-}(OCH_2CH(CH_3))_n\text{-}NH_2 \longrightarrow \left(CH_2\text{-}CH_2\text{-}CH\text{-}CH\right)_n$$

functionalization, the theoretical percentage concentration of surface nitrogen expected at conversion x can be predicted according to Equation 1:

$$\%[N] = \frac{[O]_0(1+x/3)}{[C]_0 + [O]_0(1+2x)} \times 100 \qquad \text{(Equation 1)}$$

where $[O]_0$ and $[C]_0$ are the oxygen and carbon concentration levels present in ethylene maleic anhydride copolymer prior to functionalization (which were determined by experiment to be 30 % and 70 % respectively). The actual nitrogen concentration at the surface of the functionalized copolymer can be measured from the area of the N(1s) XPS peak, Figure 3(b), and can be assigned to amide nitrogen[8] (RH$\underline{N}$-C=O ~ 401.9 eV). Therefore, a graph of experimental conversion factor (x) vs. reaction time can be plotted using the above equation, Figure 4(a). This shows that the aminolysis reaction proceeds with an initial rate of reaction x = 0.078 ± 0.02 min^{-1} (calculated from the slope of the graph) and a limiting level of nitrogen incorporation occurring after a reaction time of approximately 20 min. Assuming that all of the oxygen atoms present at the surface of the unreacted copolymer are associated with the anhydride functionality, then Equation 1 yields a conversion factor of x = 0.95 ± 0.01 following 100 min of reaction.
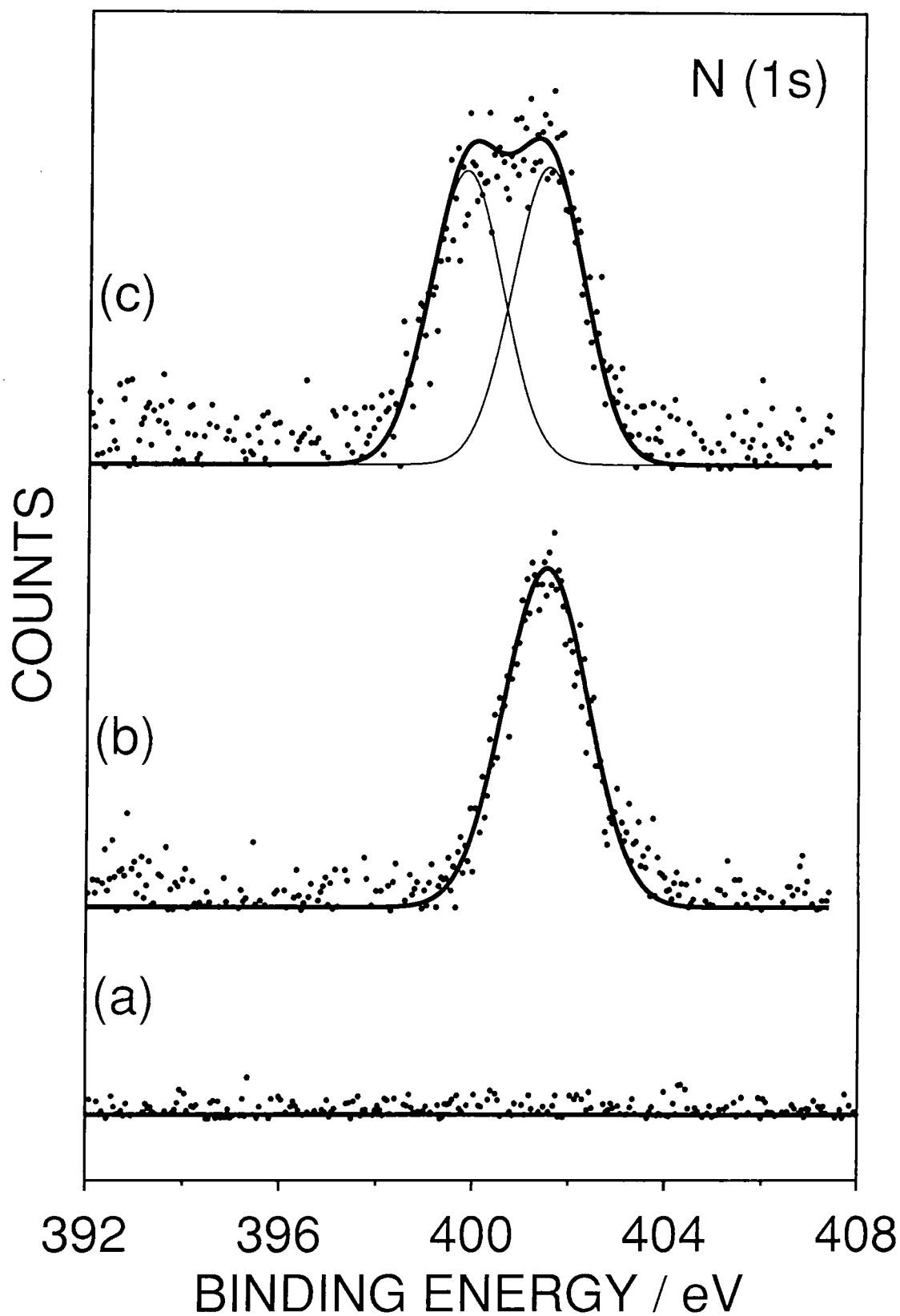
Figure 3. N(1s) XPS spectra of ethylene maleic anhydride copolymer:
(a) untreated; (b) functionalized with trifluoroethylamine; and (c) functionalized
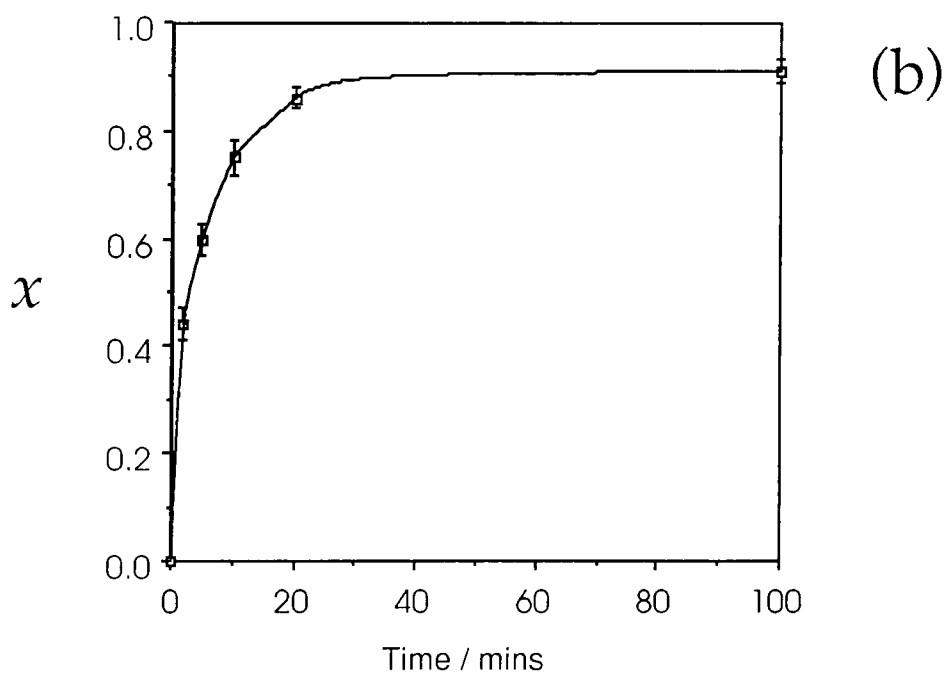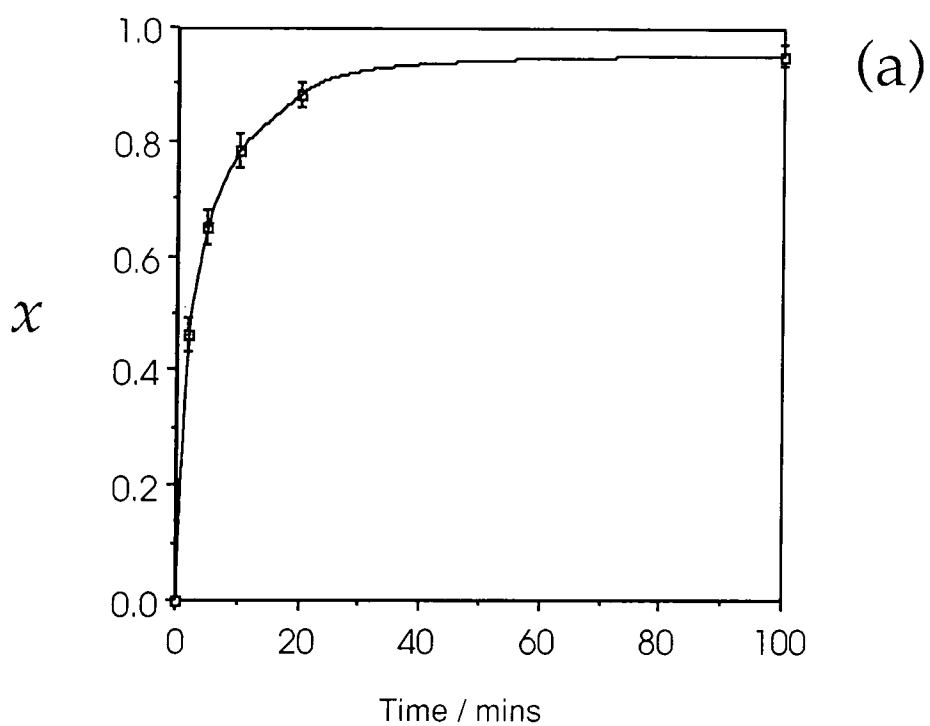with Jeffamine.

Figure 4. Experimental conversion factors (x) as a function of reaction time for ethylene maleic anhydride copolymer functionalized with (a) trifluoroethylamine and (b) Jeffamine.

6.3.3 Functionalization of the Copolymer Surface with Jeffamine

The reaction of poly(propyleneglycol)-bis (2-aminopropyl ether) (also known as Jeffamine) with ethylene maleic anhydride copolymer is described in Scheme 2. The C(1s) spectrum of the copolymer surface following reaction, Figure 2(c), could be fitted to five different functionalities:[8] hydrocarbon ($\underline{C}H_x$ ~ 285.0 eV), carbon singly bonded to an amide / carboxylic acid group or an amine group ($\underline{C}$-C-NHR(=O) / $\underline{C}$-C-OH(=O) / $\underline{C}$-NH$_2$ ~ 285.7 eV), carbon singly bonded to oxygen or singly bonded to an amide nitrogen (-$\underline{C}$-O / $\underline{C}$-NH-C=O ~ 286.5 eV), amide group (RHN-$\underline{C}$=O ~ 288.7 eV), and a carboxylic acid group (O-$\underline{C}$=O ~ 289.3 eV). The N(1s) XPS region comprises two components arising from amide (RH$\underline{N}$-C=O ~ 401.9 eV) and amine nitrogens (R-$\underline{N}$H$_2$ ~ 399.9 eV) in approximately equal concentrations, Figure 3(c), which is consistent with only one end of the Jeffamine molecule participating in the surface functionalization reaction.

The conversion factor has again been calculated by measuring the area of the N(1s) XPS peak following surface reaction, Figure 3(c). This extent of conversion was then plotted as a function of treatment time, Figure 4(b). The initial rate of reaction (x = 0.075 ± 0.02 min^{-1}) and overall conversion factor (x = 0.91 ± 0.02 after 100 min of reaction) for the copolymer functionalized with Jeffamine was comparable to that for trifluoroethylamine.

66

6.4   DISCUSSION

The reaction of ammonia or primary / secondary amines with anhydride groups is referred to as 'Nucleophilic Acyl Substitution'.[6] The tetrahedral intermediate, formed during nucleophilic attack on the anhydride group in the copolymer, expels one of the substituents originally bonded to the anhydride carbon centre resulting in the formation of a half amide, Scheme 3. In the case of maleic anhydride, the half amide derivative is named maleamic acid. Previous solution phase studies have shown that primary amines produce good to excellent yields of the N-alkylmaleamic acids, where the rate of reaction is found to rise with increasing basicity of the amine reagent.[4] The present surface functionalization results for ethylene maleic anhydride copolymer are consistent with this description.

It is important to note that the initial rates of reaction and overall yields for both trifluoroethylamine and Jeffamine are much higher than those found in corresponding experiments concerning the reaction of alcohols with maleic anhydride copolymer surfaces.[12] This can be attributed to the greater nucleophilicity of amines compared to alcohols.[9] Therefore, it can be deduced that, in the general case an amine of the type XCH_2NH_2 (where X could be a long alkyl chain, etc.) can be expected to undergo acylation at the maleic anhydride copolymer surface with high levels of conversion.

6.5   CONCLUSIONS

Vapour phase chemical functionalization of ethylene maleic anhydride copolymer surfaces with trifluoroethylamine and Jeffamine produces a half amide linkage, and is found to proceed to virtually 100 % conversion. The much higher reaction rates and yields obtained for amines compared to corresponding studies with alcohols can be attributed to the greater nucleophilicity of the former.

REFERENCES

[1]   Ho, R. M.; Su, A. C.; Wu, C. H.; Chen, S. I. *Polymer* **1993**, *34*, 3264.

[2]   Chilkoti, A.; Ratner, B. D.; Briggs, D. *Chem. Mater.* **1991**, *3*, 51.

[3]   Hamilton, L. M.; Green, A.; Edge, S.; Badyal, J. P. S.; Feast, W. J.; Pacynko, W. F. *J. Appl. Poly. Sci.* **1994**, *52*, 413.

[4]   Trivedi, B. C.; Culbertson, B. M. *Maleic Anhydride*; Plenum: New York, **1982**.

[5]   Everhart, D. S.; Reilley, C. S. *Anal. Chem.* **1981**, *53*, 665.

[6]   Nakayama, Y.; Takahagi, T.; Soeda, F.; Hatada, K.; Nagaoka, S.; Suzuki, J.; Ishitani, A. *J. Polym. Sci.* **1988**, *26*, 559.

[7]   Tasker, S.; Badyal, J.P.S. *Polymer* **1994**, *35*, 22.

[8]   Beamson, G.; Briggs, D. *High Resolution XPS of Organic Polymers*; Wiley: Chichester, **1992**.

[9]   McMurry, J. *Organic Chemistry*; Brooks/Cole: California, **1988**; pp 652-653.

[10]   Sutherland, I.; Sheng, E.-S.; Brewis, M.; Heath, R.J. *J. Mater. Chem.* **1994**, *4*, 683.

[11]   Popat, R.P.; Sutherland, I.; Sheng, E.-S. *J. Mater. Chem.* **1995**, *5*, 713.

[12]   Evenson, S.A.; Badyal, J.P.S. *To be Published.*

CHAPTER 7

SURFACE FUNCTIONALIZATION OF MALEIC

ANHYDRIDE PLASMA POLYMER FILMS

7.1   INTRODUCTION

Polymeric surfaces containing anhydride groups are widely sought after since they can improve interfacial adhesion[1] and polymer/polymer compatibility,[2] as well as being able to undergo functionalization reactions.[3] Conventional homopolymerization,[4] copolymerization,[5] and graft polymerization[6] of maleic anhydride have all been extensively studied in the past. These methods tend to suffer from a lack of control over the concentration of surface anhydride groups, thereby severely restricting their suitability for subsequent functionalization reactions.   More recently, it has been demonstrated that pulsed plasma polymerization of maleic anhydride can yield well-adhered polymeric layers, where the overall anhydride incorporation can be controlled by varying the specific electrical discharge parameters (e.g. duty cycle, power, etc.).[7] Clearly, this approach offers great scope for tailoring surfaces of complex shaped solid substrates via subsequent chemical functionalization reactions. For instance, anhydride groups are susceptible to nucleophilic attack by amines, alcohols, etc.[8] Whereas alternative reaction conditions require organic solvents[9-11] or molten polymer (reactive extrusion)[12,13] in conjunction with elevated temperatures and/or pressures, here we describe the direct vapour-phase functionalization of pulsed maleic anhydride plasma polymer surfaces using 2,2,2-trifluoroethylamine and Jeffamine®-D. The former was chosen as a model nucleophile in order to demonstrate the viability of the proposed reaction methodology, whilst surfaces functionalized with the latter reagent are of potential interest for biomedical purposes.[14]

71

7.2   EXPERIMENTAL

Briquettes of maleic anhydride (Aldrich, 99% purity) were ground into a fine powder and loaded into a monomer tube. Plasma polymerization experiments were carried out in an electrodeless cylindrical glass reactor (4.5 cm diameter, 460 cm^3 volume, base pressure of 5.2×10^{-3} mbar, with a leak rate lower than 1.0×10^{-10} kg s^{-1}) enclosed in a Faraday cage. The reactor was fitted with a gas inlet, a thermocouple pressure gauge, a 30 L min^{-1} two-stage rotary pump attached to a liquid nitrogen cold trap, and an externally wound copper coil (4 mm diameter, 9 turns, spanning 8 - 15 cm from the gas inlet). All joints were grease free. An L-C matching network was used to match the output impedance of the R.F. generator (13.56 MHz) to that of the partially ionized gas load; this was achieved by minimising the standing wave ratio (SWR) of the transmitted power. Pulsed plasma polymerization experiments were carried out by using a signal generator to trigger the R.F. power supply. A cathode ray oscilloscope was used to monitor the pulse width and amplitude. The average continuous wave power output (P_{cw}) of the R.F. supply spanned 5 - 90 W. Pulse on-times (t_{on}) and off-times (t_{off}) could be varied between 5 - 800 and 5 - 1200 μs respectively. The average power <P> delivered to the system during pulsing was calculated using the following expression: $<P> = P_{cw} \{ T_{on} / (T_{on} + T_{off}) \}$ where $T_{on} / (T_{on} + T_{off})$ is defined as the duty cycle.[15]

Prior to each experiment, the reactor was cleaned by scrubbing with detergent, rinsing in isopropyl alcohol, followed by oven drying and a 30 min high-power (50 W) air plasma treatment. The reactor was then vented to air and

the substrate to be coated placed at the centre of the chamber followed by evacuation back down to base pressure. Subsequently, the monomer vapour was introduced into the reaction chamber at a constant pressure of 2.6×10^{-1} mbar (the vapour pressure of maleic anhydride at room temperature), and a flow rate of approximately 1.6×10^{-9} kg s^{-1}. At this stage, the plasma was ignited and run for 10 min. Upon completion of deposition, the R.F. generator was switched off, and the monomer feed allowed to continue to flow through the system for a further 5 min prior to opening up to atmospheric pressure.

Next, the deposited maleic anhydride pulsed plasma polymer coatings were reacted with either 2,2,2-trifluoroethylamine (Fluorochem, 99.5%) or Jeffamine®-D [poly(propylene glycol) bis(2-aminopropyl ether)] (Aldrich, average molecular weight $M_n = 230$) in a vapor-phase labelling apparatus, Figure 1.[16] The reaction procedure and XPS / IR experiments were carried out as in Chapter 5. Instrumentally determined sensitivity factors were taken as C(1s) : O(1s) : F(1s) : N(1s) equals 1.00 : 0.55 : 0.67 : 0.74. XPS measurements were carried out to chemically analyse the surfaces before and after functionalization to verify the attachment of the amines.

The stability of the Jeffamine functionalized maleic anhydride plasma polymer layers towards washing was examined in the presence of a range of polar and nonpolar solvents: (i) water, (ii) methanol, (iii) chloromethane, (iv) hexane, and (v) toluene. Following removal of the coated substrate from each solvent, the surface was examined by XPS to check for any chemical changes.
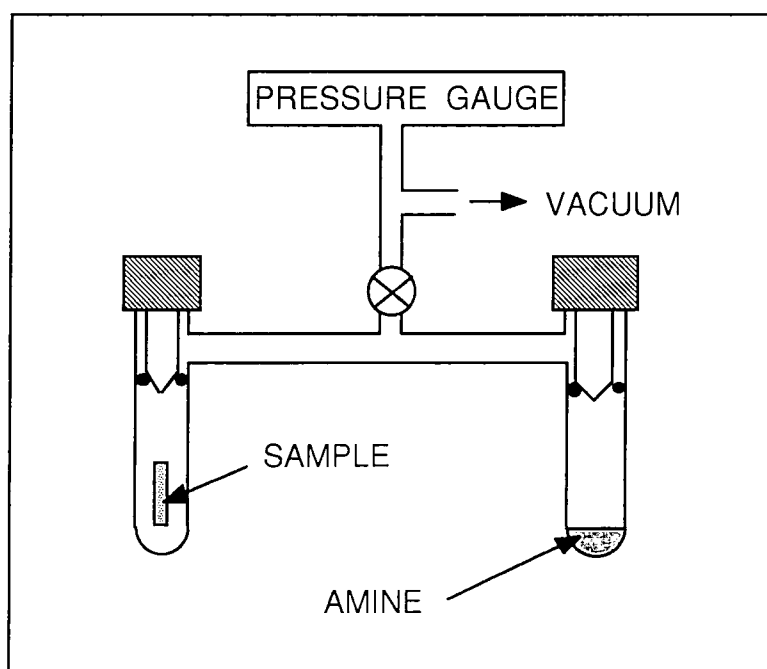
Figure 1. Vapour phase functionalisation apparatus.

7.3 RESULTS

7.3.1 Plasma Polymerization of Maleic Anhydride

Plasma polymerization of maleic anhydride produced a well-adhered coating containing a variety of oxygenated carbon functionalities. Complete coverage of the substrate was confirmed by checking for the absence of any XPS signals peering through from the underlying substrate (e.g. Si(2p) in the case of glass slides). Pulsing the electrical discharge on the μs - ms timescale provided control over the coating composition (i.e. the concentration of anhydride functionalities). Typical ranges are quoted in Table 1. Greater retention of anhydride functionalities could be achieved at low duty cycles compared to continuous wave conditions.[7]

The high resolution C(1s) XPS spectra of maleic anhydride pulsed plasma polymer deposited under optimum conditions for anhydride group retention (P_{cw} = 5W, T_{on} = 20 μs, and T_{off} = 1200 μs) is shown in Figure 2(a), and could be fitted to five different types of carbon functionality:[17] hydrocarbon ($\underline{C}H_x$ ~ 285.0 eV), carbon singly bonded to an anhydride group ($\underline{C}$-C(O)=O ~ 285.7 eV), carbon singly bonded to oxygen (-$\underline{C}$-O ~ 286.6 eV), carbon doubly bonded to oxygen (O-$\underline{C}$-O / -$\underline{C}$=O ~ 289.1 eV), and anhydride groups (O=$\underline{C}$-O-$\underline{C}$=O ~ 289.4 eV).

Corresponding infrared analysis displayed absorbance bands which were consistent with a maleic anhydride plasma polymer layer:[7,18] 1849 cm^{-1} and 1780 cm^{-1} (asymmetric and symmetric C=O stretch in cyclic anhydrides), 1238 - 1135

	O : C Ratio	% Anhydride Carbon Centres
Continuous Wave (5W)	0.18 ± 0.02	10 ± 0.05
Pulsed (Low Duty Cycle)	$0.25 - 0.43 \pm 0.02$	$11 - 29 \pm 0.02$
Maleic Anhydride Monomer	0.75	50

Table 1. A comparison between typical compositions for the maleic anhydride plasma polymer coatings and the starting monomer.

Figure 2. C(1s) XPS spectra of the maleic anhydride pulsed plasma polymer layer: (a) untreated; and functionalised with (b) trifluoroethylamine; and (c) Jeffamine.
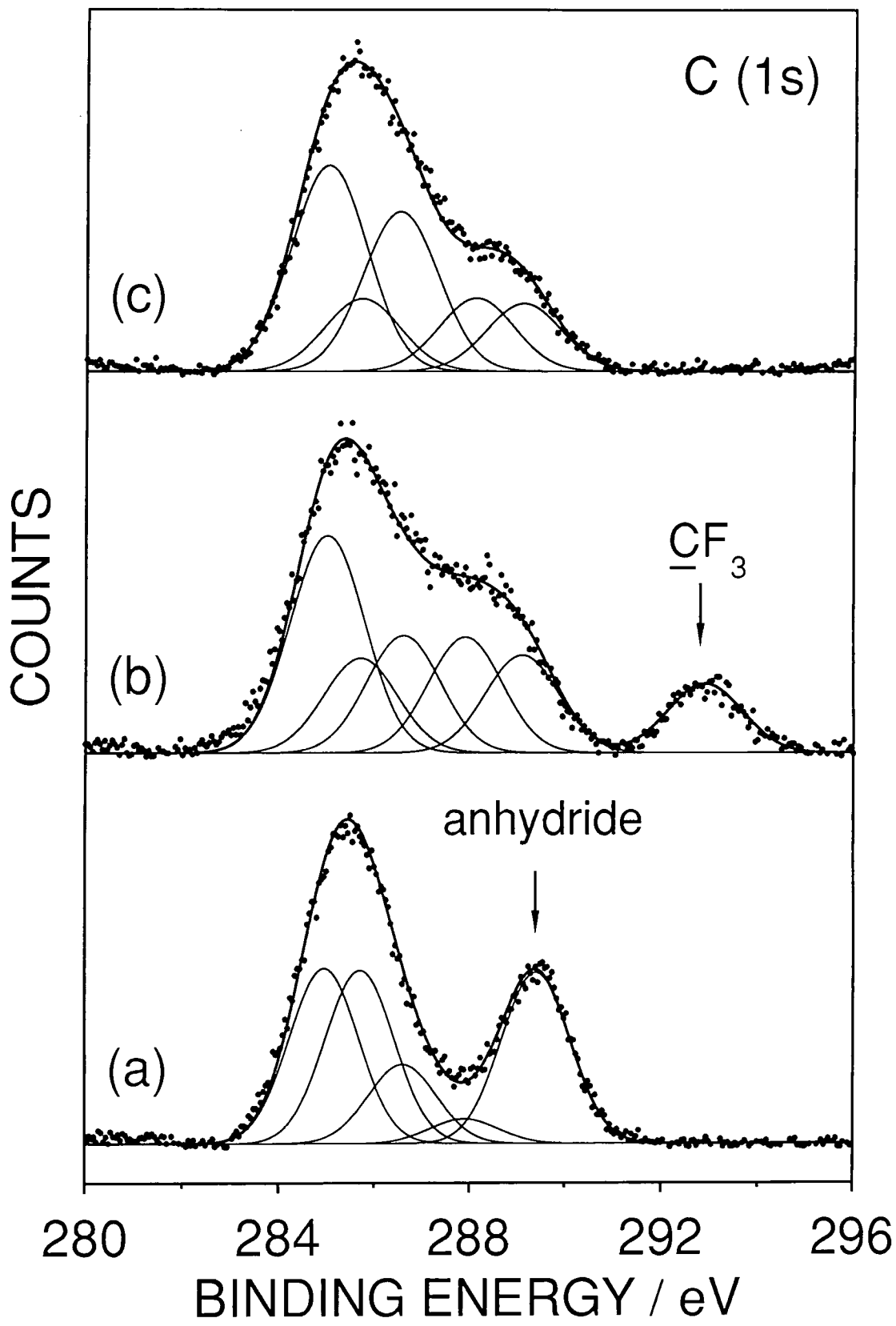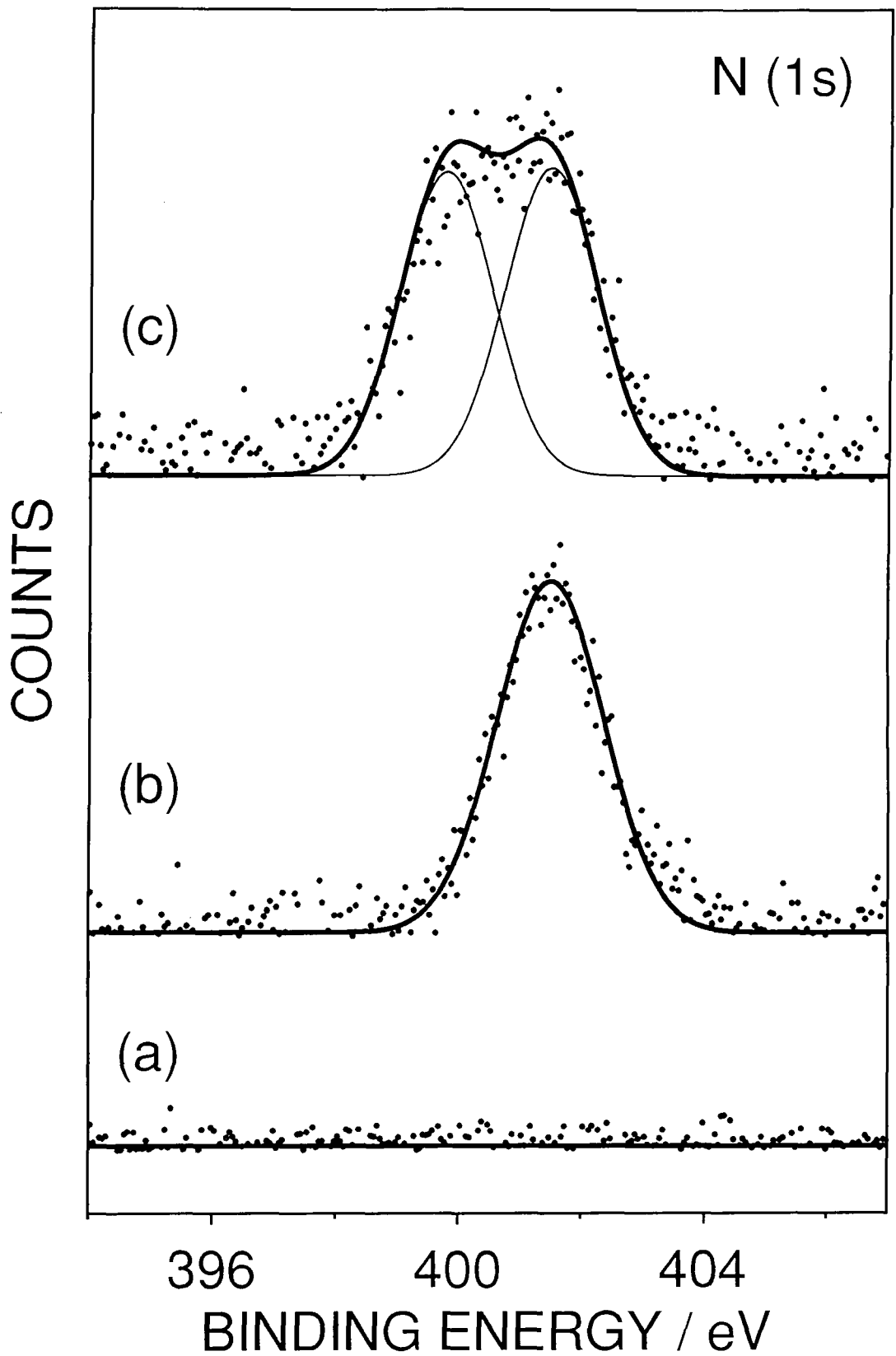
Figure 3. N(1s) XPS spectra of the maleic anhydride pulsed plasma polymer layer: (a) untreated; and functionalised with (b) trifluoroethylamine; and (c) Jeffamine.

cm^{-1} and 980 - 902 cm^{-1} (anhydride group stretching vibrations in cyclic anhydrides), and 1110 - 1056 cm^{-1} (C-O stretch in cyclic anhydrides), Figure 4(a).

7.3.2 Functionalisation Reactions with Trifluoroethylamine

A key reaction between maleic anhydride and primary amines is aminolysis.[19] The deposited maleic anhydride pulsed plasma polymer layer was exposed to trifluoroethylamine, with the aim of producing half amide linkages at the surface, as depicted in Scheme 1 (Chapter 6). The C(1s) XPS spectra following reaction, Figure 2(b), could be fitted to five different types of carbon functionality:[17] hydrocarbon (CH$_x$ ~ 285.0 eV), carbon singly bonded to an amide / carboxylic acid group (C-C-NHR(=O) / C-C-OH(=O) ~ 285.7 eV), carbon singly bonded to both nitrogen and a trifluoromethyl carbon (N-C-CF$_3$ ~ 287.3 eV), amide / carboxylic acid group (RHN-C=O / O-C=O ~ 289.1 eV), and trifluoromethyl carbon (-CF$_3$ ~ 292.9 eV). The unambiguous assignment of the trifluoromethyl C(1s) peak, as well as the contribution from the three trifluoromethyl fluorines (-CF$_3$ ~687.7 eV)[17] to the F(1s) region, confirmed that surface functionalisation had indeed taken place. The N(1s) XPS peak areas were used to calculate the overall aminolysis efficiency since the amide nitrogens (RHN-C=O ~ 401.9 eV)[17] can be taken as a measure of surface nitrogen concentration following functionalisation, Figure 3(b).[19,20] Reaction between the plasma polymer and trifluoroethylamine eventually reached a limiting level of nitrogen incorporation around 30 mins exposure, which corresponds to an overall conversion factor of 0.93 ± 0.01 down to a depth of at least 2.5 nm.[17]
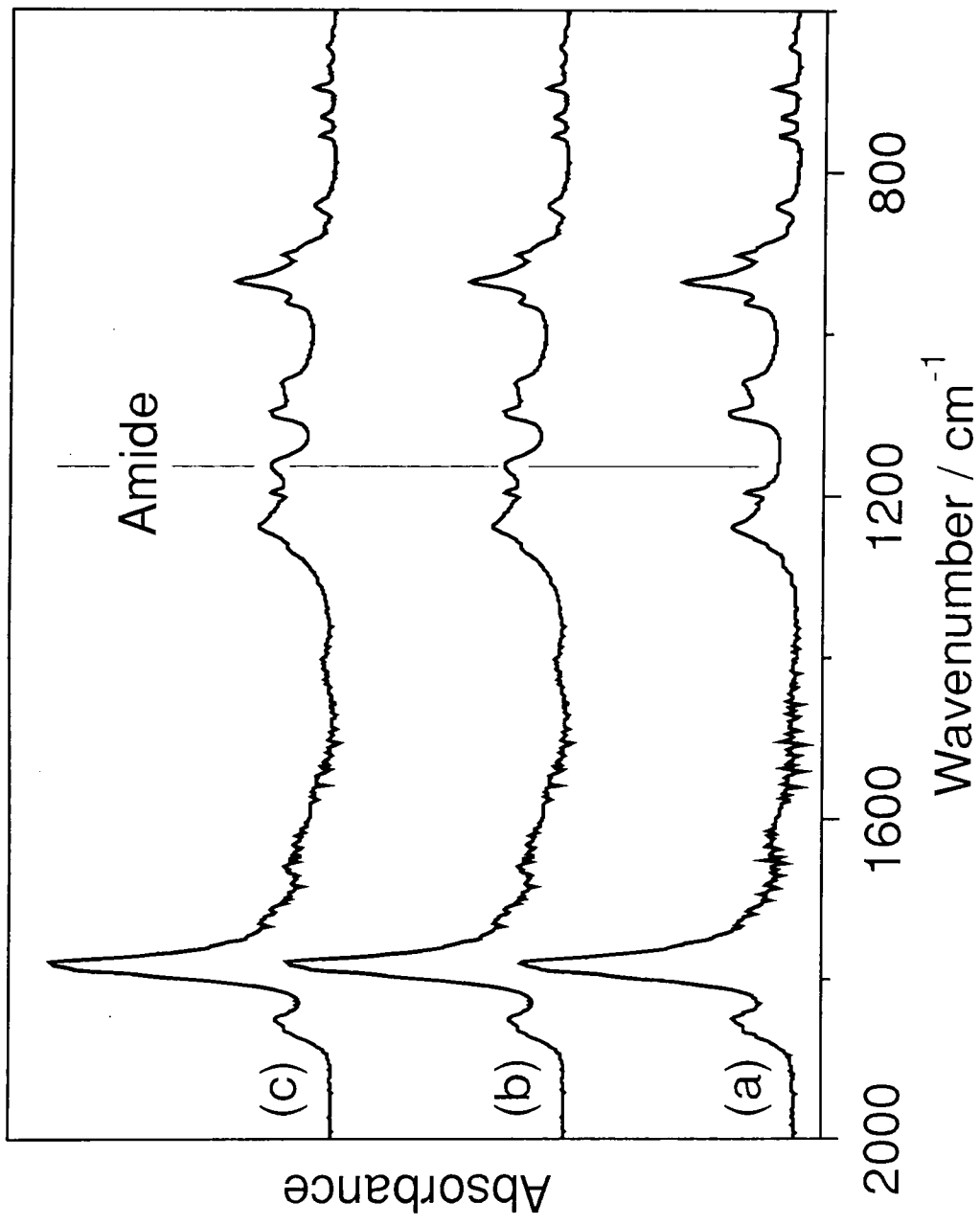
Figure 4. Infrared absorbance spectra of the maleic anhydride pulsed plasma polymer layer: (a) untreated; and functionalised with (b) trifluoroethylamine; and (c) Jeffamine.

Infrared spectroscopy also provided evidence the formation of half amide linkages as seen by the appearance of new absorbances at:[18] 1656 cm^{-1} (amide I and amide II bands overlapping), 1280 cm^{-1} (carboxylic acid stretch), 1153 cm^{-1} (non-cyclic anhydride stretch), Figure 4(b). All of these features can be attributed to the opening up of the cyclic anhydrides to yield carboxylic acid and amide groups. The apparent discrepancy between the disproportionately higher intensities of anhydride group absorbance bands at 1849 cm^{-1} and 1780 cm^{-1} compared to what would be expected on the basis of the 0.93 ± 0.01 conversion factor obtained by XPS indicates that the aminolysis reaction occurs only at the surface of the plasma polymer whilst leaving the underlying anhydride groups unfunctionalised (since the infrared sampling depth is far greater than the 2.5 nm sensitivity of XPS).[18]

7.3.3   Functionalisation Reactions with Jeffamines

Reaction between the maleic anhydride pulsed plasma polymer layer and Jeffamine-D resulted in the stable attachment of Jeffamines onto the substrate, Sch. 2 Ch. 6. In this case, five different carbon functionalities were identified in the C(1s) XPS spectra, Figure 2(c):[17] hydrocarbon ($\underline{C}H_x \sim 285.0$ eV), carbon singly bonded to amide / carboxylic acid groups or amine groups ($\underline{C}$-C-NHR(=O) / $\underline{C}$-C-OH(=O) / $\underline{C}$-NH$_2$ ~ 285.7 eV), carbon singly bonded to oxygen or singly bonded to amide nitrogen (-$\underline{C}$-O / $\underline{C}$-NH-C=O ~ 286.5 eV), amide groups (RHN-$\underline{C}$=O ~ 288.7 eV), and carboxylic acid groups (O-$\underline{C}$=O ~ 289.3 eV). Also, the N(1s) XPS region indicated the presence of two types of nitrogen environment

corresponding to amide (RH$\underline{N}$-C=O ~ 401.9 eV)[17] and amine groups (R-$\underline{N}$H$_2$ ~ 399.9 eV)[17] in approximately equal concentrations, Figure 3(c); this suggests that only one end of the Jeffamine molecule has undergone reaction with the maleic anhydride plasma polymer surface, Scheme 2. On this basis, the extent of conversion was calculated to be 0.91 ± 0.02 from the N(1s) peak areas after 30 min reaction time. Again, the appearance of new bands in the infrared spectra at:[18] 1656 cm^{-1} (overlapping amide I and amide II bands), 1280 cm^{-1} (carboxylic acid stretch), and 1153 cm^{-1} (non-cyclic anhydride stretch) confirms that the surface anhydride rings have undergone opening to form carboxylic and amide groups, Figure 4(c).

7.3.4 Solubility Experiments

The stability of these surfaces was checked by comparing the C(1s) XPS spectra taken for the Jeffamine functionalized maleic anhydride plasma polymer layers both before (*), and after (i - v) washing in a range of solvents, Figure 5. The similarity between all of these spectra as well as a good correlation between the O : C : N elemental ratios prior to and following solvent washing confirmed that the plasma polymer layer is indeed well-adhered to the underlying substrate, and also that the Jeffamines are securely bonded to the coating surface.
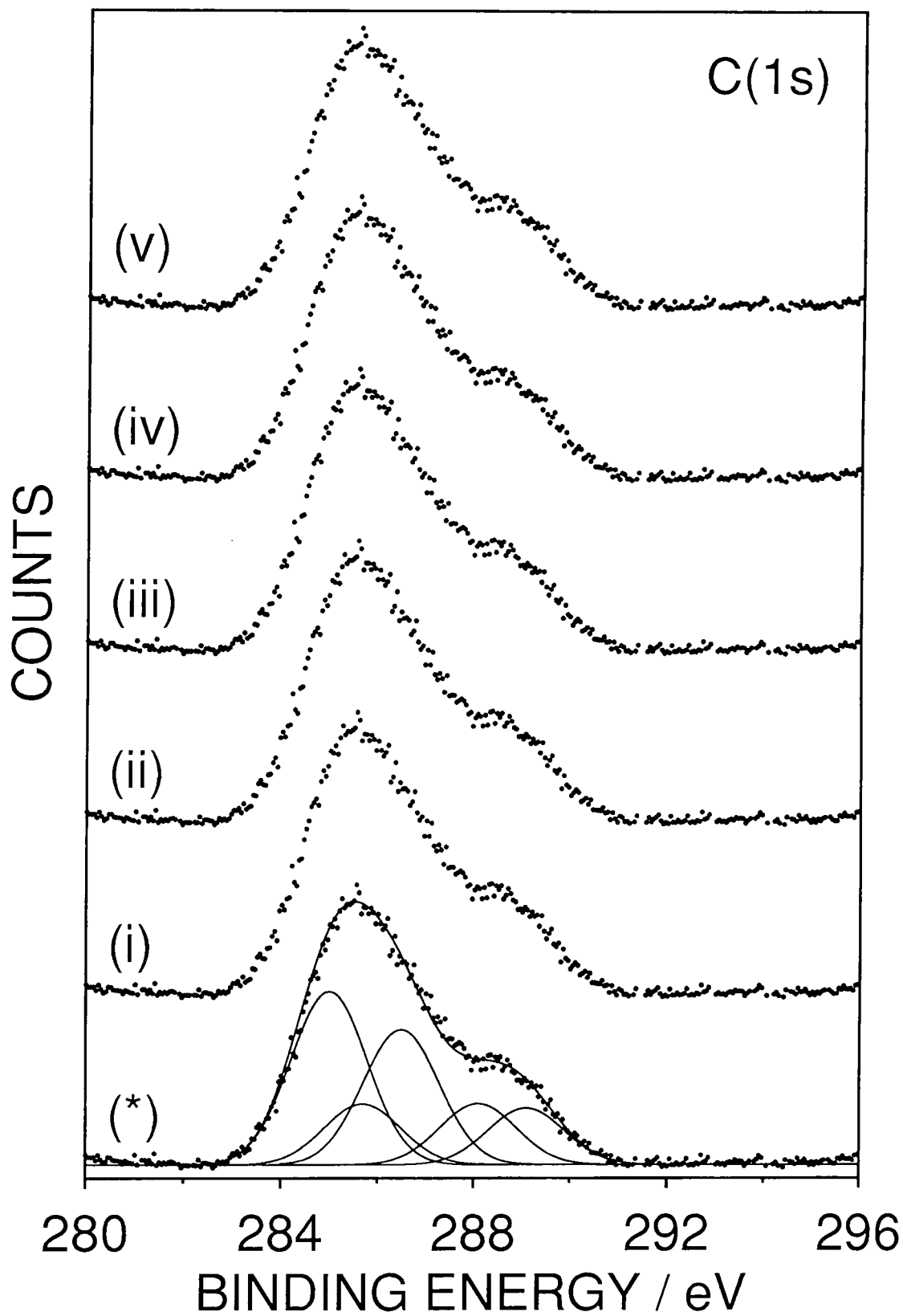
Figure 5. C(1s) XPS spectra of the Jeffamine functionalised maleic anhydride pulsed plasma polymer layer: (∗) before washing; and after washing in (i) water, (ii) methanol, (iii) chloromethane, (iv) hexane, and (v) toluene.

7.4 DISCUSSION

A wide range of polymers including urethanes, silicones, methacrylates, hydrogels, fluorocarbons, and polyolefins are used in biomedical applications.[21] Since only the surfaces of these polymers are exposed to the biological environment, it is the interfacial properties of the biomedical material which ultimately govern the success, failure, or rejection of the device. In the past it has been shown that radiation grafting of monomers onto inert polymeric supports can produce materials which combine the desirable surface properties of the graft with the good mechanical properties of the underlying substrate,[22] although the total number of grafting sites can be limited by the nature of the copolymer backbone. Continuous wave plasma deposition of thin films has also been used within this context,[23] however the use of derivatization techniques have shown that the concentration of desired functional groups tends to be low due to extensive fragmentation of the precursor during deposition.[23] More recently, it has been demonstrated that pulsed plasma polymerization can lead to a dramatic improvement in the extent of functional group retention at low duty cycles as a result of less fragmentation of the precursor molecule, reduced damage of the growing plasma polymer layer during the duty cycle on-time, as well as radical-initiated polymerization within the off-period.[7,24]

In the case of pulsed plasma polymerization of maleic anhydride , the high density of surface anhydride groups enables extensive vapour-phase aminolysis. This approach alleviates the drawbacks associated with conventional solution-phase and extrusion techniques (e.g. reorientation of

surface functional groups and solvent extraction of low molecular weight species).[25] The overall measured reaction yields for 2,2,2-trifluoroethylamine and Jeffamine-D correlate well with previously reported values for the vapour-phase aminolysis of ethylene maleic anhydride copolymer surfaces.[26] Furthermore, whereas functionalized maleic anhydride copolymers can be removed by solvent washing,[27] the current method produces well-adhered polymer networks which overcome these limitations.

Such an ability to be able to tailor stable, functionalized plasma polymer layers makes this methodology attractive for an extensive range of applications. These include the control of hydrophilicity, biocompatability,[14] stabilizing dispersions and polymer blends,[13] modification of polymer adsorption characteristics,[11] ion conducting membranes, thin film electrodes,[27] and catalysts.

7.5   CONCLUSIONS

Amine terminated nucleophiles can be chemically fixed onto any shaped solid substrate via reaction with a well-adhered maleic anhydride pulsed plasma polymer layer.   The intermolecular spacing and concentration of amine molecules attached to the surface can be engineered to a pre-selected level by controlling the level of anhydride group incorporation during deposition of the plasma polymer coating or alternatively by changing the reaction time between the amine and the plasma polymer surface.

REFERENCES

[1] Hindryckx, F.; Dubois, P.; Patin, M.; Jerome, R.; Teyssie, P. *J. Appl. Poly. Sci.* **1995**, *56*, 1093.

[2] Oostenbrink, A. J.; Gaymans, R. J. *Polymer* **1992**, *31*, 3086.

[3] Gaboury, S. R.; Urban, M. W. *Langmuir* **1994**, *10*, 2289.

[4] Tsiourvas, D.; Paleos, C. M. ; Dais, P.; *J. Appl. Poly. Sci.* **1989**, *38*, 257.

[5] Kuo, P. -L.; Ni, S. - C.; Lai, C. -C. *J. Appl. Poly. Sci.* **1992**, *45*, 611.

[6] Samay, G.; Nagy, T.; White, J. L. *J. Appl. Poly. Sci.* **1995**, *56*, 1423.

[7] Ryan, M. E.; Hynes, A. M.; Badyal, J. P. S.; *Chem. Mater.* **1996**, *8*, 37.

[8] Trivedi, B. C.; Culbertson, B. M. *Maleic Anhydride*; Plenum: New York, **1982**.

[9] Harris, R. F.; Lopez, K. M *J. Appl. Poly. Sci.* **1993**, *50*, 559.

[10] Harris, R. F.; DePorter, C. D.; Potter, R. B. *Macromolecules* **1991**, *24*, 2973.

[11] Felix, J. M.; Gatenholm, P. *J. Appl. Poly. Sci.* **1991**, *42*, 609.

[12] Vermeesch, I.; Groeninckx, G. *J. Appl. Poly. Sci.* **1994**, *53*, 1365.

[13] Koning, C.; Ikker, A.; Borggreve, R.; Leemans, L.; Moller, M. *Polymer* **1993**, *34*, 4410.

[14] Dérand, H.; Wesslén, B. *J. Poly. Sci.: Part A* **1995**, *33*, 571.

[15] Savage, C. R.; Timmons, R. B. *Chem. Mater.* **1991**, *3*, 575.

[16] Tasker, S.; Badyal, J. P. S. *Polymer* **1994**, *35*, 22.

[17] Beamson, G.; Briggs, D. *High Resolution XPS of Organic Polymers*; Wiley: Chichester, **1992**.

[18]   Silverstein, R. M.; Bassler, G. C.; Morril, T. C. *Spectrometric Identification of Organic Compounds*; Wiley: Singapore, **1991**.

[19]   Sutherland, I.; Sheng, E.-S.; Brewis, M.; Heath, R.J. *J. Mater. Chem.* **1994**, *4*, 683.

[20]   Popat, R.P.; Sutherland, I.; Sheng, E.-S. *J. Mater. Chem.* **1995**, *5*, 713.

[21]   Castner, D. G.; Ratner, B. D. *J. Vac. Sci. Technol. A* **1988**, *6*, 964.

[22]   Cohn, D.; Hoffman, A. S.; Ratner, B. D. *J. Appl. Poly. Sci.* **1984**, *29*, 2645.

[23]   Chilkoti, A.; Ratner, B. D.; Briggs, D. *Chem. Mater.* **1991**, *3*, 51.

[24]   Rinsch, C. L.; Chen, X.; Panchalingham, V.; Everhart, R. C.; Wang, J.; Timmons, R. B. *Langmuir* **1996**, *12*, 2995.

[25]   Nakayama, Y.; Takahagi, T.; Soeda, F.; Hatada, K.; Nagaoka, S.; Suzuki, J.; Ishitani, A. *J. Polym. Sci.* **1988**, *26*, 559.

[26]   Evenson, S. A.; Badyal, J. P. S. *To be Published.*

[27]   Rietman, E. A.; Kaplan, M. L. *J. Poly. Sci. C: Poly. Letts.* **1990**, *28*, 187.

CHAPTER 8

CHEMICAL ATTACHMENT OF PAMAM

DENDRIMERS TO SOLID SURFACES

8.1   INTRODUCTION

Dendrimers are highly ordered, three dimensional, tree-like, functional polymers which comprise branched repeat units emanating from a central core.[1] This type of structure can give rise to high solubility, whist the presence of many terminal groups offers a large number of reactive sites.[2] Potential applications for dendritic polymers include:[3] nanoscale catalysts, micelle mimics, drug delivery agents, chemical sensors, high performance polymers, adhesives, and coatings.

Most previous studies aimed at producing dendritic coatings have attempted to use solvent casting methods.[4-11] Various combinations of dendrimers and solvents have been examined in conjunction with different types of substrate (Table 1). The major drawback associated with this approach is understood to be the poor adhesion between the dendrimer coating and the substrate. Covalent attachment of dendrimers to solid surfaces was first achieved by using an intermediate mercaptoundecanoic acid (MUA) self-assembled monolayer (SAM) deposited onto gold,[14] thereby enabling amine terminated dendrimers to bond to gold via amide linkages with the SAM. The limited choice of substrate and the inability to control the concentration of reactive groups at the surface of the SAM restricts the more widescale applicability of this technique.

Here we describe an alternative methodology which allows amine terminated dendrimers to be bonded, at a predetermined concentration, onto any type of solid substrate. First, a maleic anhydride plasma polymer coupling

Dendrimer	Substrate	Deposition Method	Structure	Analysis	Ref.
Phenylacetylene	Carbon coated mica sheets	Solvent cast from toluene	Crystallites	TEM	4
PS, PEG, PEO - Dendrimer block copolymers	Glass	Solvent cast from THF	Spherulites, axialites, dendritic films	Optical	5, 6
PS - poly(propyleneimine) block copolymer	Not stated	Solvent cast	Large network structures	TEM	7
Carbosiloxane	Mica, pyrolytic graphite	Solvent cast from hexane	Single molecules, complete layer	SFM	8
PAMAM (G = 9.5)	Silicon	Solvent cast from methanol	Dendritic cells, microfibrils	AFM, optical	9
PAMAM (G = 4)	Modified silicon oxide (glass, Si wafer, ITO slides)	Solvent cast from methanol	Thin film covered in Au colloids	XPS, FTIR, AFM	10, 11
Polyether	Water	Film compressed in Langmuir trough	Bilayer structure	Neutron reflectivity	12
Octaferrocenyl	Pt wire electrode	Redox reaction	Sheet like compact morphology	SEM	13
PAMAM (G = 0,2,4,6,8)	Gold	Covalently attached via a MUA self assembled monolayer on Au	Monolayer	XPS	14

Table 1. Previously reported dendrimer modified substrates.

layer is deposited, where the level of anhydride functional group incorporation into the coating can be controlled by altering the electrical discharge parameters (e.g. duty cycle, power, etc.). Amine terminated dendrimers are then able to react with this well-adhered plasma polymer layer, Scheme 1:
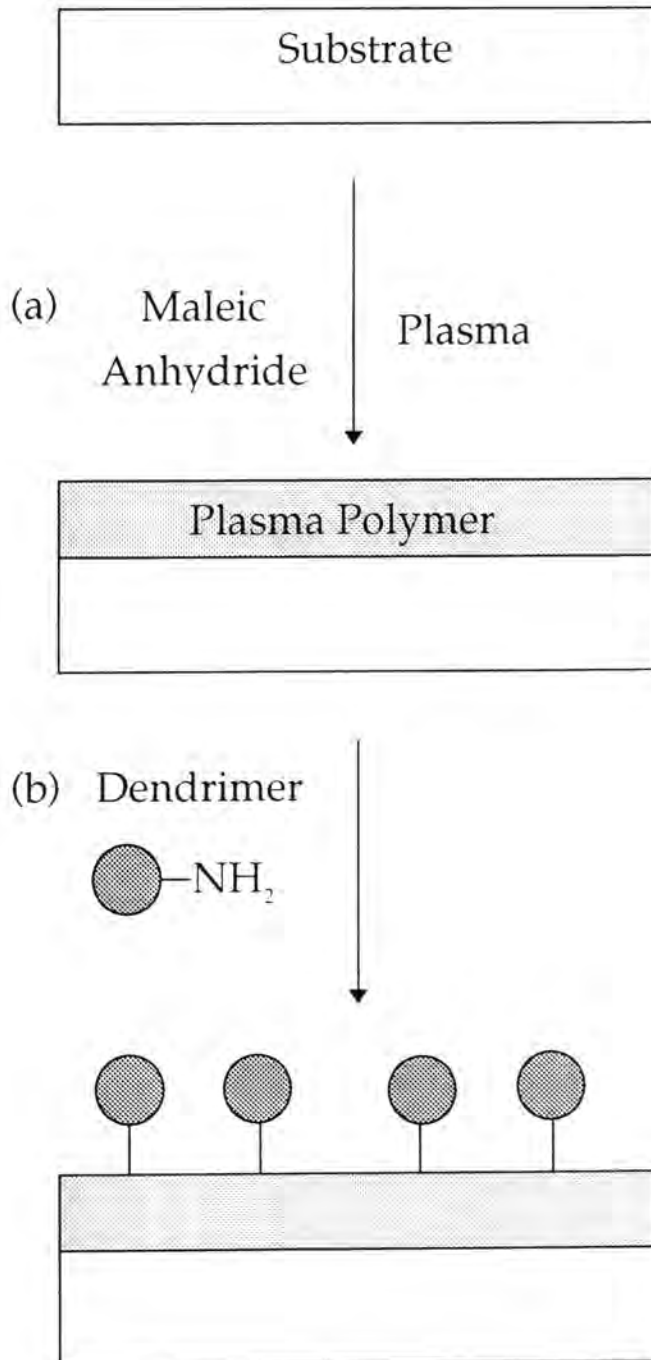
8.2 EXPERIMENTAL

Briquettes of maleic anhydride (Aldrich, 99% purity) were ground into a fine powder and loaded into a monomer tube. Plasma polymerization experiments were carried out as in Chapter 7. The average continuous wave power output (P_{cw}) of the R.F. supply spanned 5 - 90 W. Pulse on-time (t_{on}) and off-times (t_{off}) could be varied between 5 - 800 and 5 - 1200 µs respectively. The average power <P> delivered to the system during pulsing was calculated using the following expression: $<P> = P_{cw} \{T_{on} / (T_{on} + T_{off})\}$ where $T_{on} / (T_{on} + T_{off})$ is defined as the duty cycle.[15]

Next, the plasma polymer modified substrates were reacted with generation 4 polyamidoamine Starburst™ dendrimers (PAMAM SBD's). The functionalization reactions were carried out by placing 3 drops of the dendrimer solution (Aldrich, 10% wt./vol. in methanol, MW ~ 14,215) onto the plasma polymer modified substrates, under a nitrogen atmosphere. The surface was then rinsed with methanol to remove any unreacted dendrimers. Solutions containing different dendrimer concentrations were also employed in order to vary the molecular packing density at the surface.

A number of techniques were used to characterize the substrate surface at each stage of the described functionalization methodology. X-ray photoelectron spectroscopy (XPS) was carried out as in Chapter 5. Instrumentally determined sensitivity factors were taken as C(1s) : O(1s) : N(1s) equals 1.00 : 0.55 : 0.74. Complete coverage of the substrate by the maleic anhydride plasma polymer layer was confirmed by the absence of any XPS signals showing through from

the underlying substrate (e.g. Si(2p) in the case of glass slides). XPS measurements were also carried out to chemically analyse the modified surfaces and to verify the attachment of dendrimers. A Digital Instruments Nanoscope III atomic force microscope was used to examine the physical structure of the resultant dendrimer films. The microscope was operated in tapping mode, where changes in the oscillation amplitude of the cantilever tip serve as a feedback signal for measuring topographic variations across a surface.[16]

8.3   RESULTS

8.3.1   Plasma Polymerization of Maleic Anhydride

Plasma polymerization of maleic anhydride produced a well-adhered coating containing a variety of oxygenated carbon functionalities. The high resolution C(1s) XPS spectra of maleic anhydride pulsed plasma polymer (P_{av} = 5 W; T_{on} = 20 µs; T_{off} = 1200 µs), Figure 1(a), can be fitted to five different carbon functionalities:[17] hydrocarbon ($\underline{C}H_x$ ~ 285.0 eV), carbon singly bonded to an anhydride group ($\underline{C}$-C(O)=O ~ 285.7 eV), carbon singly bonded to oxygen (-$\underline{C}$-O ~ 286.6 eV), carbon doubly bonded to oxygen (O-$\underline{C}$-O / -$\underline{C}$=O ~ 289.1 eV), and an anhydride group (O=$\underline{C}$-O-$\underline{C}$=O ~ 289.4 eV).

Pulsing the electrical discharge on the ms - µs timescale provided control over the coating composition (i.e. the concentration of anhydride functionalities).[18] Typical ranges are quoted in Table 2:
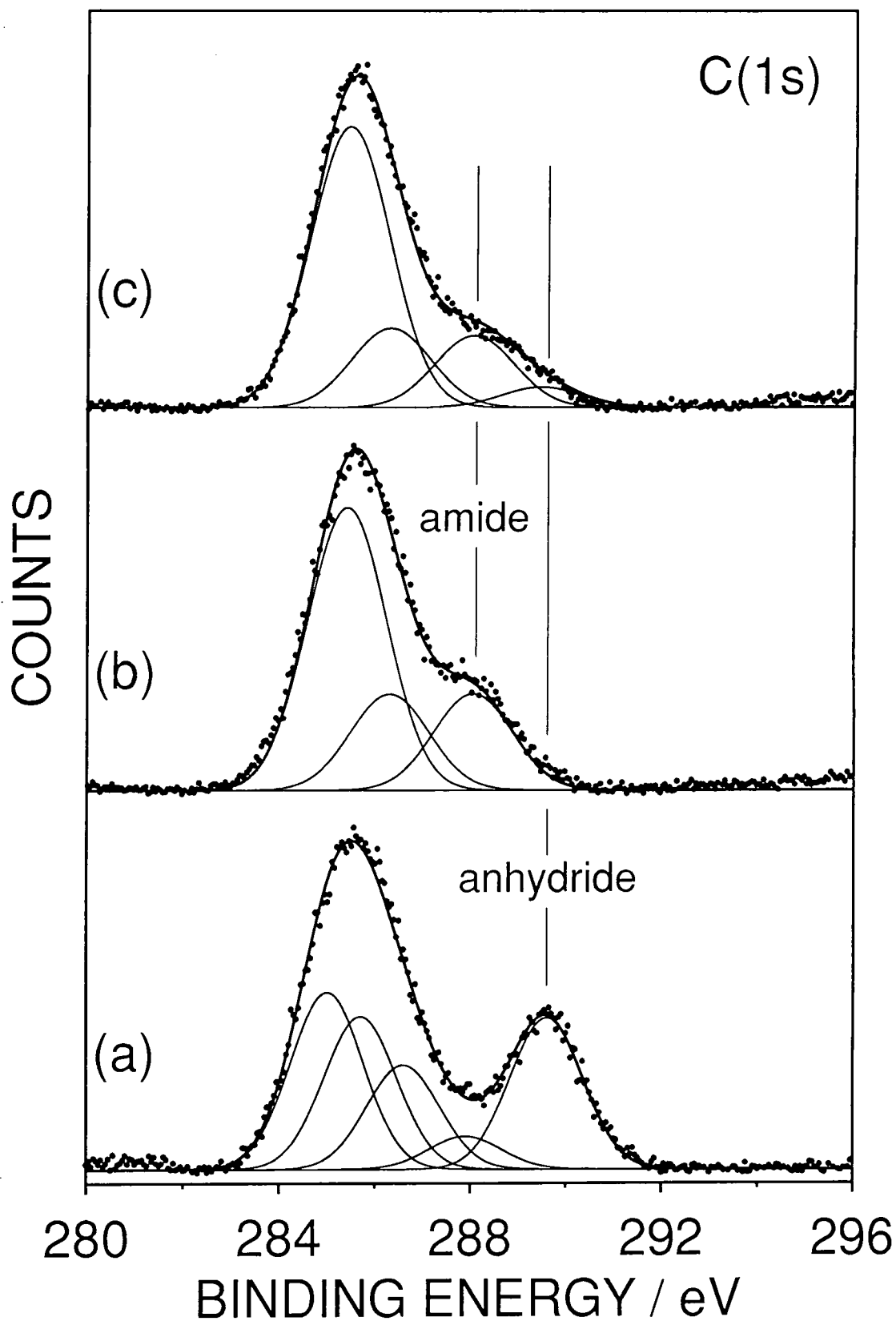
Figure 1. C(1s) XPS spectra of: (a) the maleic anhydride pulsed plasma polymer layer; and the plasma polymer functionalised with a (b) 10% wt./vol. and (c) 2.5% wt./vol. solution of PAMAM dendrimers.

	O : C Ratio	% Anhydride Carbon Centres
Continuous Wave (5W)	0.18 ± 0.02	10 ± 0.05
Pulsed (Low Duty Cycle)	$0.25 - 0.43 \pm 0.02$	$11 - 29 \pm 0.02$
Maleic Anhydride Monomer	0.75	50

Table 2. A comparison between typical compositions for the maleic anhydride plasma polymer coatings and the starting monomer.

Greater retention of anhydride functionalities was achieved whilst pulsing at low duty cycles compared to continuous wave plasma polymerization. This can be attributed to less fragmentation of the precursor molecule and reduced damage of the growing plasma polymer layer during the duty cycle on-time, combined with radical-initiated polymerization of maleic anhydride within the off-period.[18]

The almost flat morphology of the underlying glass substrate, Figure 2(a), is mirrored by the deposited plasma polymer layer, Figure 2(b).

8.3.2 Functionalization Reactions with PAMAM Dendrimers

Functionalization of the plasma polymer layer, by reacting with a solution of dendrimers dissolved in methanol, resulted in the stable attachment of PAMAM dendrimers onto the substrate. These could not be washed away by repeated rinsing with methanol. XPS characterization of the dendrimer functionalized
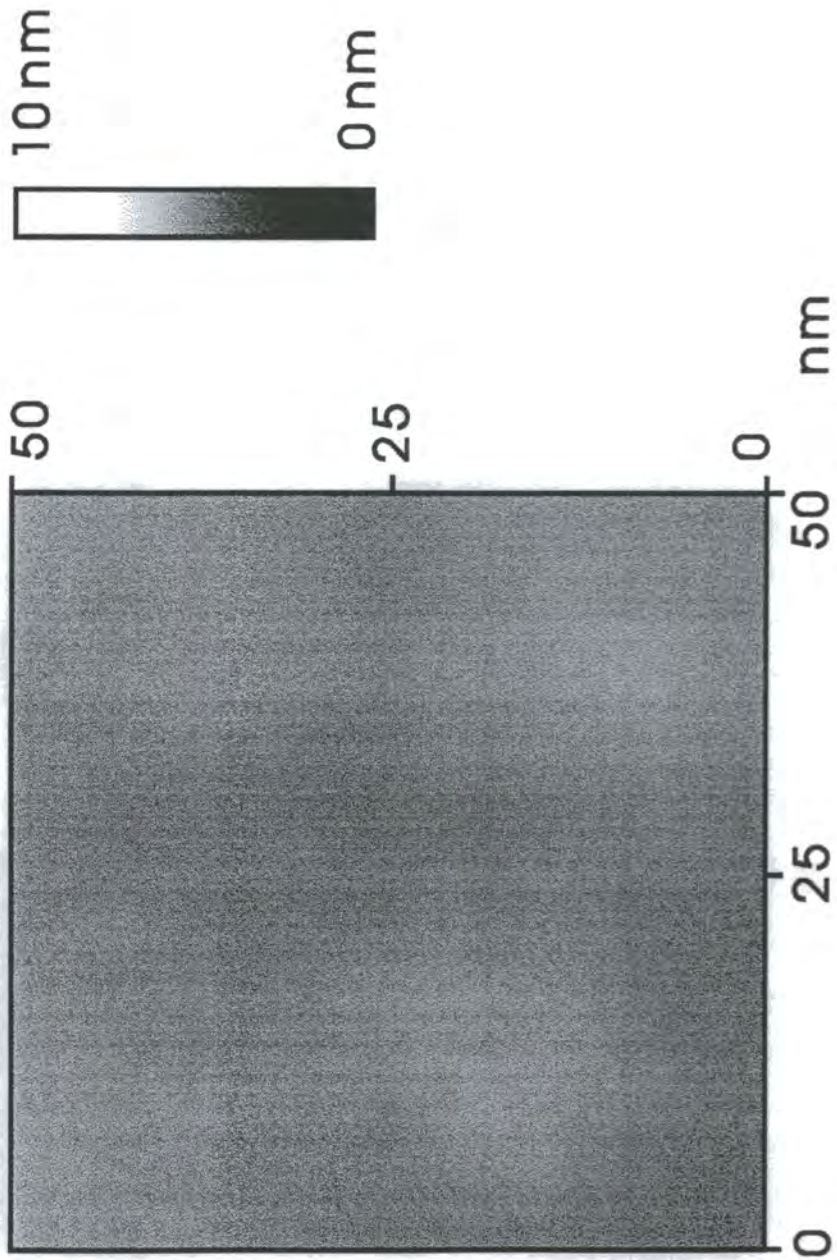
Figure 2(a). Low resolution tapping mode atomic force micrograph of the glass substrate.
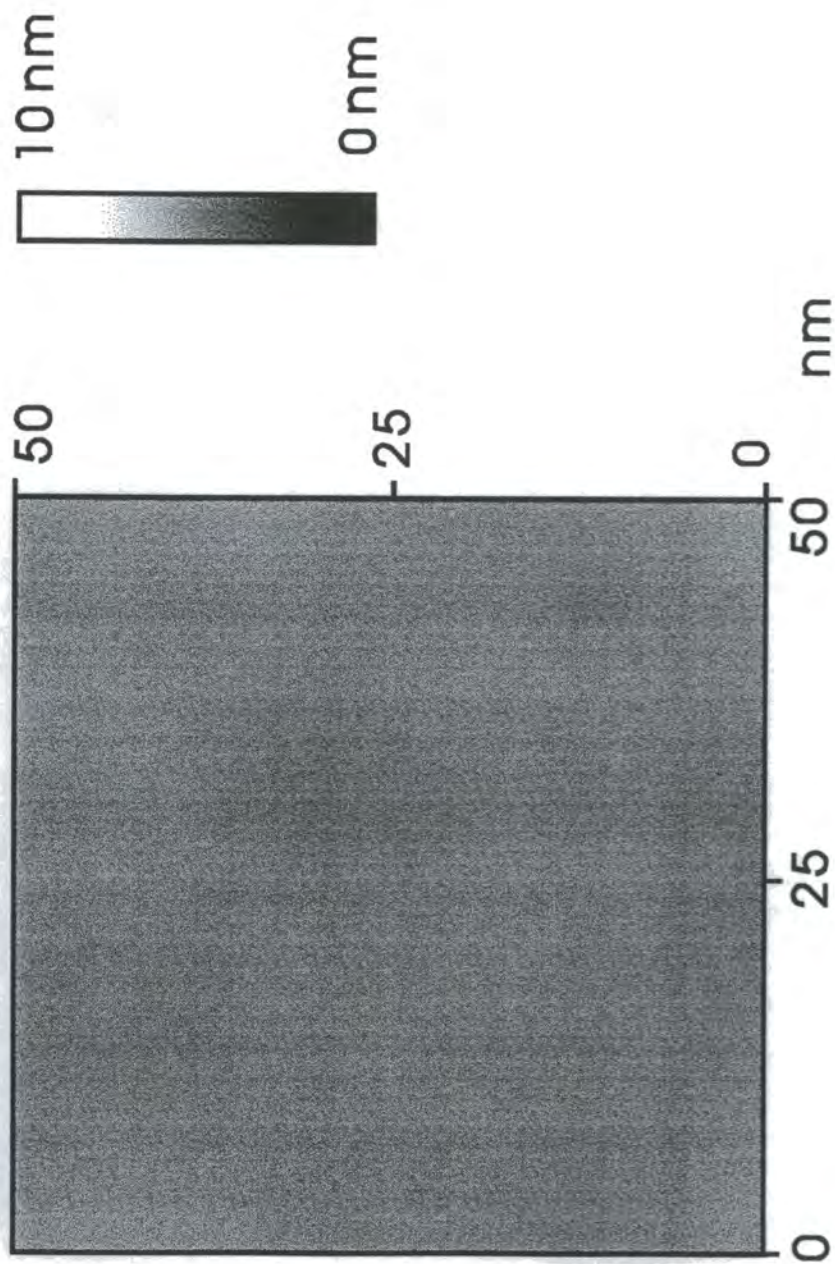
Figure 2(b). Low resolution tapping mode atomic force micrograph of the maleic anhydride pulsed plasma polymer deposited onto glass (P_{cw} 5W; T_{on} 20μs; T_{off} 1200μs).
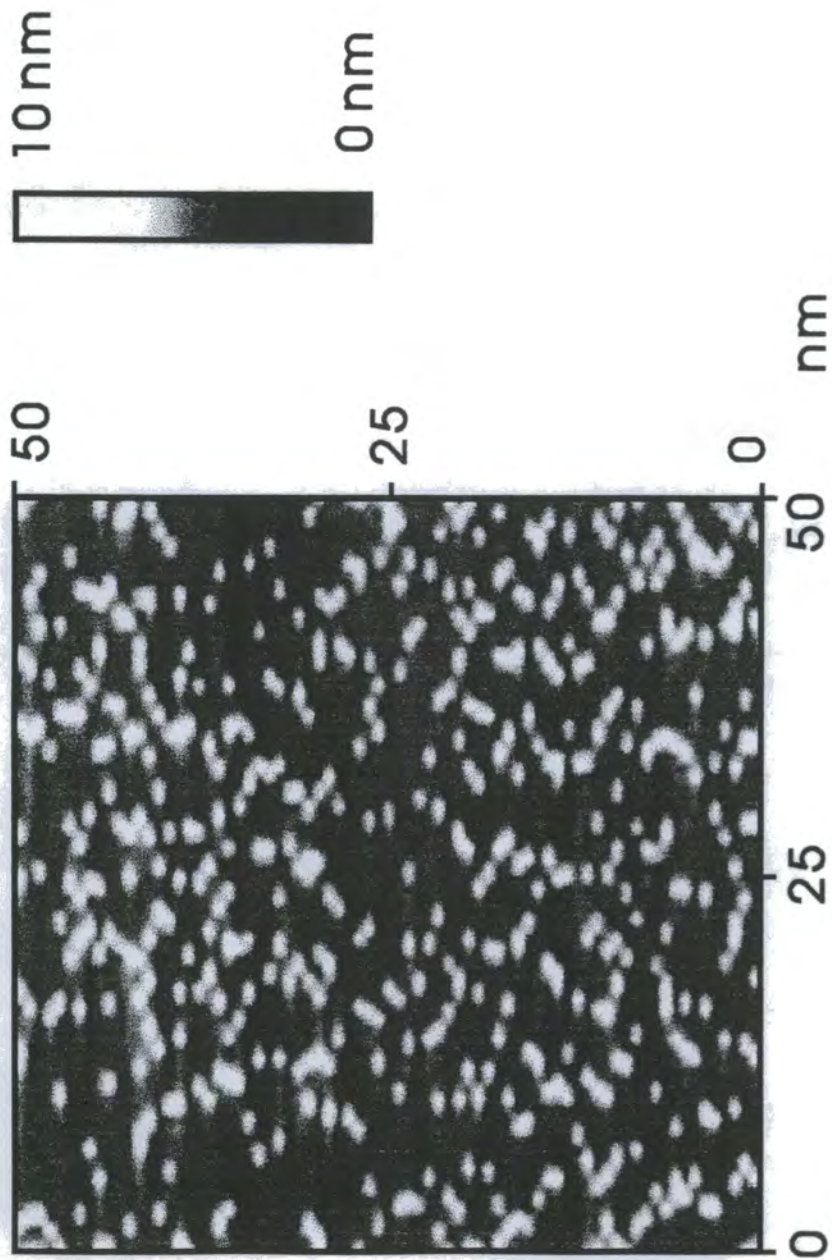
Figure 2(c). Low resolution tapping mode atomic force micrograph of generation 4 PAMAM dendrimers (white spots) attached to the maleic anhydride pulsed plasma polymer layer (darker background).

maleic anhydride plasma polymer layers showed changes in the widescan and core level spectra, thereby indicating that the dendrimers are indeed chemically bonded to the substrate. The corresponding high resolution C(1s) spectra can be fitted to three different carbon functionalities:[17] carbon singly bonded to an amide carbon / amine nitrogen ($\underline{C}$-C-NHR(=O) / $\underline{C}$-N ~ 285.7 eV), carbon singly bonded to an amide nitrogen (-$\underline{C}$H$_2$-NH-C=O ~ 286.6 eV), and an amide group (RHN-$\underline{C}$=O ~ 287.9 eV), Figure 1(b). The core level binding energies and peak area ratios of these environments are consistent with those predicted for a complete PAMAM dendrimer film. Furthermore, the disappearance of the anhydride group in the C(1s) envelope (O=$\underline{C}$-O-$\underline{C}$=O ~ 289.4 eV) confirms that the surface is completely covered by dendrimers. The appearance of a peak in the N(1s) region at ~ 401.9 eV is also consistent with amine terminated dendrimers being attached to the maleic anhydride plasma polymer layer via amide linkages.[17]

The packing density of dendrimers attached to the substrate could be varied by diluting the solution, Figure 3. The surface concentration of nitrogen (% N) was found to slowly decrease as the dendrimer solution was diluted (% wt. / vol.). Eventually, a sharp fall in the amount of nitrogen detected at the surface was noted at just below a concentration of 2.5% wt. / vol.; this ties in with the reappearance of the anhydride group peak (O=$\underline{C}$-O-$\underline{C}$=O ~ 289.4 eV) in the C(1s) envelope, Figure 1(c), thus indicating that the surface coverage of dendrimer is no longer complete.

The morphology, size and intermolecular spacing of the attached dendrimer layers were determined using atomic force microscopy. AFM
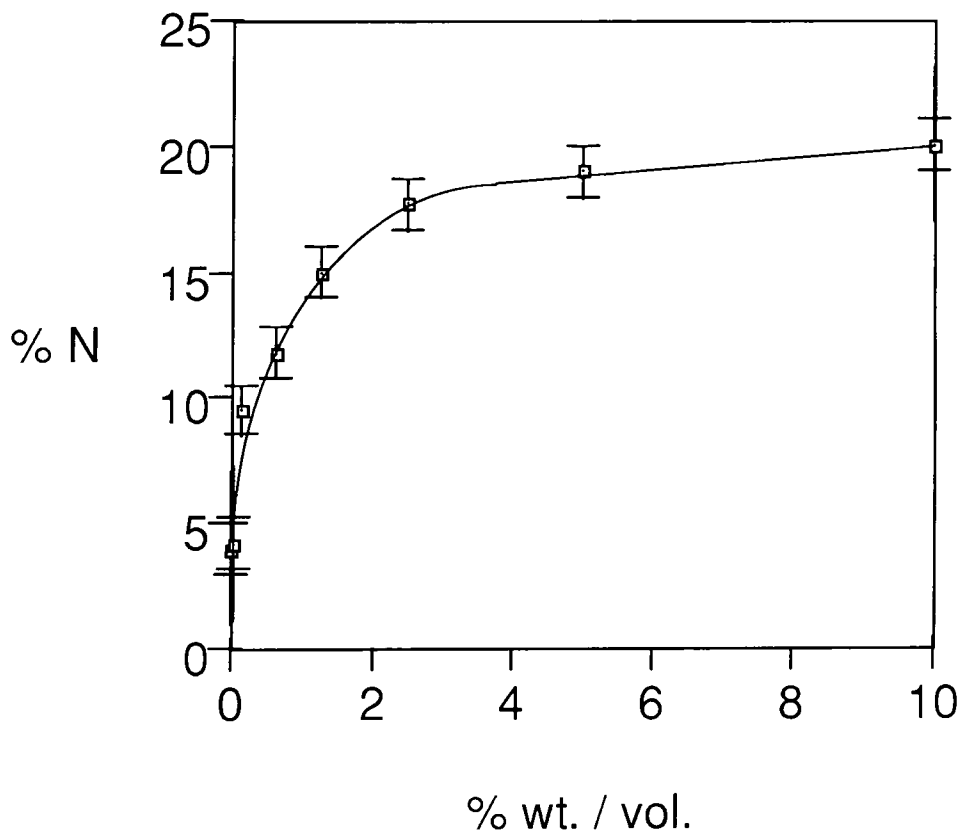
Figure 3. Nitrogen concentration (% N) at the surface of the plasma polymer layer after functionalization versus the dilution of dendrimer molecules (% wt./vol.).

micrographs of PAMAM dendrimers covalently bonded to the maleic anhydride plasma polymer layer display small white dots (height = 2.0 ± 0.03 nm; width = 3.3 ± 0.04 nm), which represent individual dendrimers attached to the underlying (darker shading) plasma polymer surface, Figures 2(c) and 4.

8.4   DISCUSSION

Generation 4 Starburst dendrimers occur around the threshold at which PAMAM dendrimers adopt a globular geometry (generations 0 - 3 are non-spheroidal).[19]   Electron paramagnetic resonance (EPR) spectroscopy[20] and computer assisted molecular simulations[21] have previously been used to show that these fourth-generation PAMAM dendrimers exist in solution as soft spheroids with a packed external structure. However, very little work has been undertaken in the past to characterize and image dendrimers attached to surfaces. Theoretical and computer modelling studies have calculated contact forces and possible geometries of dendrimers located on surfaces;[22] these predict a flattening and spreading out of the dendrimer molecules over the surface, in an analogous manner to water droplets present on a windowpane. Such behaviour can account for the observed greater width of the PAMAM dendrimers bonded to the surface of the plasma polymer layer compared to their height, Figure 4. It also explains the slight discrepancy between the experimentally measured width of 3.3 ± 0.04 nm and the theoretical diameter of 3.06 nm predicted using a Corey-Pauling-Koltun (CPK) three dimensional contracted model of the fourth generation PAMAM dendrimer.[1]
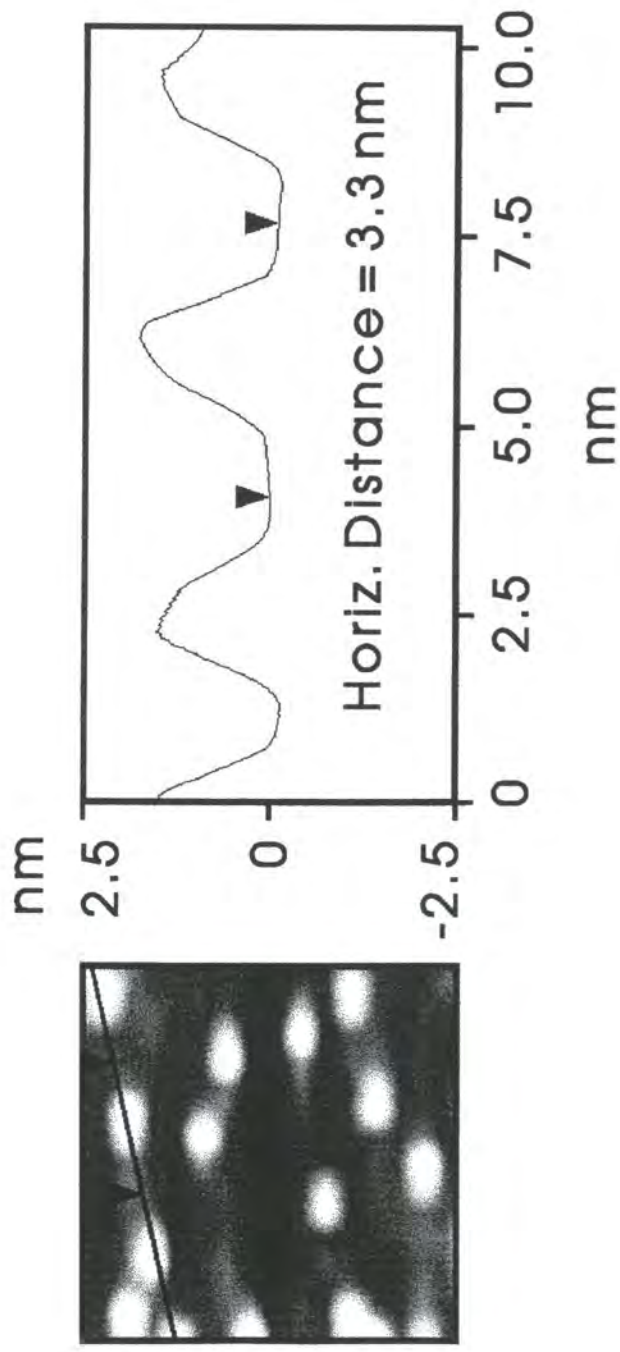
Figure 4. High resolution tapping mode AFM image of generation 4 PAMAM dendrimers and the associated cross-section. The distance between consecutive markers corresponds to the size of individual dendrimers.

Compared to previous solvent casting and self-assembly techniques, the current method offers the capability to control the number of reactive anhydride groups at the surface thereby regulating the dendrimer surface density. It also provides additional benefits, such as good adhesion between the plasma polymer layer and the underlying substrate, and complete coverage of the substrate by the plasma polymer layer.

8.5 CONCLUSIONS

Starburst PAMAM dendrimers can be chemically fixed onto any shaped solid substrate (glass, quartz, silicon, polymer, elastomer, etc.) by pre-depositing a well-adhered plasma polymer layer of maleic anhydride. The intermolecular spacing and concentration of dendrimer molecules attached to the surface can be engineered to a pre-selected level by controlling the level of anhydride group incorporation into the plasma polymer coating and also by changing the dilution of the dendrimer solution. Such an ability to be able to tailor the surface properties makes this methodology attractive for a wide range of applications including adhesion, wetting, catalysis, biocompatability, and chemical sensors. Furthermore, the fixed dendrimers themselves present external chemical groups which are capable of participating in further reactions to generate surfaces with different physiochemical properties.

REFERENCES

[1]   Tomalia, D. A.; Naylor, A. M.; Goddard III, W. A. *Angew. Chem. Int. Ed. Engl.* **1990**, *29*, 138.

[2]   Tomalia, D. A. *Macromol. Symp.* **1996**, *101*, 243.

[3]   Dagani, R. *Chem. & Eng. News* **1996**, *June 3*, 30.

[4]   Buchko, C. J.; Wilson, P. M.; Xu, Z.; Zhang, J.; Moore, J. S.; Martin, D. C. *Polymer* **1995**, *36*, 1817.

[5]   Gitsov, I.; Fréchet, J. M. J. *Macromolecules* **1993**, *26*, 6536.

[6]   Fréchet, J. M. J.; Gitsov, I. *Macromol. Symp.* **1995**, *98*, 441.

[7]   van Hest, J. C. M.; Baars, M. W. P. L.; Elissen-Roman, C.; van Genderen, M. H. P.; Meijer, E. W. *Macromolecules* **1995**, *28*, 6689.

[8]   Sheiko, S. S.; Eckert, G.; Ignat'eva, G.; Muzafarov, A. M.; Spickerman, J.; Räder, H. J.; Möller, M. *Macromol. Rapid Commun.* **1996**, *17*, 283.

[9]   Evenson; S. A.; Badyal, J. P. S., submitted for publication in *Chem. Mater.*

[10]   Rubin, S.; Bar, G.; Taylor, T. N.; Cutts, R. W.; Zawodzinski Jr., T. A. *J. Vac. Sci. Technol. A.* **1996**, *14*, 1870.

[11]   Bar, G.; Rubin, S.; Cutts, R. W.; Taylor, T. N.; Zawodzinski, T. A. *Langmuir* **1996**, *12*, 1172.

[12]   Saville, P. M.; Reynolds, P. A.; White, J. M.; Hawker, C. J.; Frechet, J. M. J.; Wooley, K. L.; Penfold, J.; Webster, J. R. P. *J. Phys. Chem.* **1995**, *99*, 8283.

[13]   Alonso, B.; Moran, M.; Casado, C. M.; Lobete, F.; Losado, J.; Cuadrado, I. *Chem. Mater.* **1995**, *7*, 1440.

[14] Wells, M.; Crooks, R. M. *J. Am. Chem. Soc.* **1996**, *118*, 3988.

[15] Savage, C. R.; Timmons, R. B. *Chem. Mater.* **1991**, *3*, 575.

[16] Babcock, K. L.; Prater, C. B. *Phase Imaging: Beyond Topography*, Digital Instruments Application Note: California **1995**.

[17] Beamson, G.; Briggs, D. *High Resolution XPS of Organic Polymers*; Wiley: Chichester, **1992**.

[18] Ryan, M. E.; Hynes, A. M.; Badyal, J. P. S.; *Chem. Mater.* **1996**, *8*, 37.

[19] Gopidas, K. R.; Leheny, A. R.; Caminati, G.; Turro, N. J.; Tomalia, D. A. *J. Am. Chem. Soc.* **1991**, *113*, 7335.

[20] Ottaviani, M. F.; Cossu, E.; Turro, N. J.; Tomalia, D. A.; *J. Am. Chem. Soc.* **1995**, *117*, 4387.

[21] Naylor, A.M.; Goddard III, W.A.; Kiefer, G.E.; Tomalia, D.A.; *J. Am. Chem. Soc.* **1989**, *111*, 2339.

[22] Mansfield, M. L.; *Polymer* **1996**, *37*, 3835.

CHAPTER 9

CONTROLLED POLYMERIZATION OF

1,2-ETHANEDITHIOL

9.1 INTRODUCTION

Sulfur containing polymers show outstanding properties including super electroconductivity, specific ion exchange, radiation / high temperature resistance, and biocompatability.[1] They include polythioethers, polythioesters, polythiols, polysulfoxides, polysulfones, poly(sulfonic acid)s, etc.[2] In particular, thiols have been of foremost importance in the development of the functional group concept in biochemistry.[3] This is highlighted by the fact that thiol groups can potentially form disulfide 'bridges' with protein chains to stabilize the three-dimensional conformation of proteins at surfaces.[4]

The introduction of thiol groups onto polyethylene surfaces was first achieved by the pyrolysis and photolysis of carbon disulfide.[5] Early plasma polymerization studies involving sulfur compounds concentrated on producing thin films containing sulfonic acid and sulfonic ester groups, for use in cation-exchange systems.[6,7] Recently, plasma treatment of a wider range of sulfur monomers (thiophene, carbon disulfide, dimethyl sulfide, ethanethiol, ethanedithiol, etc.) has been examined for the introduction of thiol groups onto polyethylene surfaces.[8] The results indicated that the plasma polymer obtained from 1,2-ethanedithiol contained the highest concentration of thiol groups.

More recently, it has been demonstrated that varying the specific electrical discharge parameters during plasma polymerization provides greater control over the overall surface composition.[9,10] In the current study, the plasma polymerization of 1,2-ethanedithiol is examined over a range of output powers in order to maximize the level of surface thiol group incorporation.

94

9.2 EXPERIMENTAL

1,2-ethanedithiol (Aldrich, 99% purity) was further purified by several freeze-pump-thaw cycles.[11] Plasma polymerization experiments were carried out as in Chapter 7. X-ray photoelectron spectroscopy (XPS) and infrared (IR) spectroscopy were then used to measure the extent of thiol group incorporation and overall S : C ratio in the resultant polymer.

XPS analysis was carried out as in Chapter 5. Instrumentally determined sensitivity factors were taken as C(1s) : S(2p) equals 1.00 : 0.54. In addition, both the ethanedithiol monomer and plasma polymer were examined by infrared analysis on a Mattson Polaris instrument operating at 4 cm^{-1} resolution over a 400 to 4000 cm^{-1} range. The Golden Gate™ Single Reflection Diamond ATR accessory was used for improved qualitative and quantitative analyses of liquids and films. This is achieved by optimal beam condensation and maximum throughput as a result of the transfer optics system comprising a complex combination of mirrors and lenses.[12]

A Digital Instruments Nanoscope III atomic force microscope (AFM) and an Olympus BX40 optical microscope were used to examine the physical structure of the resultant films. The AFM was operated in TappingMode, where changes in the oscillation amplitude of the cantilever tip serve as a feedback signal for measuring topographic variations across a surface.[13]

9.3 RESULTS

Plasma polymerization of 1,2-ethanedithiol produced a well-adhered coating containing surface thiol groups. The surface was analysed by XPS, IR, AFM, and optical microscopy:

9.3.1 X-ray Photoelectron Spectroscopy

The high resolution C(1s) XPS spectra of 1,2-ethanedithiol plasma polymer (average power output $<P> = 40$ W), Figure 1, can be fitted to one single carbon functionality:[14] carbon singly bonded to sulfur ($\underline{C}$-S ~ 285.5 eV). The corresponding S(2p) region of the spectra also revealed one peak corresponding to sulfur singly bonded to carbon (C-$\underline{S}$ centred at ~ 163.8 eV), Figure 2. This envelope can be fitted with two components since the S(2p) core level has two different spins, C-$\underline{S}$($2p_{1/2}$) ~ 163.5 eV and C-$\underline{S}$($2p_{3/2}$) ~ 164.7 eV.[14] The experimentally observed intensity ratio between the two deconvoluted components [$S(2p_{3/2})$: $S(2p_{1/2})$] ranges from 1.8 - 2.0, which corresponds favourably with the theoretical value of 1.95, estimated from the cross section for ionization of these core levels [0.590 for $S(2p_{1/2})$ and 1.15 for $S(2p_{3/2})$].[1]

Complete coverage was confirmed by checking for the absence of any XPS signals showing through from the underlying substrate (e.g. Si(2p) in the case of glass slides).
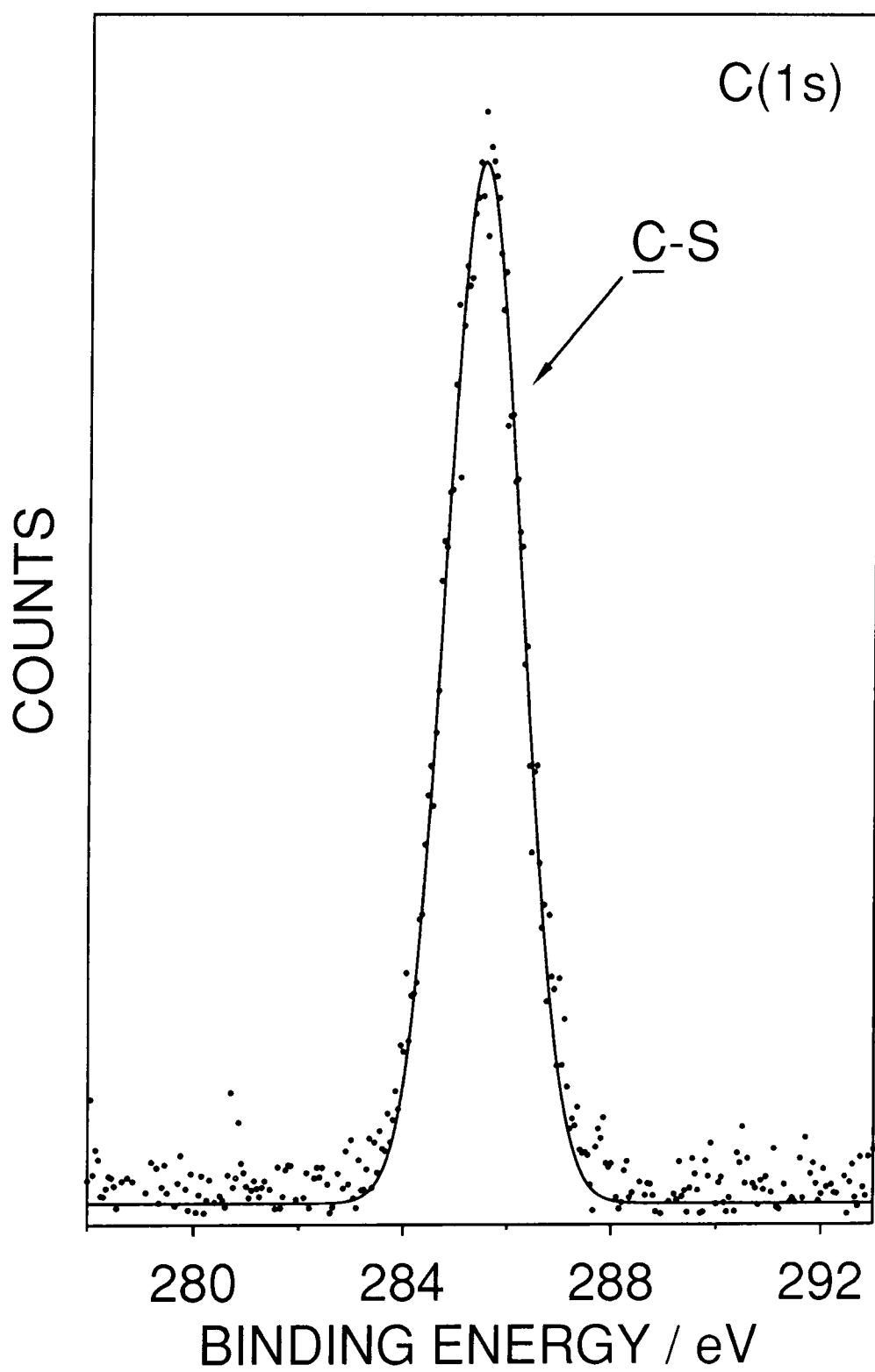
Figure 1. C(1s) XPS spectrum of the 1,2-ethanedithiol plasma polymer layer deposited at 40 W average power output.
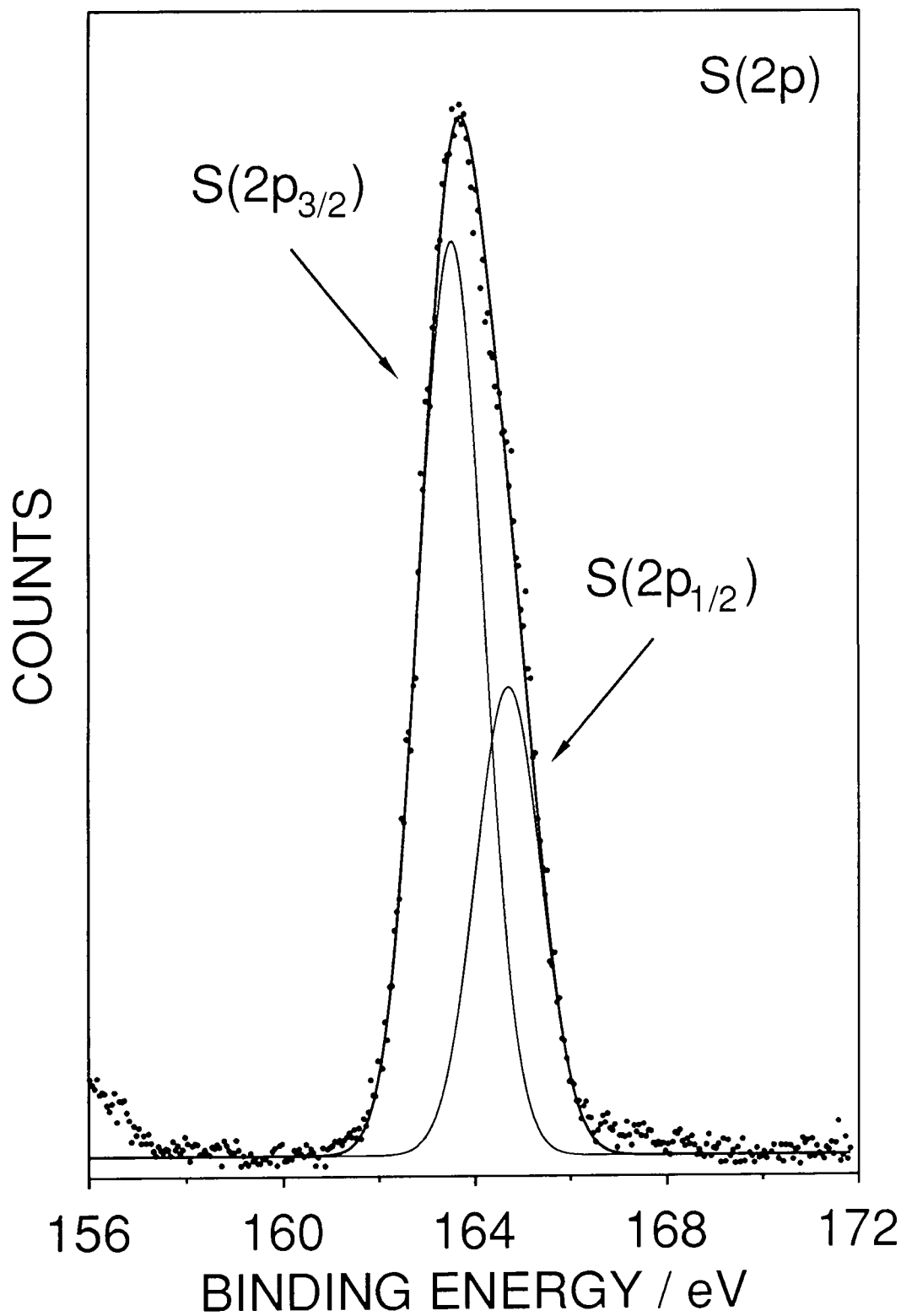
Figure 2. S(2p) XPS spectrum of the 1,2-ethanedithiol plasma polymer layer deposited at 40 W average power output.

9.3.2 Infrared Spectroscopy

Infrared analysis of the 1,2-ethanedithiol liquid monomer before plasma treatment, Figure 3(a), displayed absorbance bands at:[15] 2910 cm^{-1} (C-H stretching), 2551 cm^{-1} (S-H stretching in thiols), 1432 cm^{-1} (CH$_2$ bending), 1280 cm^{-1} and 1220 cm^{-1} (CH$_2$ wagging), and 1150 cm^{-1} (CH$_2$ twisting). These are all consistent with previous reports for 1,2-ethanedithiol in argon and nitrogen matrices.[16]

All of the infrared absorption features characteristic of the monomer are retained during plasma polymerization at <P> = 40 W, Figure 3(b), indicating retention of the monomer structure within the plasma polymer layer. The bands generally appear broader and less well defined than in the monomer, due to the increased variety of chemical environments for each functional group.[17] Additional bands were observed at:[15] 2362 cm^{-1} and 2343 cm^{-1} arising from Si-H and Si-H$_2$ stretching vibrations at the interface of the plasma polymer and the underlying glass substrate. The absorbance at 2551 cm^{-1} (S-H stretching) further confirms the existence of thiol groups at the surface of the plasma polymer.

9.3.3 Average Power Output Study

The average power output <P> was gradually reduced from 40 W down to 0.1 W in order to optimise the retention of thiol groups in the plasma polymer. Average powers below 5 W were achieved by pulsing the electrical discharge. Negligible variation in the C(1s) and S(2p) XPS peak shapes was found over the
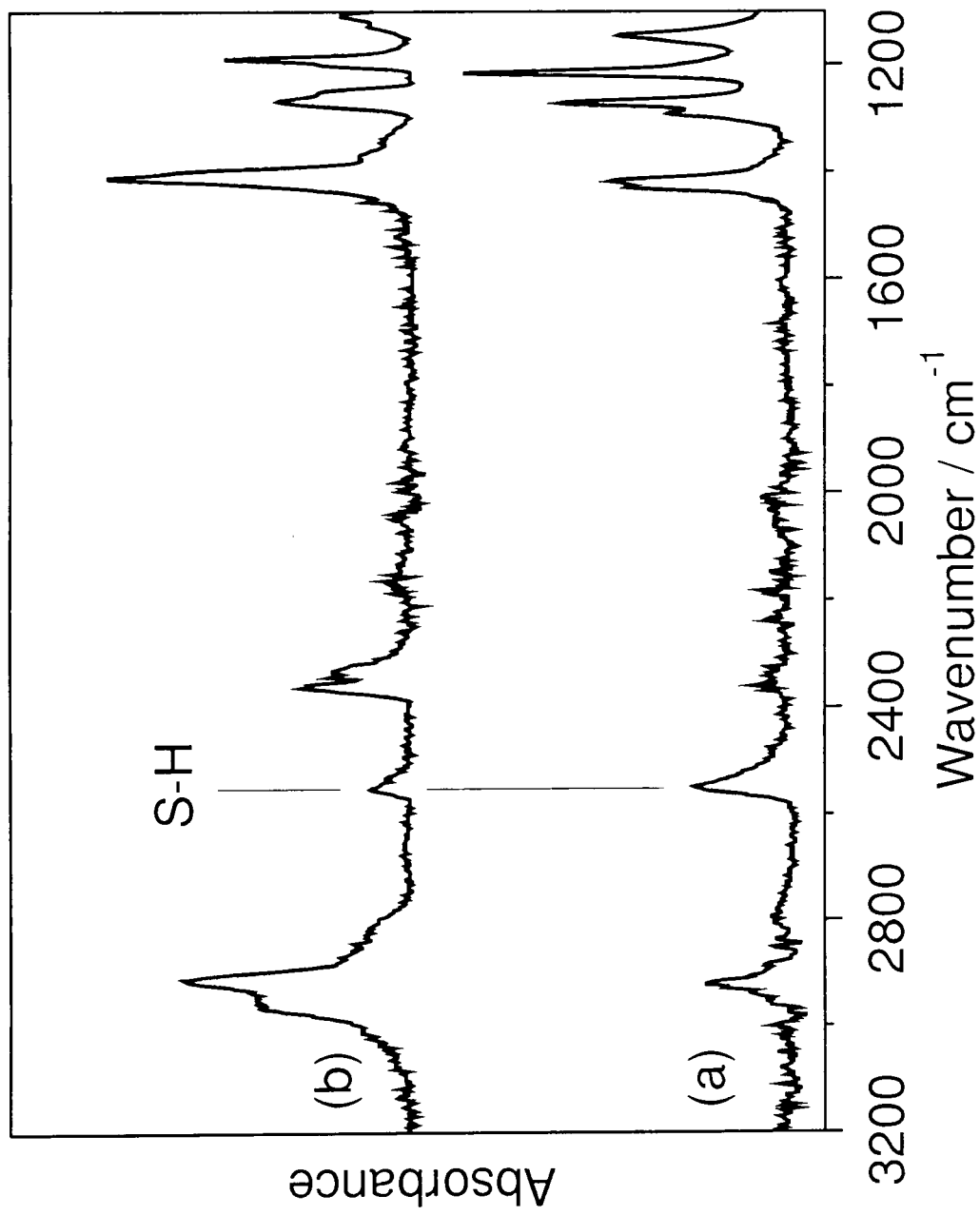
Figure 3. Infrared absorbance spectra of the 1,2-ethanedithiol: (a)monomer,.and (b) plasma polymer layer.

output power range 40 W - 20 W and all of the IR bands appeared at the same wavenumbers. The only observed differences were (i) the intensity of the IR band at 2551 cm^{-1} (S-H stretching in thiols) and (ii) the overall sulfur : carbon elemental ratio (S : C) in the plasma polymer measured by XPS, Figure 4. This ratio increased from 0.64 ± 0.02 to 1.41 ± 0.07 as the average power was reduced from 40 W to 20 W, and was accompanied by a slight increase in the intensity of the IR band at 2551 cm^{-1}. Reducing the average power below 15 W sees the appearance of Si(2p) and O(1s) XPS signals showing through from the underlying glass substrate, the intensity of which increase in line with the reduction in average power output. This indicates incomplete deposition and suggests that the monomer is not undergoing polymerization.

9.3.4   Atomic Force Microscopy and Optical Microscopy

These variations in surface chemical composition are accompanied by morphological and structural changes at the interface, as observed by AFM and optical microscopy. Films deposited at low average powers (0.1 - 15 W) contain micro-droplets, the diameters of which increase with the output power: 5 μm at <P> = 1 W, Figure 5(a), up to 10 - 50 μm at <P> = 5 W, Figure 5(b). As the average power is increased above 20 W the micro-droplets disappear and the surfaces are completely flat, Figure 5(c). This dramatic change in the surface structure of the plasma polymer occurs at the same average power at which Si(2p) and O(1s) XPS signals from the underlying substrate are no longer observed.
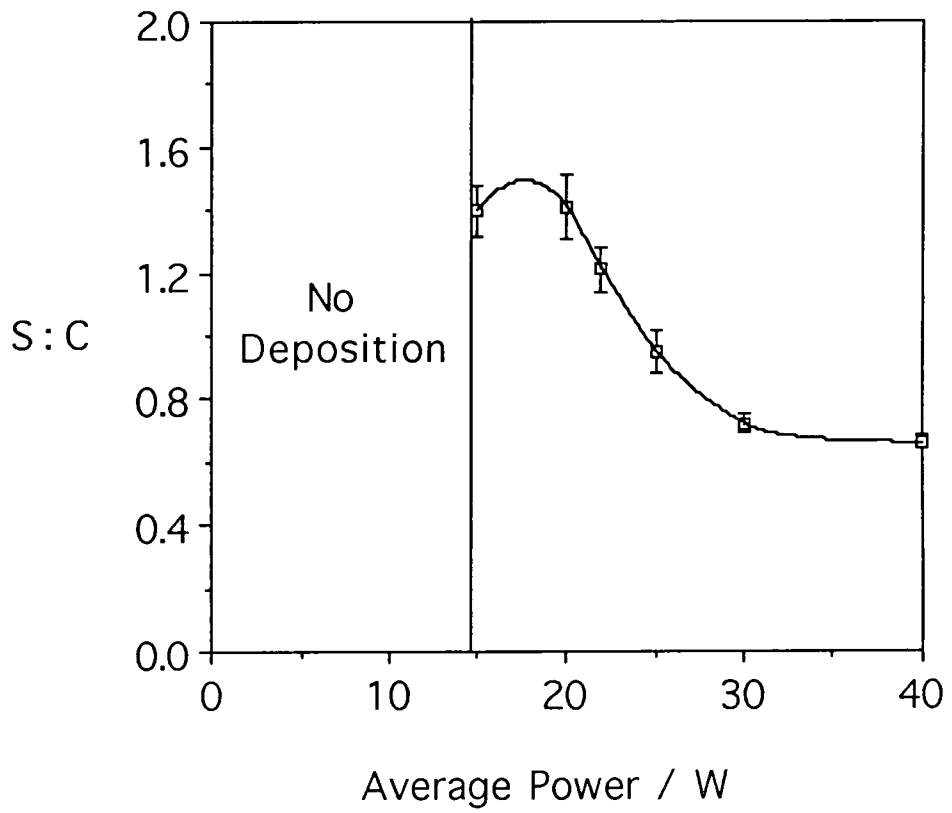
Figure 4. A graph of the overall sulfur : carbon (S : C) elemental ratio at the surface of the 1,2-ethanedithiol plasma polymer versus average power output <P> to the plasma.

1.0 μm

0.0 μm

μm
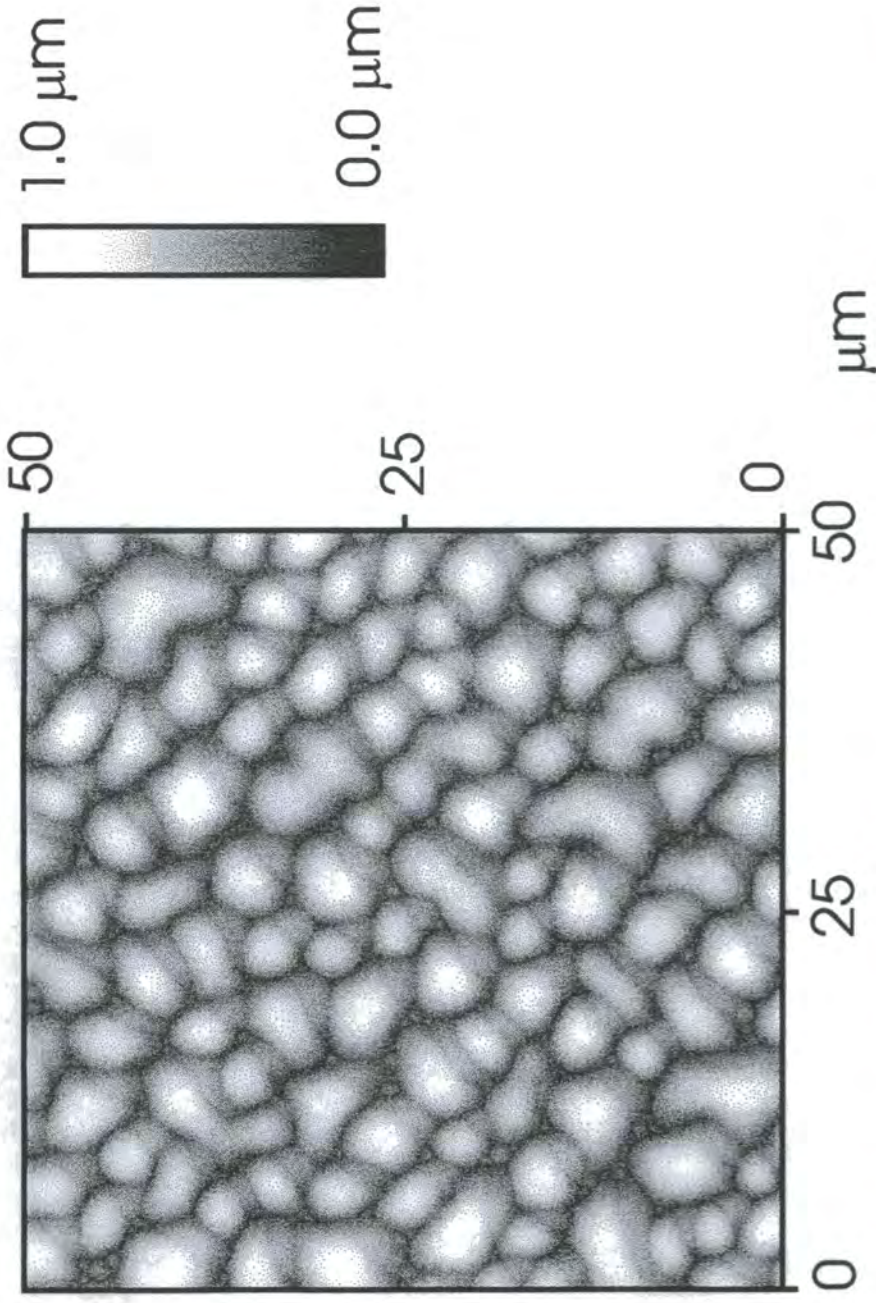
Figure 5(a). Low resolution atomic force micrograph of the micro-droplets formed during plasma deposition of 1,2-ethanedithiol onto glass at 1 W average power output.

100 µm

Figure 5(b). Optical micrograph of the micro-droplets formed during plasma deposition of 1,2-ethanedithiol onto glass at 15 W average power output.

Figure 5(c). Low resolution atomic force micrograph of the plasma polymer formed during plasma polymerization of 1,2-ethanedithiol onto glass at 40 W average power output.

9.4   DISCUSSION

The introduction of thiol groups onto surfaces by plasma treatment is a relatively new type of surface modification. Early plasma polymerization experiments using sulfur compounds resulted in pol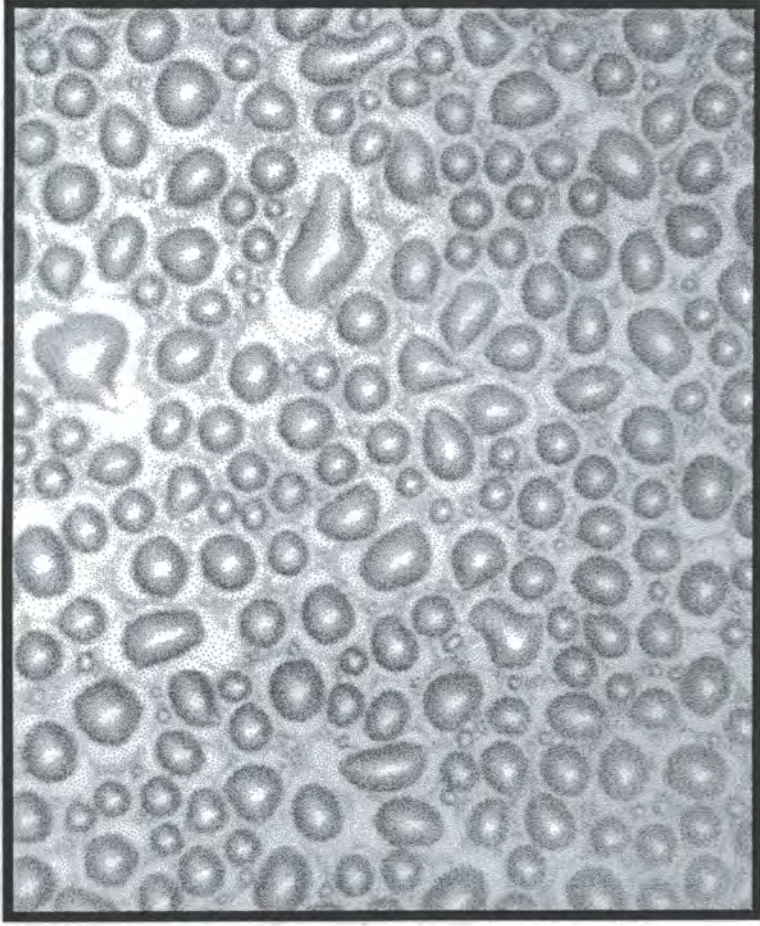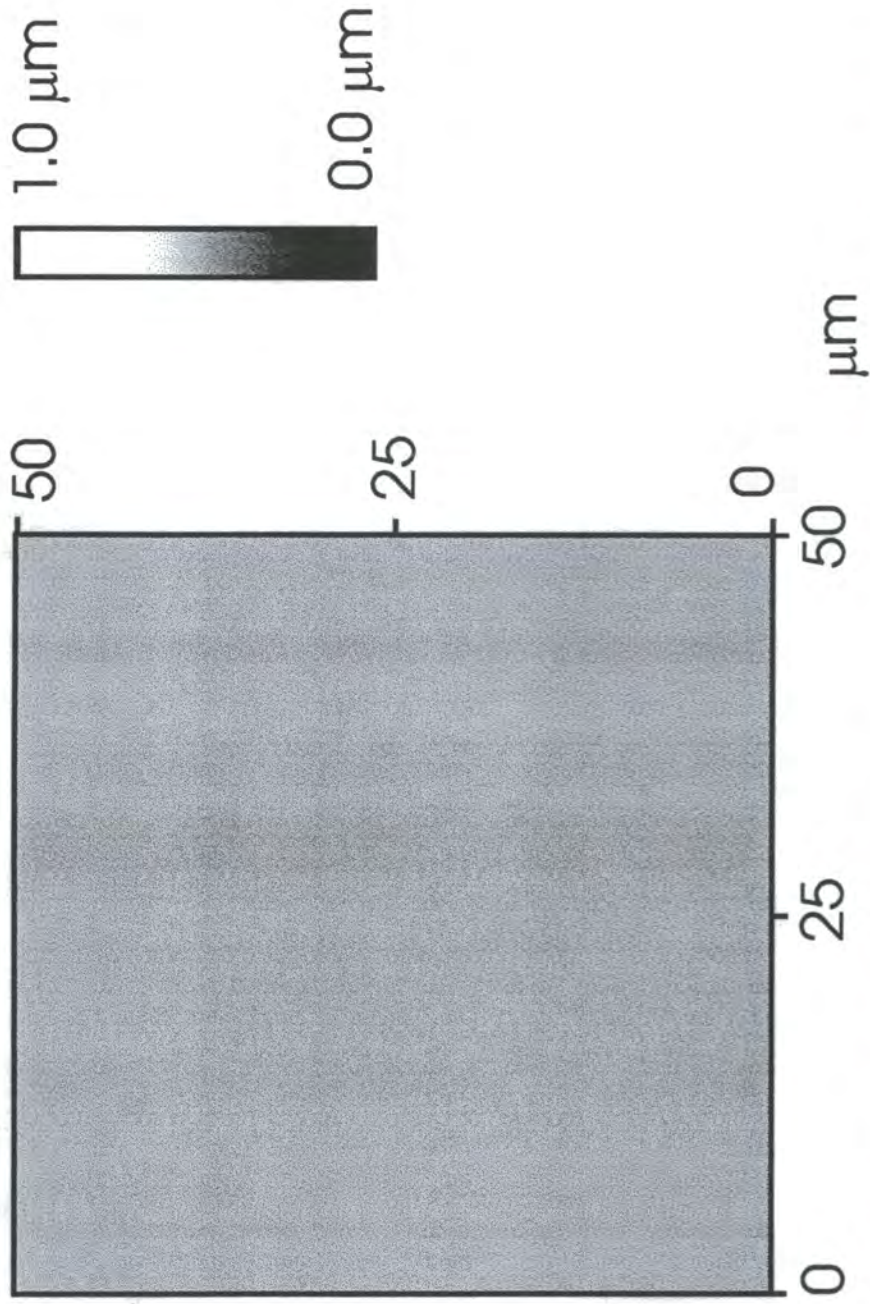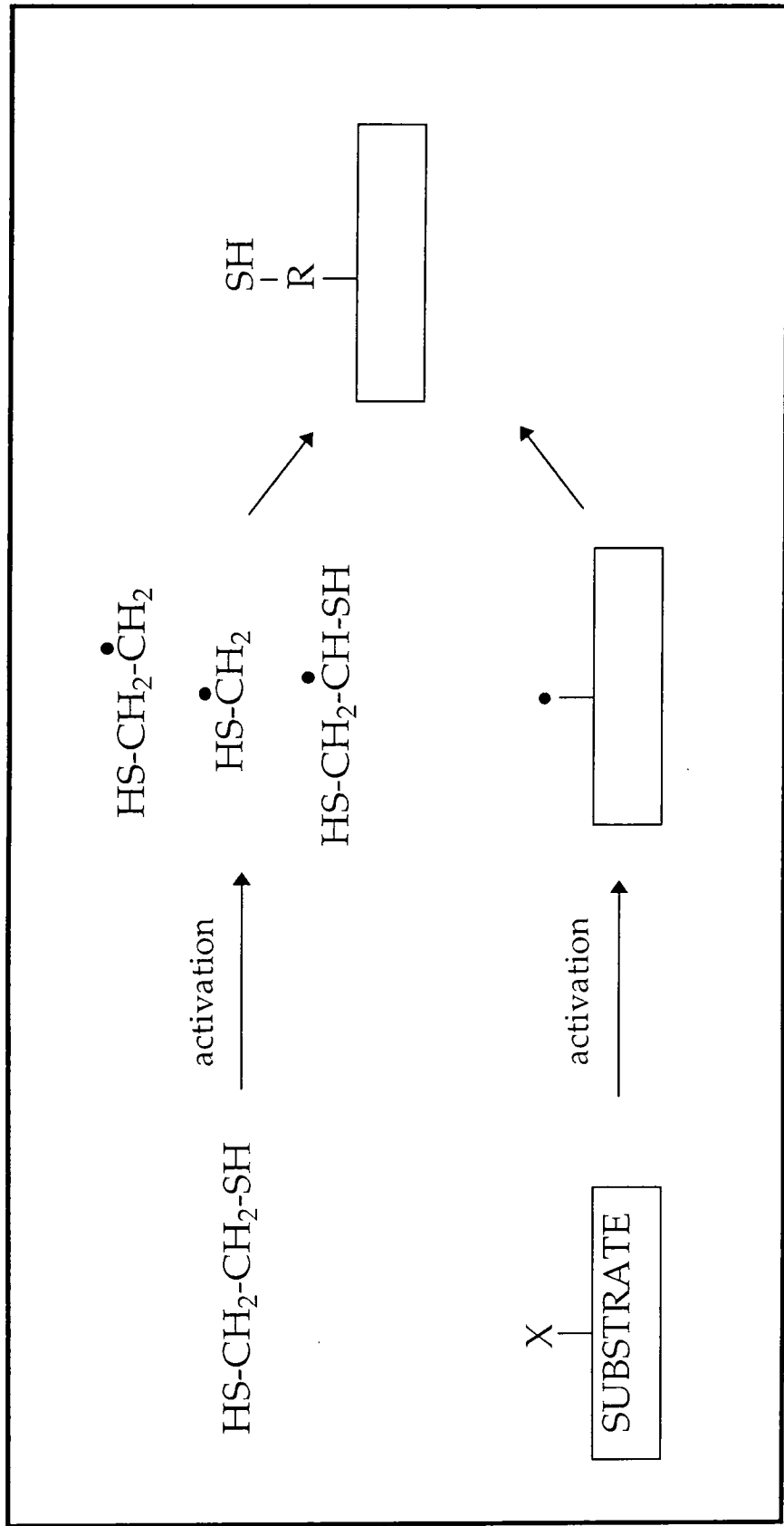ymers containing thiol functionalities, regardless of whether the thiol group is present in the starting monomer or not.[1] Subsequently, a wider range of monomers were polymerized under fixed plasma conditions (40W, 35 mTorr, 1 min).[8] The results suggested that the concentration of thiol groups introduced onto the surface is related to the amount of radical species in the plasma having terminal thiol groups. According to their experiments, the 1,2-ethanedithiol plasma contains most of the aforementioned species and thus the resultant plasma polymer boasted the highest percentage of surface thiol groups.

Fine tuning the electrical discharge parameters during plasma deposition potentially offers greater control over the concentration of surface sulfur groups.[9,10] In the present study, the overall S : C ratio and concentration of thiol functionalities was found to be strongly dependant on the average power output <P> of the system. The greatest retention of thiol groups was achieved at <P> = 20 W. This improvement, compared to the value attained at <P> = 40 W, can be attributed to less fragmentation of the precursor molecule (i.e. more thiol containing radical species in the plasma) and reduced damage of the growing plasma polymer layer during deposition.[10]

The proposed reaction mechanism for the plasma polymerization of 1,2-ethanedithiol is shown in Scheme 1.[8] This is supported by previous

HS-CH$_2$-CH$_2$-SH

HS-CH$_2$-$\overset{\bullet}{C}$H$_2$

$\xrightarrow{\text{activation}}$

HS-$\overset{\bullet}{C}$H$_2$

HS-CH$_2$-$\overset{\bullet}{C}$H-SH

SH
|
R
|

X
|
SUBSTRATE

$\xrightarrow{\text{activation}}$

Scheme 1. Proposed reaction mechanism for the introduction of thiol groups onto surfaces during the plasma polymerization of 1,2-ethanedithiol.

fragmentation studies of 1,2-ethanedithiol,[18] which have been shown to produce relatively stable CH_3SH, CH_2SH, CH_2SH_2, CH_3CHS, and SH_2 radicals in comparison to those formed from the corresponding oxygen analogue ($HOCH_2CH_2OH$). The bond dissociation energies of thiols RS-H (89 kcal mol^{-1}) and R-SH (67 kcal mol^{-1}) further confirm that the thiol group (-SH) is likely to stay intact upon impact, producing SH radicals.[19]

It is believed that at average powers below 20 W, insufficient reactive species are generated from which a complete plasma polymer coating can be formed. This accounts for the appearance of Si(2p) and O(1s) signals in the XPS spectrum and the incomplete film structure observed by AFM. This theory is reinforced by the knowledge that the concentration of reactive species in the plasma increases with applied R.F. power.

Furthermore, it is believed that the value of 1.41 ± 0.07 is one of the highest reported S : C ratios in a plasma polymer film. Previous studies aimed at increasing this ratio in plasma polymers have concentrated on increasing the proportion of sulfur in the starting monomer(s). For instance, plasma polymerization of carbon disulfide can result in S : C ratios of 0.16 up to 14.0 as the power is reduced,[20] whereas the only other relatively high ratio of 0.63 was obtained from an 80% SO_2 / 20% C_2H_2 starting mixture.[1]

9.5 CONCLUSIONS

Thiol groups can be introduced onto any shaped solid by depositing a plasma polymer layer of 1,2-ethanedithiol. The level of thiol group incorporation at the surface can be engineered to a pre-selected level by controlling the plasma operating conditions. Furthermore, the overall S : C ratio was found to be strongly dependant on the average power output <P> of the system, with the highest value of 1.41 ± 0.07 being attained at <P> = 20 W. This ratio increases at higher average powers due to increased monomer fragmentation in the plasma. Such an ability to be able to tailor the surface properties makes this methodology attractive for a wide range of applications including electroconductivity, catalysis, specific ion exchange, and biocompatability.

REFERENCES

[1]   Inagaki, N.; Tasaka, S.; Miyazaki, H. *J. Appl. Poly. Sci.* **1989**, *38*, 1829.

[2]   Belen'kii, L. I. *Chemistry of Organosulfur Compounds*; Ellis Horwood: New York, **1992**.

[3]   Fluharty, A. L. In *The Chemistry of the Thiol Group*; Patai, X.; Ed.; Wiley: London, **1974**, Chapter 13.

[4]   McMurry, J. *Organic Chemistry*; Brooks/Cole: California, **1988**.

[5]   Olsen, D. A.; Osteraas, A. J. *J. Poly. Sci. A* **1969**, *7*, 1913.

[6]   Yasuda, K.; Uchimoto, Y.; Ogumi, Z.; Takehara, Z. *J. Electrochem. Soc.* **1994**, *141*, 2350.

[7]   Terlingen, J. G. A.; Feijen, J.; Hoffman, A. S.; *J. Coll. Int. Sci.* **1993**, *155*, 55.

[8]   Muguruma, H.; Karube, I.; Saito, M. *Chem. Letts.* **1996**, 283.

[9]   Savage, C. R.; Timmons, R. B. *Chem. Mater.* **1991**, *3*, 766.

[10]   Ryan, M. E.; Hynes, A. M.; Badyal, J. P. S.; *Chem. Mater.* **1996**, *8*, 37.

[11]   Huntley, D. R. *J. Phys. Chem.* **1995**, *99*, 12907.

[12]   *Golden Gate Single Reflection Diamond ATR User Manual*, Graseby Specac: Fairfield CT.

[13]   Babcock, K. L.; Prater, C. B. *Phase Imaging: Beyond Topography*, Digital Instruments Application Note, California **1995**.

[14]   Beamson, G.; Briggs, D. *High Resolution XPS of Organic Polymers*; Wiley: Chichester, **1992**.

[15]   Silverstein, R. M.; Bassler, G. C.; Morril, T. C.; *Spectrometric Identification of Organic Compounds*; Wiley: Singapore, **1991**.

[16]   Li, Y. -S.; Li, S. *Spectrochemica Acta*. **1994**, *50A*, 509.

[17]   Shard, A. *Plasma Assisted Thin Film Deposition*; PhD. Thesis: University of Durham, **1992**.

[18]   Sekiguchi, O.; Kosaka, T.; Kinoshita, T.; Taijama, S. *Int. J. Mass. Spec. and Ion Processes* **1995**, *145*, 25.

[19]   Bernadi, F.; Csizmadia, I. G.; Mangini, A. *Organic Sulfur Chemistry Theoretical and Experimental Advances*; Elsevier: Amsterdam, **1985**.

[20]   Asano, Y.; *Jap. J. Appl. Phys.* **1983**, *22*, 1618.

CHAPTER 10

CONCLUSIONS

10.1 CONCLUSIONS

This thesis has examined the processes available for tailoring surfaces at the molecular level. Pulsed plasma polymerization and subsequent surface functionalization reactions are found to be the best techniques for securing polyamidoamine Starburst dendrimers and high molecular weight Jeffamines, at a predetermined concentration, onto the surface of any shaped solid substrate.

The initial step involved mastering the technique of atomic force microscopy (AFM) used to study the packing and structure of molecules at surfaces. Nanometer resolution images of arachidic acid Langmuir-Blodgett (LB) films deposited onto hydrophobic silicon were obtained. The long axes of the fatty acid molecules are found to tilt away from the substrate normal (along the deposition direction) as the surface pressure is decreased. A similar distorted orthorhombic packing arrangement is observed for mixed LB films of arachidic acid/cadmium arachidate, although the acid regions can be removed by solvent washing to leave behind islands of cadmium arachidate molecules.

This technique was then used to study generation 9.5 polyamidoamine Starburst dendrimers (PAMAM SBDs) solvent cast onto hydrophobic silicon substrates. Dendritic cellular features are formed on the macroscopic scale due to the dewetting of the dendrimer film from the underlying substrate. At the microscopic level, these dendrimers were found to pack into microfibrils, which is similar to the complexation observed for micelles at high concentrations. The highlight of this study was the first true visualization of these individual spherical shaped nanoscopic dendrimers at surfaces.

The next goal was to develop a system for bonding these macromolecules onto chemically inert solid surfaces. Ethylene maleic anhydride copolymer thin films were deposited by spin coating techniques to produce materials with a fixed concentration of surface anhydride groups. Reaction between these moieties and trifluorinated amines / alcohols tested the viability of vapor-phase functionalization to yield securely attached molecules. The much higher reaction rates and yields obtained for amines compared to corresponding alcohols can be attributed to the greater nucleophilicity of the former. Unfortunately, this copolymer only provides a surface with a fixed concentration of anhydride groups. Furthermore, although the molecules are bonded to the copolymer film, the film itself is not securely fixed to the underlying substrate and can be removed by solvent washing.

Pulsed plasma polymerization of maleic anhydride goes one stage further, to produce thin films which are both well-adhered to the underlying substrate and contain a predetermined concentration of surface anhydride groups. Subsequent vapor-phase functionalization reactions produce solid surfaces to which generation 4 PAMAM dendrimers, high molecular weight Jeffamines, and trifluorinated amines have been attached at a desired packing density. Again AFM has been used to image these even smaller dendrimers (diameter = 3.5 nm), however this time they are securely bonded to the substrate surface. Initial biological tests have proven these coatings to be stable in the presence of synthetic culture media from Life Technologies. Further cell proliferation, cell toxicity, friction and adhesion tests are planned to examine the overall biocompatability of these surfaces.

Thiol groups have similarly been introduced onto surfaces via the plasma polymerization of 1,2-ethanedithiol. The average power output to the plasma was found to have a profound effect over the level of thiol group incorporation and overall sulfur : carbon elemental ratio in the resultant polymer. In fact, the value of 1.41 ± 0.07 is the one of the highest reported S : C ratios achieved for a plasma polymer film.

In summary, this thesis has shown that with careful choice of both physical and chemical functionalization techniques, PAMAM dendrimers and high MW Jeffamines can be securely bonded to the surface of any solid substrate. Finally, the technique of pulsed plasma polymerization can be extended to a wider range of monomers, thus producing alternative surface reactive groups to which even more complex macromolecules can be attached. Ultimately this allows the structure and properties of any shaped solid surface to be tailored at the molecular level.

APPENDIX

COLLOQUIA, SEMINARS, PRESENTATIONS

AND LECTURE COURSES

UNIVERSITY OF DURHAM

BOARD OF STUDIES IN CHEMISTRY

COLLOQUIA AND SEMINARS FROM INVITED SPEAKERS

.

1994

October 19	Prof. N. Bartlet, University of California
	Some Aspects of Ag(III) and Ag(III) Chemistry
October 26	Dr. G. Rumble, Imperial College
	Real or Imaginary 3rd Order Non-Linear Optical Materials
December 7	Prof. D. Briggs, ICI and University of Durham
	Surface Mass Spectrometry

1995

March 1	Dr. M. Rosseinsky, Oxford University
	Fullerene Intercalation Chemistry
April 26	Dr. M. Schroder, University of Edinburgh
	Redox Active Macrocyclic Complexes
May 3	Prof. E. W. Randall, Queen Mary & Westfield College
	New Perspectives in NMR Imaging
October 4	Prof. D. Tuck, University of Windsor, Ontario
	Electron Transfer Processes in Main Group Chemistry

October 11	Prof. P. Lugar, University of Berlin
	Low Temperature Crystallography
November 17	Prof. D. Bergbreiter, Texas A&M
	Design of Smart Catalysts, Substrates and Surfaces
November 22	Prof. I. Soutar, Lancaster University
	A Water of Glass? Luminescence Studies of Water Soluble Polymers
December 8	Prof. M. Reetz, Mullheim
	Size Selective Synthesis of Metal Clusters

1996

January 10	Dr. B. Henderson, Waikato University
	Electrospray Mass Spectrometry - A New Technique
January 17	Prof. J. W. Emsley, Southampton University
	Liquid Crystals: More than Meets the Eye
January 31	Dr. G. Penfold
	Soft Soap and Surfaces
February 14	Prof. R. Nolte
	Design Strategies for Supramolecular Architectures
March 6	Dr. R. Whitby, University of Southampton
	New Approaches to Chiral Catalysts
March 12	Prof. V. Balzani, University of Bologna
	Supramolecular Photochemistry

October 22	Prof. B. J. Tighe, Aston University
	Polymers for Biomedical Application
October 23	Prof. H. Ringsdorf, Johannes Gutenberg-Universitat
	Function Based on Organisation
November 6	Dr. K. Reid, Nottingham University
	Probing Dynamic Processes with Photoelectrons
November 18	Prof. Olah
	Crossing Conventional Lines in my Chemistry of the Elements
November 20	Prof. J. Earnshaw, Belfast University
	Surface Light Scattering: Ripples and Relaxation
December 4	Prof. K. Muller-Dethlefs, York University
	Very High Resolution ZEKE Spectroscopy

1997

February 6	Prof. P. Bartlet, Southampton University
	Integrated Chemical Systems
February 19	Brian E. Hayden
	Dynamics of Dissociation at Surfaces
March 3	Dr. M. Owen and Dr. D. Gravier, Dow Corning
	Siloxanes at Surfaces
March 6	Prof. K. Toth
	Advances in Scanning Electrochemical Microscopy

PRESENTATIONS ATTENDED

December 1996   ICI, Zeneca, Tioxide Poster Competition

"Dendrimers Mimic Plant Cells" - 3rd Prize

April 1997   North-Eastern Universities Graduate Symposium

"Dendrimers Mimic Plant Cells" - 2nd Prize

EXAMINED LECTURE COURSES

Oct. - Dec. 1994   Polymer Physical Chemistry (Dr. R. W. Richards)

Oct. 1994 - Jan. 1995   General Laboratory Techniques (Dr. D. P. Hampshire)

Electron Microscopy (Dr. K. Durose)

Spectroscopy (Dr. D. P. Halliday)